OXYGEN TRANSFER IN RECIRCULATING FLOW

by

Tuck Foo Thum

Thesis submitted to the Graduate Faculty of the
Virginia Polytechnic Institute and State University
in partial fulfillment of the requirements for the degree of

MASTER OF SCIENCE

in

Mechanical Engineering

APPROVED:

T. E. Diller, Chairman

D. R. Jaasma

J. Moore

January, 1985

Blacksburg, Virginia

OXYGEN TRANSFER IN RECIRCULATING FLOW

by

Tuck Foo Thum

(ABSTRACT)

An experimental investigation was done on oxygen transfer into a laminar flow of whole blood and saline solutions downstream of an abrupt pipe expansion. This was used as the experimental model for regions of separated flow in the arterial system. The flow was fully-developed prior to the expansion with Reynolds numbers between 160 to 850. The results showed high transfer rates over most of the region downstream of the step, with maximum transfer occurring near the reattachment point. In addition, oscillations of the transfer rate were measured at the larger Reynolds numbers of 450 and 850.

ACKNOWLEDGEMENTS

I would like to extend my gratitude to Dr. T. E. Diller for his patience, guidance and support during the course of this project. The help, suggestions and encouragement of my committee members Dr. J. Moore and Dr. D. R. Jaasma are gratefully acknowledged. The help I received from and Dr. L. J. Arp in the lab is gratefully acknowledged. I am very grateful to my mom, brothers and sisters for their moral support during the course of my studies. The financial support of the Whittaker Foundation made this project possible. Many thanks to for typing this thesis. I would like to thank my relatives and friends for their support and encouragement during the past year. Finally, I want to express my sincere appreciation to my special friend, , for her support and caring.

TABLE OF CONTENTS

TABLE OF CONTENTS (continued)

LIST OF FIGURES

LIST OF FIGURES (continued)

LIST OF FIGURES (continued)

LIST OF TABLES

LIST OF TABLES (continued)

LIST OF TABLES

NOMENCLATURE

C_{Hb} = hemoglobin concentraton

C = capacitance

d = upstream diameter of tube

d_i = inner diameter of silicon tube

D = downstream diameter of silicon tube

D_c = diffusivity of oxygen

D_m = diffusivity of silicon membrane

D_o = reference value for oxygen diffusivity

h_d = mass transfer coefficient

k = constant for Margaria equation

L = length of silicon tube

M = oxygen sink strength

m = constant for Margaria equation

P = gas pressure

$\hat{P}$ = dimensionless oxygen partial pressure

P_b = partial pressure of oxygen in blood

P_i = initial oxygen partial pressure

P_o = partial pressure of oxygen surrounding the transfer tube

P_s = measured partial pressure of oxygen

PO_2 = oxygen partial pressure

Q = volume flow rate

r_i = inside tube radius

r_o = outside tube radius

R_l = convection resistance

R_2 = convection resistance

R_3 = convection resistance

R_m = membrane resistance

Re = Reynolds number = $\frac{\bar{V}d}{\nu}$

r = radial coordinate

S = oxygen saturation of hemoglobin

Sh_w = wall Sherwood number

Sh = Sherwood number

Sh_{exp} = experimental Sherwood number

t = time elapsed since calibration

u_m = mean fluid velocity at upstream of tube

$\bar{V}$ = average fluid velocity in tube

x = axial coordinate

x^+ = dimensionless axial coordinate

Greek Symbols

α_b = oxygen solubility in blood or saline

α_m = oxygen solubility in membrane

η = dimensionless radial coordinate

θ = dimensionless transfer, eq. 4.3

ϕ_m = membrane permeability, eq. 4.1

ν = kinematic viscosity

γ_w = shear rate

ϕ = slope of the oxygen-hemoglobin saturation curve

1. INTRODUCTION

Atherosclerosis is known to develop in the human circulatory system at branchings, sharp curvatures, and in regions of bifurcations where flow separation and the resulting fluid recirculation occur. The mechanisms and formation processes of atherosclerotic plaques in these recirculating regions is not presently understood.

One aspect of the problem which has not been well studied in the past is the convective mass transfer process in recirculating flows in blood. Heat transfer studies in recirculation regions have demonstrated the complexity of the problem in single phase systems [1]. Figure 1 shows the recirculating region behind a backward-facing step in a tube [5]. The flow separates at the edge of the step and reattaches some distance downstream (x_r). The position of the reattachment point may actually fluctuate in time, in which case x_r is an average value. Far enough downstream the flow again becomes fully developed. This region downstream of the reattachment point is termed the redevelopment region. When blood is used as the fluid, additional complications occur. Goldsmith has recorded particle paths of red blood cells in recirculating flow regions of blood [2,3]. Typically the cells follow a spiral orbit in the recirculating region until they finally escape into the main flow. There is a lower hematocrit in the recirculating region than the other regions of the flow. It has therefore been postulated that in a flow separation region there may be a reduction in the supply of oxygen from the blood to the arterial walls. Buerk et al. [4] have shown from measurements of oxygen partial pressure profiles through the

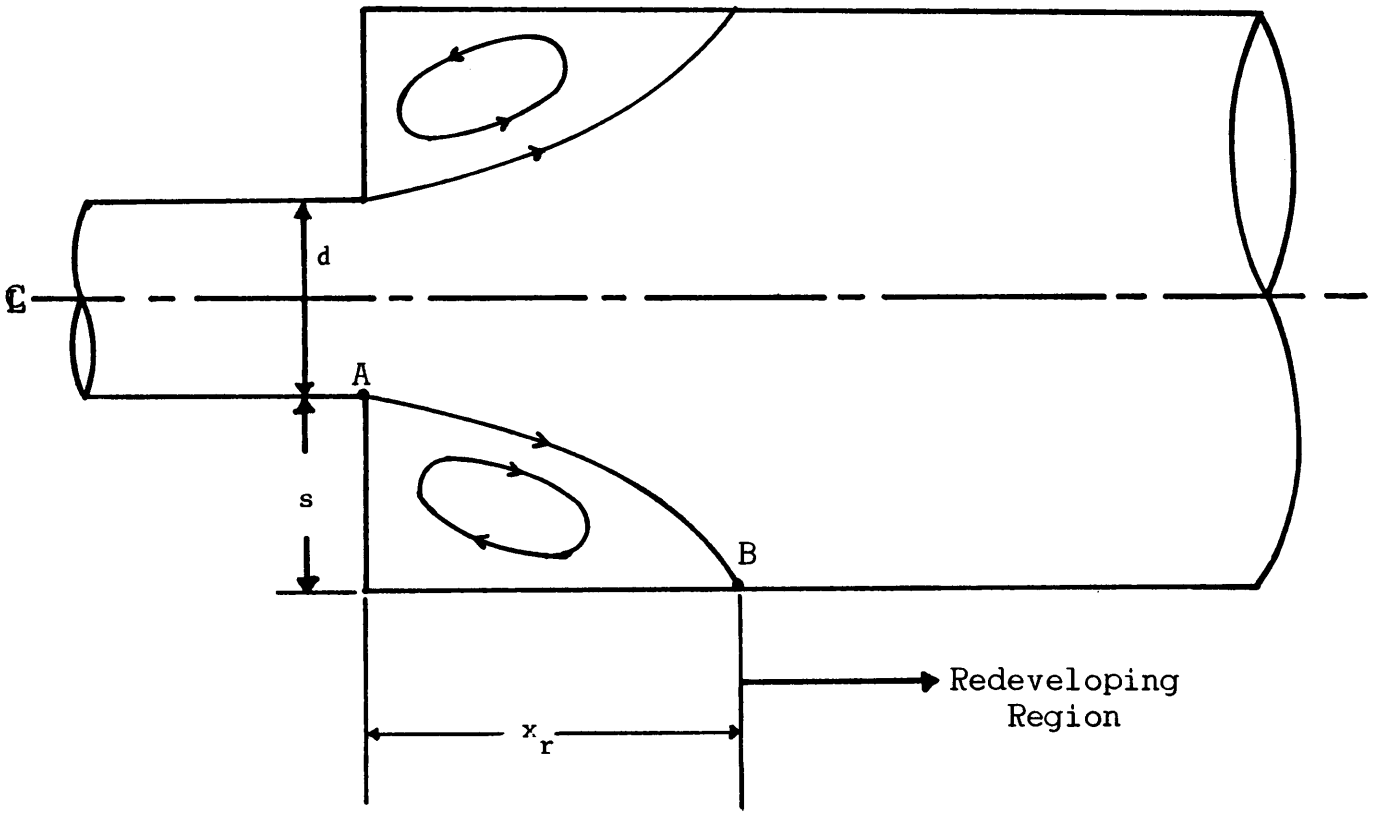

A: Flow Separation Point

B: Reattachment Point

Fig.1 Schematic Diagram of Abrupt Expansion

arterial wall that there is a minimum value of the oxygen partial pressure which is apparently dependent on the blood-side transfer.

The present research attempts to investigate the transfer processes occurring in the recirculating flow region by experimentally measuring the mass transfer. An experimental model with an abrupt backward facing step in a tube is used. This has the advantages of a known separation point and a previously well-documented flow field. The main disadvantage of the step model is that exact geometric similarity is not maintained with the stenoses and arterial branchings found in the human body. Other researchers, however, have also previously used the backward facing step as a model to study recirculating flow effects in biological experiments [5]. An attempt was made, however, to match the approximate flow conditions found in the body. Table 1 shows the representative flow parameters for the larger vessels of man. The experimental model had an upstream tube diameter of 0.5 cm with corresponding Reynolds numbers ranging from 160 to 850. As seen from Table 1, this is a good match for large arteries.

Table 1 Systemic Circulation of Man 6

Structure	Diameter (cm)	Velocity (cm/s)	Reynolds Number	Shear Rate at Wall (s^{-1})
Ascending Aorta	2.0-3.2	63	3600-5800	190
Descending Aorta	1.6-2.0	27	1200-1500	120
Large Arteries	0.2-0.6	20-50	110-850	700

2. LITERATURE REVIEW

2.1 Introduction

Many experimental and numerical studies of fluid flow and heat transfer in separated regions have been done. These can be arranged in categories of external and internal flow, each of which can be laminar or turbulent. For internal flow, like fluid flow inside a tube, the Reynolds number for laminar flow is less than approximately 2300. While there are many fluid flow studies for both laminar and turbulent flows, most heat or mass transfer studies have been for turbulent flow.

2.2 Fluid Mechanics

Back et al. [7] studied the flow field of water downstream of the abrupt expansion in a circular channel for a large range of Reynolds numbers ($20 < Re < 4200$). Their velocity profile immediately upstream of their step was nearly uniform. They examined how the growth of the shear layer between the central jet and the reverse flow along the wall in the separated flow region determined the location of the reattachment point. Their experimental investigation found that there were basically three flow regimes. At low Reynolds numbers (20-250), the growth of the laminar shear layer between the central jet and the reverse flow along the wall determined the reattachment point. The reattachment point increased with increasing Reynolds number in this regime. At intermediate Reynolds numbers (400-1000) there was instability in the vortex sheet-like shear layer. Reattachment was determined when the

lateral extent of the undulating motion extended to the wall. The reattachment point moved back toward the step as Reynolds numbers increased in this regime. At Reynolds numbers above 1000, reattachment occurred at a relatively short distance downstream of the step.

Feuerstein et al. [5] investigated the flow in an abrupt expansion for the case with a parabolic velocity profile in the upstream tube. Their experimental results showed that the reattachment length varied almost linearly with the Reynolds number up to Re = 1090. For Reynolds numbers above 1090 they found reattachment lengths considerably larger than Back et al. [7]. Roschke and Back [28] attributed this difference in results to the different inlet profiles in the upstream tube.

At relatively small Reynolds numbers (Re < 200), in an abrupt circular channel expansion, Macagno and Hung [8] also found that the reattachment location moved downstream with increasing Reynolds numbers.

In an experimental investigation of the laminar flow of air over a downstream-facing step (external boundary layer) Goldstein et al. [9] also found that for a relatively small Reynolds number, the reattachment location moved downstream with increasing Reynolds number. Secondary flows caused by the presence of the step were found in the separated region downstream of the step.

Denham and Patrick [10] used a laser anemometer to measure the velocity distribution in a two-dimensional flow channel and from the measured velocites stream function values were calculated. Flow streamlines were then plotted and the recirculation zone (distance from step height to reattachment point) determined. Their experimental

results for the length of recirculation zone agree reasonably well with those from the wind-tunnel study of Goldstein et at. [9].

Since the present experimental work involved a different geometry (sudden pipe expansion) no comparison of the recirculation length was made with Denham and Patrick [10]. But an interesting observation was found by them during their experiment. They found that at the highest Reynolds number (Re = 229) there were small periodic fluctuations in the velocities near the reattachment point. Durst et al. [11] in their experimental investigation of the laminar flow of air downstream of a plane symmetric sudden expansion using a laser Doppler anemometer found fluctuations for Reynolds numbers above 400. Using a laser Doppler anemometer, Ahmed et al. [12] made some flow disturbance measurements through a constricted tube at Reynolds numbers from 500 to 2000 and also found fluctuations.

Armaly et al. [13] also used a laser Doppler anemometer to measure the velocity distribution and reattachment length downstream of a single backward facing step mounted in a two-dimensional channel. The laminar regime (Re = 70-1200) of the flow was characterized by a reattachment length that increased with Reynolds number.

Numerical studies of backward-facing step flow have been done by Armaly et al. [13] and Mueller and O'Leary [14]. Mueller and O'Leary used an explicit time-dependent finite difference scheme to obtain the numerical solution of the modelled flow field for Reynolds numbers between 0.1 and 1500. There was good qualitative and quantitative agreement between their numerical and experimental results of finding

the reattachment point for Re < 100. Good agreement was also obtained between experimental and numerical results of the reattachment point for Reynolds numbers smaller than 400 for Armaly et al. [13] where the two-dimensionality of the flow was maintained. For Reynolds numbers greater than 400, the numerical and experimental results deviated due to the inherent three-dimensionality of the experimental flow.

2.3 Heat and Mass Transfer

Sparrow and Kalejs [15] experimentally investigated the transfer coefficient distributions in the flow separation, reattachment and redevelopment regions along the walls of a partially constricted inlet for Reynolds numbers in the laminar range (< 1500) using the naphthalene sublimation technique with air as the working fluid. They found that the presence of the inlet constriction gives rise to very low values of the transfer coefficient immediately downstream of the constriction plates, but the transfer coefficient increases rapidly as the downstream distance increases and finally attains a maximum at the point where the separated flow reattaches to the wall.

Local heat transfer of a high-temperature laminar gas flow downstream of an abrupt circular channel expansion was investigated by Back et al. [16] and they found that the highest heat transfer occurred near the reattachment point in the tube.

Runchal [17] conducted a series of experiments to provide information about the mass-transfer behavior of fluids at very high Schmidt numbers for turbulent incompressible flow behind a sudden enlargement of a pipe and generally agreed that the location of the maximum heat/mass transfer was in the vicinity of, or at, the reattachment point.

Zukauskas et al. [18] presented an experimental investigation of the heat transfer in the reattachment and redevelopment regions downstream of a two-dimensional bluff body (external boundary layer) attached on a flat plate in the region of a fully-developed turbulent

boundary layer--the heat transfer increases linearly along the separation region and reaches a maximum at the reattachment point. The radius of curvature of the surface of the obstacle had no significant effect on the heat transfer at reattachment. But the curved surface of the leading edge diminished the length of the separation region, and the intensity of heat transfer.

Larson's [19] experimental heat-transfer investigation in regions of separated flow for external surfaces also showed that the maximum heat-transfer occurred near the reattachment point of the separated boundary layers investigated.

Heat transfer coefficients on the downstream face of an abrupt enlargement or inlet constriction in a pipe for turbulent flow were measured by Sparrow and O'Brien [20]. Two flow configurations were investigated: (1) an abrupt enlargement from a smaller diameter pipe to a larger diameter pipe and (2) partial constriction of a pipe inlet by a large baffle plate. The authors found higher average transfer coefficient values for the pipe with the constricted inlet than for the pipe with the abrupt enlargement.

Schneiderman et al. [21] made a numerical study of the mass transport patterns of blood flowing through an axisymmetric constriction in a straight, cylindrical vessel with constant wall concentration and found that for Reynolds numbers larger than that required for flow separation ($Re > 16$), there was a decrease in transfer right after separation (caused by the constricted vessel) but an increase of mass flux in other regions of the vessel.

Finally, a review of separated flows by Chilcott [22] shows that in all cases the maximum local heat transfer occurred in the region around the reattachment point of the separated flow.

The literature review presented has shown that there has been little experimental work done on transfer in laminar separated flows. The few transfer experiments found had greatly different Schmidt and Prandtl numbers than those in saline or blood for oxygen transfer. In addition, most of the experiments involved external flow. The fluid flow results indicate different flow regimes within supposedly laminar flow. The numerical studies are generally done only for $Re < 400$. In terms of the heat transfer results, the highest transfer occurs at or around the reattachment point.

3. EXPERIMENTAL METHOD

3.1 Introduction

The experimental procedures described include (1) finding the reattachment point by the flow visualization technique and (2) oxygen transfer measurements to blood and saline solutions. The method for analysis of the data is also given.

3.2 Experimental Apparatus

A schematic diagram of the experimental apparatus is shown in Fig. 2. The entire apparatus was enclosed within a temperature-controlled Plexiglass structure at 37°C. The use of Plexiglass allowed everything inside of the enclosure to be seen while providing sufficiently low heat loss characteristics. The environment was kept at a constant temperature by circulating the heated air with a fan through an automatically controlled heater. Three thermistors were placed at different locations inside the environment to monitor the air temperature. An automatic controller averaged the readings from the three thermistors and used this average value to control the heater in an on-off fashion. This ensured that the average temperature varied by no more than ±0.5 C from the set point. A complete description of the set-up is given by Pattantyus [23].

A detailed sketch of the transfer chamber is shown in Fig. 3. It was constructed of Plexiglass with liquid and gas ports at each end. Inside of the transfer chamber was a 1.27 cm diameter silicon rubber

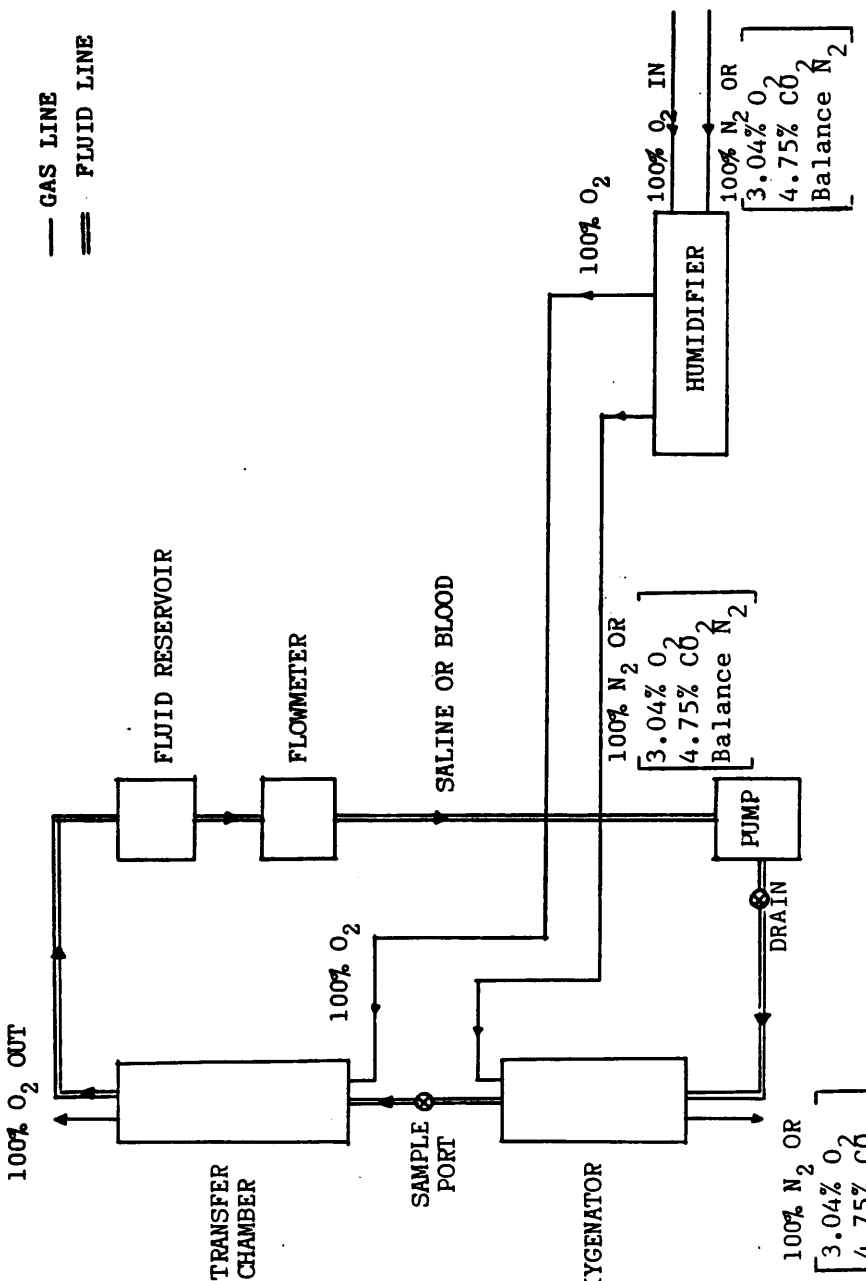

Fig. 2 Schematic Diagram of Experimental Apparatus

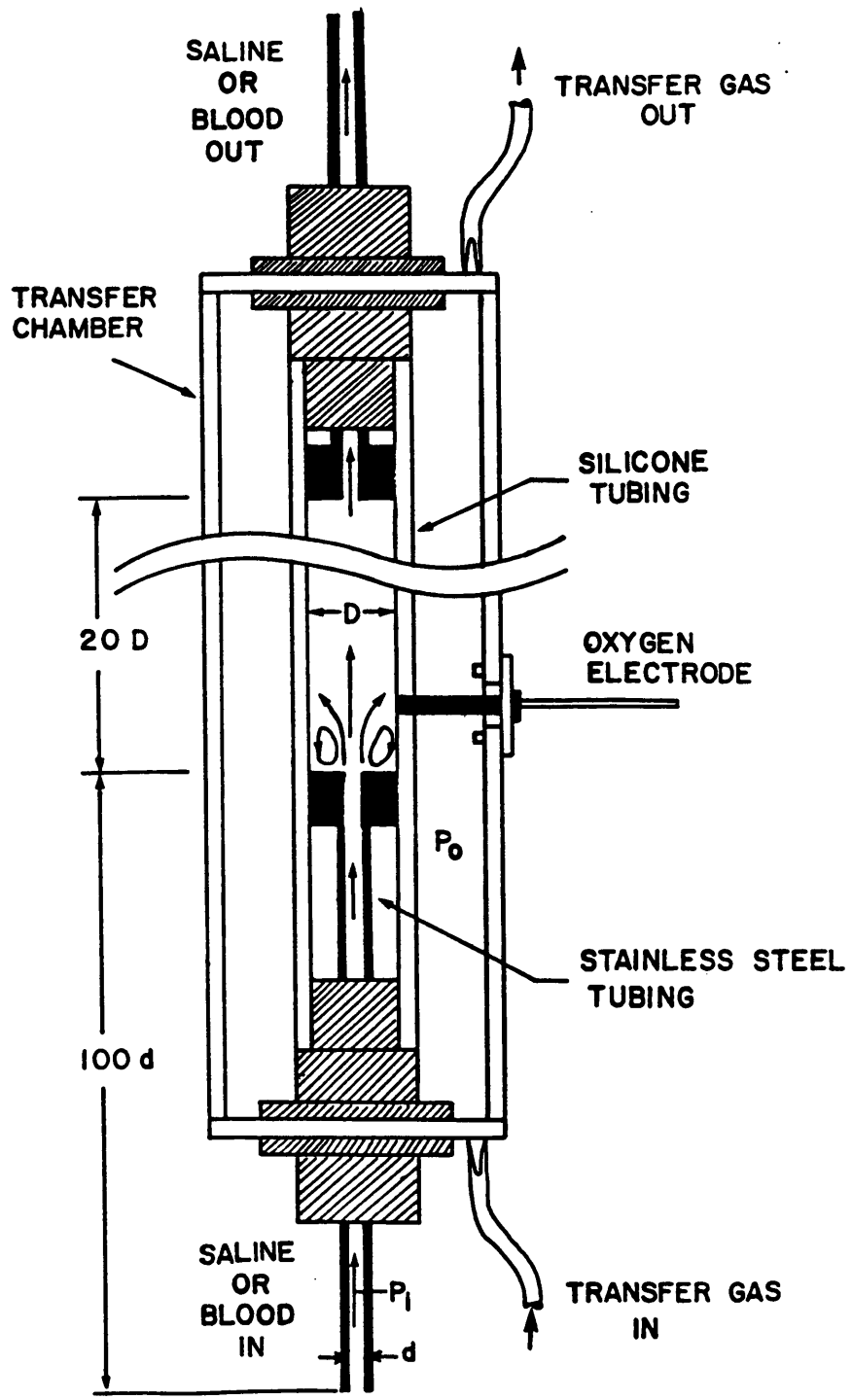

Fig. 3. Transfer chamber

tube where the oxygen transfer took place. Two stainless steel tubes of 0.49 cm inner diameter with a bushing attached were fitted into the silicon rubber tube as shown in Fig. 3 with O-ring seals to allow them to slide freely. This assembly was mounted vertically in the thermal environment. A miniature Clark electrode, 3.2 mm in diameter (Diamond Electro-Tech, Model 730) was inserted at a fixed position flush with the silicon rubber tube inner wall. It was used to measure the oxygen partial pressure at the fluid-surface boundary. The electrode was connected to the Chemical Microsensor Model 1201 manufactured by Diamond Electro-Tech, Inc. This arrangement enabled the position of the measuring electrode relative to the tube expansion to be varied, while leaving the measuring electrode fixed at one position in the tube wall.

During the transfer experiments, the gases were passed through a humidifier. The humidified gas with the lower percentage of oxygen content (3% O_2 or 0% O_2) was passed through an oxygenator (SciMed Membrane Oxygenator System Model No. 0800-2A). This oxygenator was used to provide a constant oxygen partial pressure in the fluid as it entered the transfer chamber. The humidified gas with the higher percentage of oxygen content (100% O_2) was meanwhile circulated inside the transfer chamber through the lower gas inlet.

A variable-speed, positive displacement pump (Micro Pump Model 120-415) was used to provide a constant fluid flow rate. An electromagnetic flowmeter (CME 500 Series Square-wave Flowmeter) was used in-line to continuously monitor the flow rate.

Measurements of oxygen and carbon dioxide partial pressure and pH were obtained with a Corning Model 158 blood gas analyzer. This semi-automatic, microprocessor based machine has all of the calibrating reagents and gases connected to it with automatic valving controlling the flows. It also has temperature regulation at a constant 37°C, the same as the test chamber.

The total hemoglobin concentration (THb gl/dl), percent oxyhemoglobin (% 0 Hb), percent carboxyhemoglobin (% CO Hb), percent methemoglobin (% Met Hb) and a calculated value for volume percent oxygen were measured by a CO-Oximeter Model 282 Instrumentation Laboratory. The actual measurement of these parameters was accomplished by a four wavelength spectrophotometer within the instrument. The CO-Oximeter was temperature-regulated to 37°C.

3.3 Experimental Procedures and Data Collection

There were two procedures used for finding the reattachment point. Saline was first circulated through the whole system. In the first procedure, bubbles were injected by a syringe into the tubing prior to the entrance region of the transfer tubing. The reattachment point was located by measuring the distance from the step where the bubbles appeard to stop and to come into contact with the surface of the transfer tube. In the second procedure, colored dye was injected by a syringe into the tubing prior to the entrance region of the transfer tubing. The reattachment point was estimated in the same manner as the first procedure.

The day before transfer measurements were to take place, the blood gas analyzer was started up and left on continuously. This was done so that the equipment had sufficient time to stabilize. The membranes were checked to ensure that they were not coated with residue and that they were not too old. If they were, they were changed according to the maintenance instructions listed in the blood gas analyzer manual. The barometric pressure was entered into the blood gas analyzer and the value was recorded. The analyzer was then calibrated. The analyzer was also calibrated after each experiment. Some problems that would cause an improper calibration reading were bad membranes, sample chamber waste tubing blockage, air bubbles at the bottom of the reference cavity, excess silver deposits on the PO_2 electrode tip, improper membrane positioning, or moisture under the membrane skirt or PCO_2 electrode boot. The most common problems encountered were air bubbles at the bottom of the reference cavity and moisture under the membrane skirt or PCO_2 electrode boot. The first problem was eliminated by tapping the electrode until the air bubbles were removed while the second problem was removed by wiping off the moisture with a tissue or a cotton swab.

A new membrane was also installed in the miniature Clark oxygen electrode the day preceeding a transfer test. Before installation, the tip of the electrode was dipped into KCl solution. It was ensured that there were no air bubbles under the membrane after installation. If air was noted, a new membrane was installed. Between use, the tip of the electrode was soaked in a KCl solution to prevent the filling solution from drying. The membrane was changed whenever it was damaged, if

bubbles under the membrane were detected or if the filling solution was dried.

The polarization voltage of the Clark electrode was found by plotting a characteristic curve and observing the plateau. This characteristic curve was obtained by decreasing the polarization voltage from an initial value of -1.0 volt and recording the corresponding current when the electrode was stabilized at that particular voltage. A strip chart recorder connnected to the output of the microsensor aided in observing the electrode stabilization. The voltage at the midpoint of the plateau was chosen as the operating voltage for the electrode.

On the day of the actual run, the blood gas analyzer was again calibrated before the experiment took place. At the same time, the CO-Oximeter was warmed up when blood was going to be used in the experiment. After one-half hour, all fluidics were purged of air bubbles and then calibrated for total hemoglobin using CalDye, which is a reference standard for calibrating the total hemoglobin channel of the Co-Oximeter. The Clark oxygen electrode was next inserted in a fixed position flush with the silicon tube inner wall. The fluid used in the experiment was then poured into the reservoir. The positive displacement pump was then turned on to circulate the fluid around the experimental apparatus.

Any bubbles that were attached to the tubing walls were removed by pinching the tubing. To ensure that no air bubbles remained inside the oxygenator, the red cap at the top of the oxygenator was slowly released until some fluid oozed out. It was especially important that no air

bubbles were attached to the surface of the Clark electrode as any presence of air bubbles would affect the measurements.

Saline solution tests

During the initial calibration procedure using saline solution, nitrogen gas was passed into the test chamber and the oxygenator at a rate of about 1000 cc/min. At the same time the strip chart recorder connected to the output of the microsensor was turned on to monitor the trend of the partial pressure measured by the Clark electrode. After the microsensor readings had reached a steady-state, a sample was drawn and checked with the blood gas analyzer. The microsensor and analyzer readings were recorded and compared. The zero and gain knobs in the microsensor were adjusted if necessary. The N_2 gas was then cut off and the transfer chamber and oxygenator flooded with the higher oxygen content gas. The procedure was repeated for the N_2 gas. If the zero and gain knobs were adjusted earlier, the same procedure was repeated for the higher oxygen content gas.

When the calibration procedure was completed, a flow sensitivity test was conducted. The test was done to detect any variations in the probe readings due to the changes in the flow velocity around the electrode. The flow sensitivity test was done by systematically moving the expansion tube from 1 cm to 15 cm relative to the Clark electrode and back again, with the same gas in the oxygenator and test chamber. If the Clark electrode was placed in the correct position, there was very little variation in the readings. This ensured that the partial

pressure measurements taken during the transfer experiments were reliable.

After the flow sensitivity test, the transfer experiment was then conducted. The transfer chamber was flooded with 100 percent O_2 while 100 percent N_2 was passed into the oxygenator. The partial pressures were measured by systematically moving the expansion cap from a position of 1 cm relative to the Clark electrode to a position of 15 cm relative to the Clark electrode and then back again to 1 cm. A sample was taken at various positions as the expansion cap was moved and then checked with the blood gas analyzer. All readings were recorded. After the transfer test, a calibration using N_2 gas was done to check for any drift in the electrode.

Canine Blood Tests

When blood was needed for an experiment, a fresh sample of about 350 ml to 400 ml was taken from a dog kept at the veterinary school kennels. The blood was treated with liquid heparin anti-coagulant while it was being drawn. The heparin does not affect the pH. When a fresh sample of blood was obtained, the hematocrit was checked by centrifuging the sample in a capillary tube. The hematocrit was typically between 35 and 45 percent.

Before the canine blood was used for the experiment, the microsensor was first calibrated with saline solution. This was done to prevent the canine blood from being hemolyzed before the actual transfer run took place. The calibration procedure was the same as listed under

the "saline solution tests." After the initial calibration, the saline solution was drained out. To ensure no saline remained in the system, the tubes were given a slight tap and the oxygenator was removed and the saline drained off by passing in N_2 gas at one end of the oxygenator. The canine blood was then poured into the reservoir. A small sample of blood was extracted by a syringe and then analyzed by the CO-Oximeter. All of the data was recorded. Three percent O_2 gas was then passed into both the transfer chamber and the oxygenator. The strip-chart recorder was also turned on to monitor the trend of the readings recorded from the Clark electrode connected to the microsensor.

After the microsensor readings had reached a steady-state, a sample of about 3 ml was extracted from the sample port and then analyzed in the blood gas analyzer and CO-Oximeter. When the sample was initially extracted, there were bubbles of air inside the syringe. The bubbles were removed by pushing out the sample fluid and the sample extracted again. The process was repeated until no bubbles were found inside the syringe. After extraction, the syringe needle was quickly removed and the syringe head capped. Besides recording the data on the microsensor, the blood gas analyzer and on the CO-Oximeter, the flow rate, barometric pressure, temperature and the time at each data point were also recorded.

The higher oxygen concentration gas was passed into the transfer chamber while the lower oxygen concentration gas was passed into the oxygenator during the transfer test. Similar to the saline solution tests, the partial pressures were recorded by systematically moving the

expansion cap from a position of 1 cm relative to the Clark electrode to a position of 15 cm relative to the Clark electrode and then back again to 1 cm. At various positions, a sample of about 3 ml was extracted and then analyzed by the blood gas analyzer and Co-Oximeter. Calibration was done by flooding the transfer chamber and oxygenator with 3 percent O_2 gas to record any drift in the Clark electrode. The blood was then drained off, replaced by saline, and the saline used with 100 percent N_2 gas to check for drift of the microsensor.

3.4 Data Analysis

The raw experimental data in tabular form are presented in Appendix G. Corrections were made to these sets of data to compensate for the zero shift that occurred over the length of the experiment. The initial and final calibration values of the partial pressure of oxygen recorded before and after an experiment were checked against the known values for the gases used. The barometric pressure minus the vapor pressure of water at $37^{o}C$ was multiplied by the appropriate concentration to obtain the partial pressure of the known values. If the calibration values were different from the known values the corrected value of the partial pressure was obtained by subtracting a correction based on a linear shift with time from the measured partial pressure. The equation is expressed as follows:

$$\text{Actual (corrected) Value of } P_s = \text{Measured } P_s - \Delta$$

where

$$\Delta = \begin{bmatrix}\text{Initial}\\ \text{Calibration}\\ \text{Value}\end{bmatrix} - \begin{bmatrix}\text{Blood Gas}\\ \text{Analyzer}\\ \text{Value}\end{bmatrix}$$

$$- \frac{\begin{bmatrix}\text{Initial}\\ \text{Calibration}\\ \text{Value}\end{bmatrix} - \begin{bmatrix}\text{Final}\\ \text{Calibration}\\ \text{Value}\end{bmatrix}}{\text{Total Time of Experiment}} \cdot \begin{bmatrix}\text{Time since}\\ \text{Initial}\\ \text{Calibration}\end{bmatrix}$$

Using the corrected oxygen partial pressure, (P_s), the known transfer resistance of the silicon tube wall (ϕ_m), and the known inlet (P_i) and outside partial pressures (P_o), the mass transfer coefficient, (h_d), for the fluid can be obtained.

Figure 4 shows the cross-sectional profile of the silicone membrane tubing and the fluid within the tubing. Figure 5 shows the direction in which the gas diffuses through the silicon membrane and the steady-state model of the oxygen partial pressures.

Using the network analogy,

$$\frac{P_i - P_s}{R_l} = \frac{P_s - P_o}{R_m}$$

$$\frac{P_i - P_s}{\frac{1}{2 \pi r_i L h_d (\frac{\alpha_b}{\alpha_m})}} = \frac{P_s - P_o}{\frac{\ln (r_o/r_i)}{2\pi L D_m}}$$

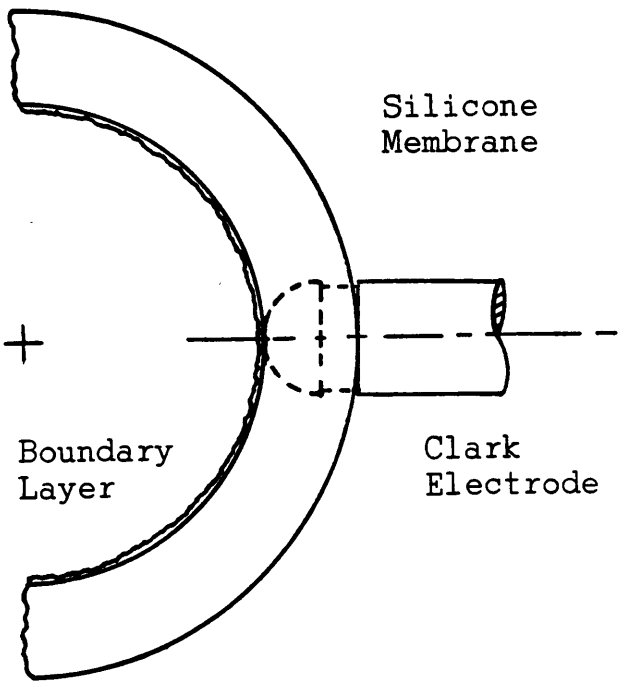

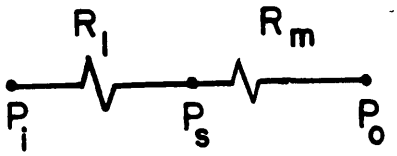

$$h_d = \frac{\Phi_m}{r_i \alpha_b \ln(r_o/r_i)}\left(\frac{P_s - P_o}{P_i - P_s}\right)$$

Fig. 4. Cross-section profile of silicon tube membrane and fluid within tube

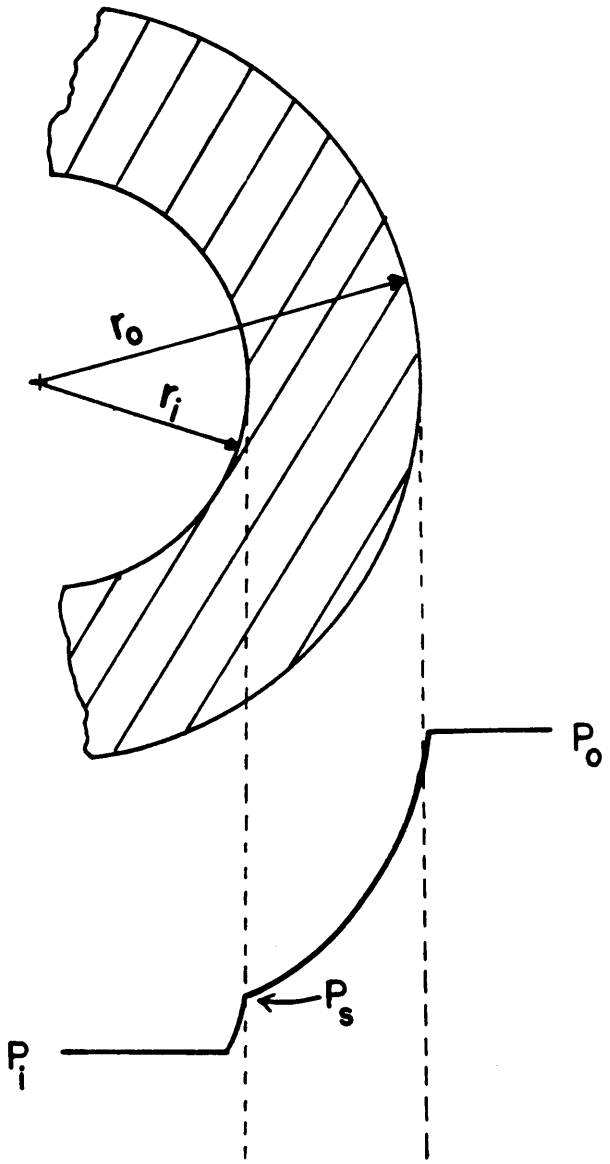

Fig. 5. Partial pressure distribution for the tube membrane

$$\frac{P_i - P_s}{\frac{1}{r_i \; h_d\left(\frac{\alpha_b}{\alpha_m}\right)}} = \frac{P_s - P_o}{\frac{\ln(r_o/r_i)}{(\phi_m / \alpha_m)}} \qquad (3.1)$$

Solving for h_d gives

$$\therefore \quad h_d = \frac{\phi_m}{r_i \; \alpha_b \; \ln\,(r_o/r_i)} \left(\frac{P_s - P_o}{P_i - P_s}\right) \qquad (3.2)$$

Oxygen solubility in saline, α_b = 0.0239 cc/cc - atm

Oxygen solubility in blood, α_b = 0.0223 cc/cc - atm

Membrane permeability, $\phi_m = 5.32 \times 10^{-6}$ cm^2/atm-s

P_s = measured partial pressure of oxygen

P_o = partial pressure of gas with higher oxygen concentration

$P_i = P_b$ = partial pressure of gas with lower oxygen concentration

Inner radius of silicon tubing, r_i = 1.27 cm.

The membrane permeability of silicone rubber, ϕ_m, and the solubility values were obtained from Diller [24].

Ratio of outer radius to inner radius, (r_o/r_i) = 1.375. Thus from Eq. (3.1), substitution of the constant values gives,

$$\text{For saline} \quad h_d = 1.101 \times 10^{-3} \frac{P_s - P_o}{P_i - P_s} \frac{cm}{s} \tag{3.3}$$

$$\text{for blood} \quad h_d = 1.179 \times 10^{-3} \frac{P_s - P_o}{P_i - P_s} \frac{cm}{s} \tag{3.4}$$

The experimental Sherwood numbers were calculated from the measured transfer coefficients using the tube diameter and oxygen diffusion coefficient of the fluid. The equation is

$$Sh_{exp} = \frac{h_d D}{D_c} \tag{3.5}$$

The diffusivity of oxygen in saline is $D_c = 2.85 \times 10^{-5}$ cm^2/s. The diffusivity of oxygen in blood is $D_c = 1.5 \times 10^{-5}$ cm^2/s. Therefore the Sherwood numbers of both saline and blood can be expressed as follows:

saline $$Sh_{exp} = 4.456 \times 10^4 \, h_d \quad (3.6)$$

blood $$Sh_{exp} = 8.467 \times 10^4 \, h_d \quad (3.7)$$

Results of the mass transfer coefficient, h_d, and the Sherwood number, Sh, for saline and blood are presented in Tables 2, 3, 4, 5 and 6 (Appendix E).

Some of the Sherwood numbers were omitted because they were too large to be measured. For these cases the values of the measured oxygen partial pressure at the surface were very close to the inlet oxygen partial pressure. From Eq. (3.2) it can be seen that if P_i is close to P_s, h_d will be very large. Correspondingly, the error will be very large.

4. ANALYTICAL SOLUTIONS

The solution for a fully-developed tube flow with a thermal entrance region starting at the step position is used to provide a comparison with the experimental results.

The analytical technique for modeling oxygen transfer in blood or saline in this region consists of numerically solving the dimensionless convective-diffusion equation. The computer program used the Crank-Nicholsen finite-difference method to solve the resulting parabolic partial differential equation. A major portion of the program was derived from EXPNUM3, a program which was developed by Pattantyus [23].

Assuming a parabolic velocity profile, a continuous homogenous fluid, and average fluid properties, the dimensionless convective-diffusion equation for steady tube flow is

$$(1 - \eta^2)(1 + \psi)\,\frac{\partial \hat{P}}{\partial x+} = \frac{\partial}{\partial \eta}\left(\eta\,\frac{\partial \hat{P}}{\partial \eta}\right) \qquad (4.1)$$

The boundary conditions are:

$$\text{(a)} \quad x^{+} = 0 \;\; ; \;\; \hat{P} = 0$$

$$\text{(b)} \quad \eta = 0 \;\; ; \;\; \frac{\partial \hat{P}}{\partial \eta} = 0$$

$$\text{(c)} \quad \eta = 1 \;\; ; \;\; \frac{\partial \hat{P}}{\partial \eta} = (1 - \hat{P})\,\frac{Sh_w}{2}$$

and the dimensionless variables are:

$$\eta = r/r_i$$

$$x^+ = \frac{\pi D_c X}{2Q}$$

$$\hat{P} = \frac{P - P_i}{P_o - P_i}$$

$$Sh_w = \frac{\phi_m}{D_c \alpha} \cdot \frac{2}{\ln (r_o/r_i)}$$

The wall Sherwood number, Sh_w, relates the diffusion resistance of the silicon tube wall and the diffusion resistance of the fluid. The parameter, ϕ_m, is the permeability of the silicon tube wall. The term ϕ is a non-linear function of P, and is proportional to the oxygen-hemogloblin saturation curve. This term accounts for the chemical reaction.

The equation of ϕ is given by

$$\phi = \frac{1.39}{\alpha_o}(C_{Hb}) \frac{\partial s}{\partial p} \frac{g/cc}{mm\ Hg}$$

$\frac{\partial s}{\partial p}$ is evaluated using Margaria equation and the hemoglobin saturation curve is shown in Fig. 6. Diller [24] gave a complete explanation of ϕ. Since Eq. (4.1) is parabolic, it is solved at each radial step of x as x is incremented in the axial direction. The Crank-Nicholsen method uses the centered difference technique where the finite difference equations are centered at half-steps between the nodes in the direction of propagation. Diller [24] gave a complete solution scheme

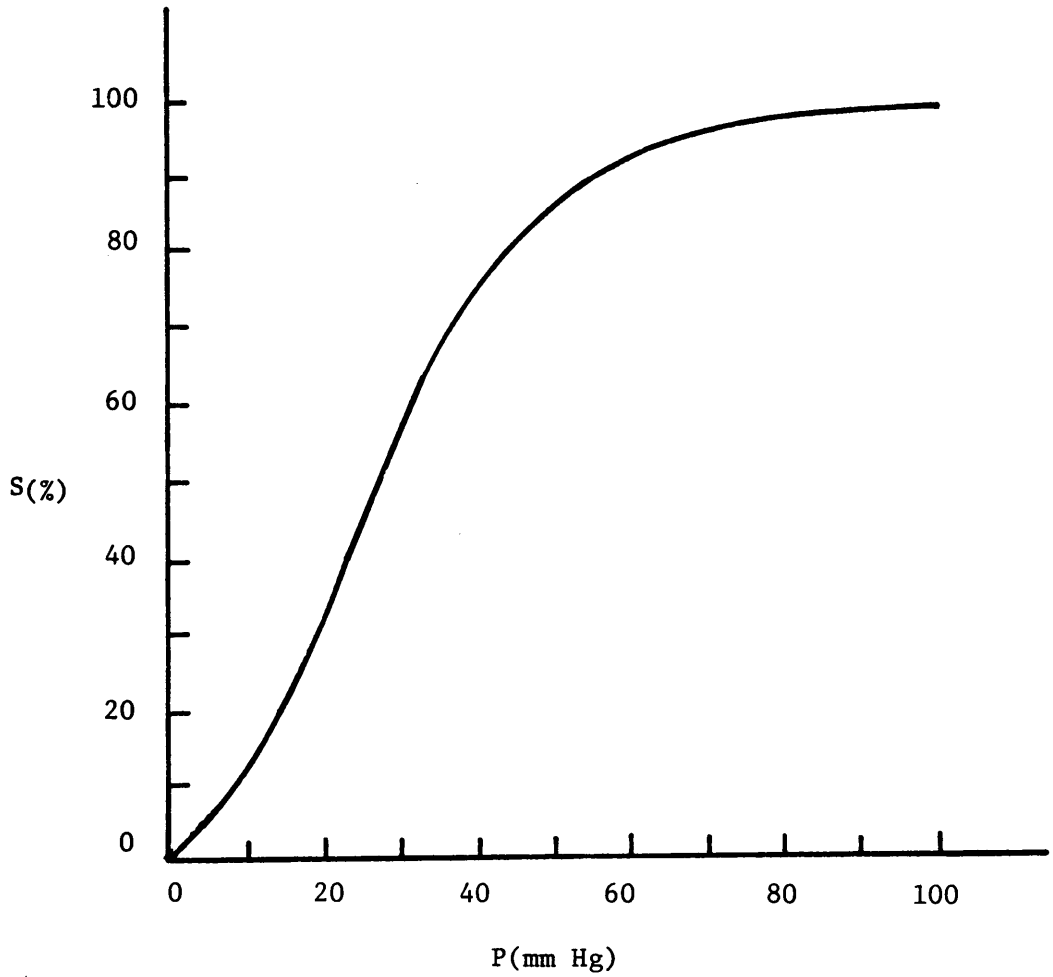

Fig. 6. Oxygen-hemoglobin saturation curve

of solving Eq. 4.1. The nodal scheme is represented in Fig. 7. The terms in Eq. 4.1 are represented in finite difference form as

$$\left.\frac{\partial \hat{P}}{\partial \eta}\right|_{i,j+1/2} = \frac{1}{4}\left[\frac{\hat{P}_{i+1,j} - \hat{P}_{i-1,j}}{\Delta\eta} + \frac{\hat{P}_{i+1,j+1} - \hat{P}_{i-1,j+1}}{\Delta\eta}\right]$$

$$\left.\frac{\partial^2 \hat{P}}{\partial \eta^2}\right|_{i,j+1/2} = \frac{1}{2}\left[\frac{\hat{P}_{i+1,j} - 2\hat{P}_{i,j} + \hat{P}_{i-1,j}}{(\Delta\eta)^2} + \right.$$

$$\left.\frac{\hat{P}_{i+1,j+1} - 2\hat{P}_{i,j+1} + \hat{P}_{i-1,j+1}}{(\Delta\eta)^2}\right]$$

$$\left.\frac{\partial \hat{P}}{\partial x}\right|_{i,j+1/2} = \frac{\hat{P}_{i,j+1} - \hat{P}_{i,j}}{\Delta x}$$

The finite difference equation is solved at each node from i=1 to i=n, where n is the number of radial divisions. As shown in Fig. 7, the nodes are shifted from the boundary one-half step to make generalization of the boundary conditions easier. A mixed boundary condition (Fig. 8) is incorporated by placing a fictitious point outside of each boundary. These variables which are discretized are then substituted into Eq. (4.1). A set of n equations is obtained for the pressures at j+1 in terms of those at j.

$$[B]\ [\hat{P}_{j+1}] = -\ [A]\ [\hat{P}_j] - [C] \qquad (4.2)$$

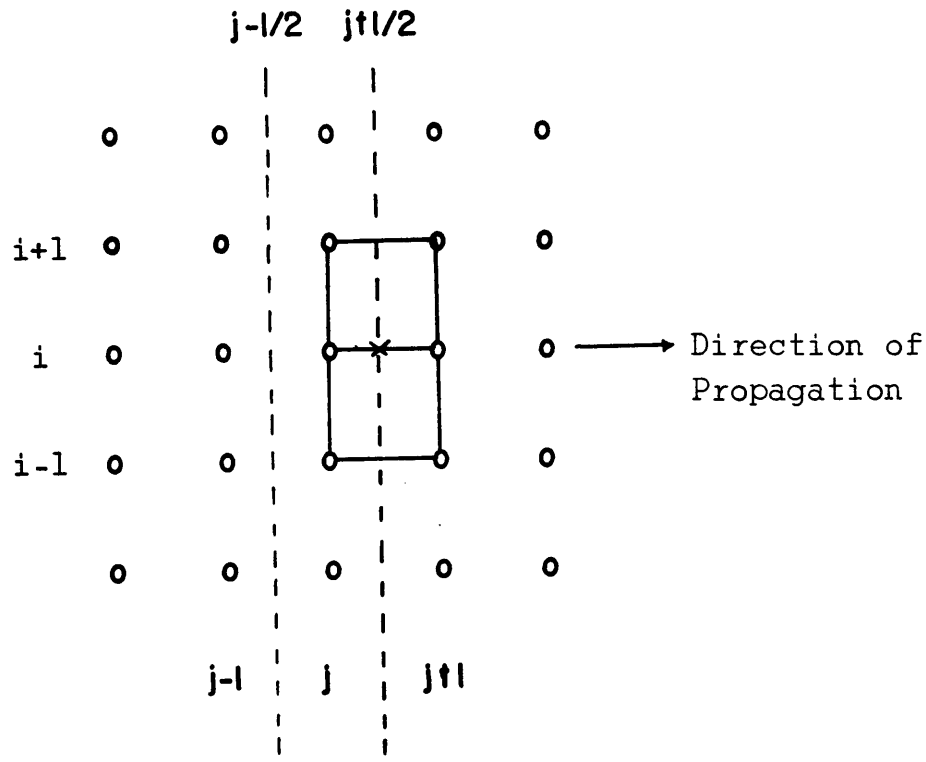

Fig. 7. Nodal scheme

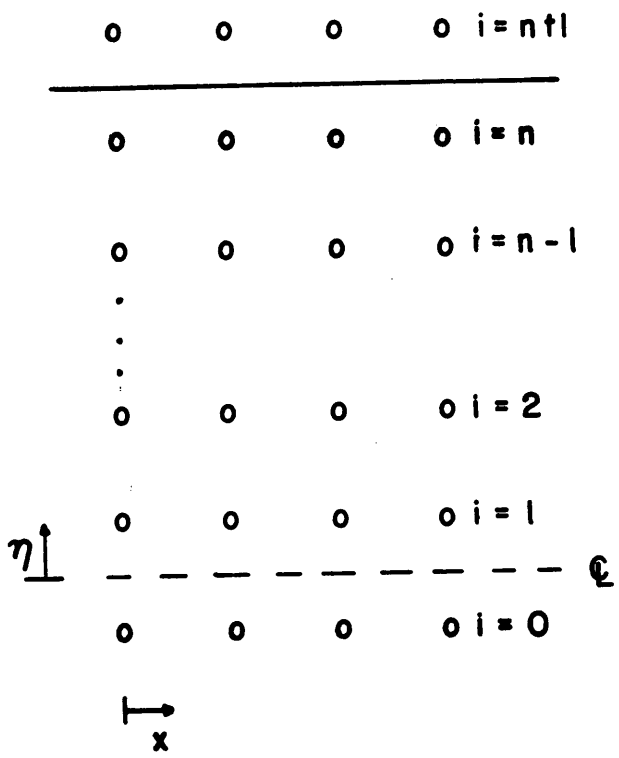

Fig. 8. Boundary nodes for numerical solution

[A] and [B] are tridiagonal matrices. The non-linear term ϕ appears in the main diagonal terms only. When solving for $[\hat{P}_{j+1}]$, the right side of Eq. (4.2) is a known matrix [D].

$$[B]\ [\hat{P}_{j+1}] = [D]$$

The Thomas algorithm is used to solve such a tridiagonal system .

For linear equations this finite-difference solution is a straightforward step-by-step progression in the x direction, which was applied to the saline cases. However, for the blood cases, the equation is not linear due to ϕ and thus iteration at each length step is necessary.

The method used by Diller [8] to solve the parabolic equation with non-linear coefficient ϕ was a forward projection of the coefficient using a truncated Taylor series about the point (i,j).

$$P_{i,j+1/2} = P_{i,j} + \left(\frac{\partial P}{\partial x}\right)_{i,j} \frac{\Delta x}{2}$$

The value of $\left.\frac{\partial P}{\partial x}\right|_{i,j}$ is obtained from Eq. (4.1) as

$$\left.\frac{\partial P}{\partial x}\right|_{i,j} = \frac{1}{(1 - \eta^2)} \frac{1}{(1 + \phi)} \frac{1}{\eta} \left(\frac{\partial P}{\partial \eta} + \frac{\partial^2 P}{\partial \eta^2}\right)$$

This value of $P_{i,j+1/2}$ was then used to evaluate $\phi_{i,j+1/2}$. After solving for $P_{i,j+1}$, ϕ was re-evaluated using the average of $P_{i,j}$ and

$P_{i,j+1}$. If this value was not within 0.02 M of the old value, the equations were re-solved with the new value. Iteration was continued until this criterion was met.

Once the values of $\hat{P}$ are found at any position in the tube the mass transfer coefficients and the Sherwood numbers can be calculated. In the calculation of the mass transfer coefficient, θ is involved. θ is the mass average concentration of oxygen in the blood (or the dimensionless transfer at that position). θ is found by calculating the change in total oxygen concentration for each node (excluding the fictitious nodes), then multiplying the fraction of the volume flow of fluid within the region of that node and finally dividing by the total transfer needed for equilibrium with the outside gas.

$$\theta = \frac{\sum_{k=1}^{n} (2\pi\, r_k \Delta r V_k)(C_k - C_i)}{\bar{V}\, \pi r_i^{\,2} (C_o - C_i)}$$

Assuming a parabolic velocity profile, this reduces to the following

$$\theta = \frac{\sum_{k=1}^{n} 4\eta_k\, \Delta\eta\, (1 - \eta_k^2)\, (C_k - C_i)}{(C_o - C_i)} \qquad (4.3)$$

Although most of the computer program was taken from Pattantyus [23], there were some changes made to it. The biggest addition was the calculation of the convective mass transfer coefficient, which was not calculated by Pattantyus. This was calculated from the balance of the

mass flux at the wall,

$$-D_c \alpha \left.\frac{\partial P}{\partial r}\right|_{wall} = h_d \alpha (\hat{P}_{av} - P_s) \qquad (4.4)$$

The above equation is non-dimensionalized in terms of the variables of Eq. (4.1) and P_s was evaluated by taking the average of $P_{n,j+1}$ and $P_{n+1,j+1}$,

$$h_d = \frac{-D_c}{r_i} \left\{ \frac{(P_i - P_{i-1})}{\frac{\Delta r}{r_i}} \frac{1}{\hat{P}_{av} - \left(\frac{P_i + P_{i-1}}{2}\right)} \right\}$$

In terms of the discretized variables h_d is given by

$$h_d = \frac{-\frac{-D_c(P_o - P_i)}{r_i \, \Delta r/r_i}[P1(H) - P1(H-1)]}{\hat{P}_{av}(P_o - P_i) - (P_o - P_i)\frac{[P1(H) + P1(H-1)]}{2}}$$

Reducing and using the substitution, gives

$\hat{P}_{av} = \theta$ and $\Delta r = r_i \Delta\eta$, gives

$$h_d = \frac{2D_c[P1(H-1) - P1(H)]}{r_i \Delta\eta[2\theta - P1(H) - P1(H-1)]} \qquad (4.5)$$

Having found the mass transfer coefficient, the Sherwood number can then be calculated using the following relation

$$Sh_{calc} = \frac{h_d D}{D_c} \tag{4.6}$$

To ensure that the program would give the correct results, it was compared with the Leveque and Graetz solutions [25] for water with no wall resistance ($Sh_w = \infty$). The maximum difference of the Sherwood number value between the calculated results and the Leveque and Graetz solutions was about 5.9 percent at a distance x of 22.3 cm. At a distance of 11.2 cm from the step, the maximum difference was about 3.7 percent. The error increased with increasing x.

For the water results, θ was checked by comparing the results with those obtained by Diller [24] for the case where the wall resistance was equal to 20. The values of θ obtained in the blood program was also checked with the results obtained by Diller.

In the radial direction, the number of divisions (Δr) had to be increased up to one hundred while the length step-size (Δx) had to be decreased to $\Delta x = 0.000005$. This was to ensure that the boundary layer development would not be missed since the fastest changes occur in the initial region. Since this would take up too many steps, a graduated step size was used, such as doubling Δx every certain number of steps. Δx was initially set at 0.000005 with the size doubled every 40 steps.

5. RESULTS

5.1 Introduction

Consistent transfer results were difficult to obtain, particularly with blood. The transfer coefficients for blood were much higher than for saline because of the chemical reaction between the oxygen and hemoglobin. The results of several whole blood and saline experiments were rejected and were not included because of two reasons:

1. The data obtained during the experiments were not repeatable. Repeatability was checked within a run by remeasuring the surface oxygen partial pressures as the electrode was moved back toward the step. If the measured values at a sample of five locations were not within ten percent of the initial values measured, the run was rejected.
2. The blood was too hemolyzed. This was most easily observed by a high methemoglobin reading. If the methemoglobin value obtained was greater than ten percent of the total hemoglobin the test was not used.

5.2 Water Results

Figure 9 shows the measured reattachment point plotted versus the Reynolds number. The parameters x_r and s are defined in Fig. 1. The present experimental data set matches the measurements of Back et al. [7] over the range of Reynolds number investigated. The reattachment point was estimated to be between x/D values of 2 and 5 for the transfer

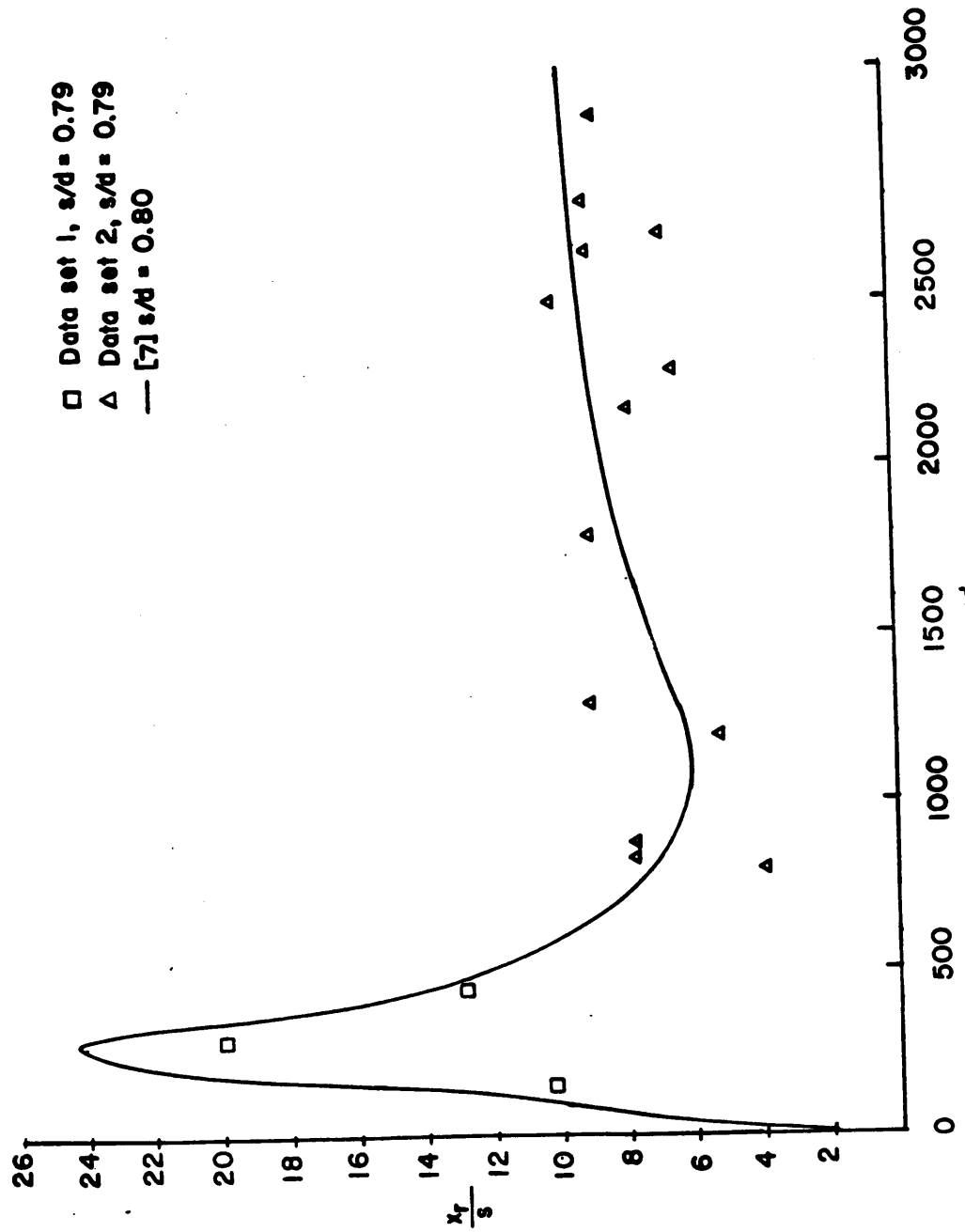

Fig. 9. Reattachment point vs. Reynolds number

measurements considered.

The measured transfer coefficients inside the tube are shown in Figs. 10, 11, and 12 for three Reynolds numbers (160, 450, 850) as a function of distance from the tube expansion, x/D, where D is the diameter of the larger tube. The error bars represent the results of an external error analysis (Appendix C). Some of the values for the higher Reynolds number were too large to be measured with the tube resistance used. As seen from Eq. 3.1, as the value of P_s approaches P_i, the value of h_d goes to infinity. For this range the values of the measured oxygen partial pressure at the surface, P_s, were very close to the oxygen partial pressure in the bulk of the fluid, P_i. The estimated error for these data points is larger than the measurement. These data points, which were also off the graphs, were discarded.

Calculated results of the Sherwood numbers were obtained by considering transfer at the beginning of a tube without a step. Transfer began at the position of the step. The velocity profile used was fully-developed parabolic. These calculated results were then used for comparison with the experimental results and are represented by the solid lines in the figures.

Measurements by Sparrow et al. [15] in a two-dimensional channel are also shown in Fig. 12. The ratio of the step height to the upstream channel height was 0.5. Their upstream flow was not fully developed, however, and the value of the Schmidt number was 2.5, compared to a value of 245 for the present results. Their results were compared by scaling the ratio of the Schmidt numbers to the 1/3 power and non-

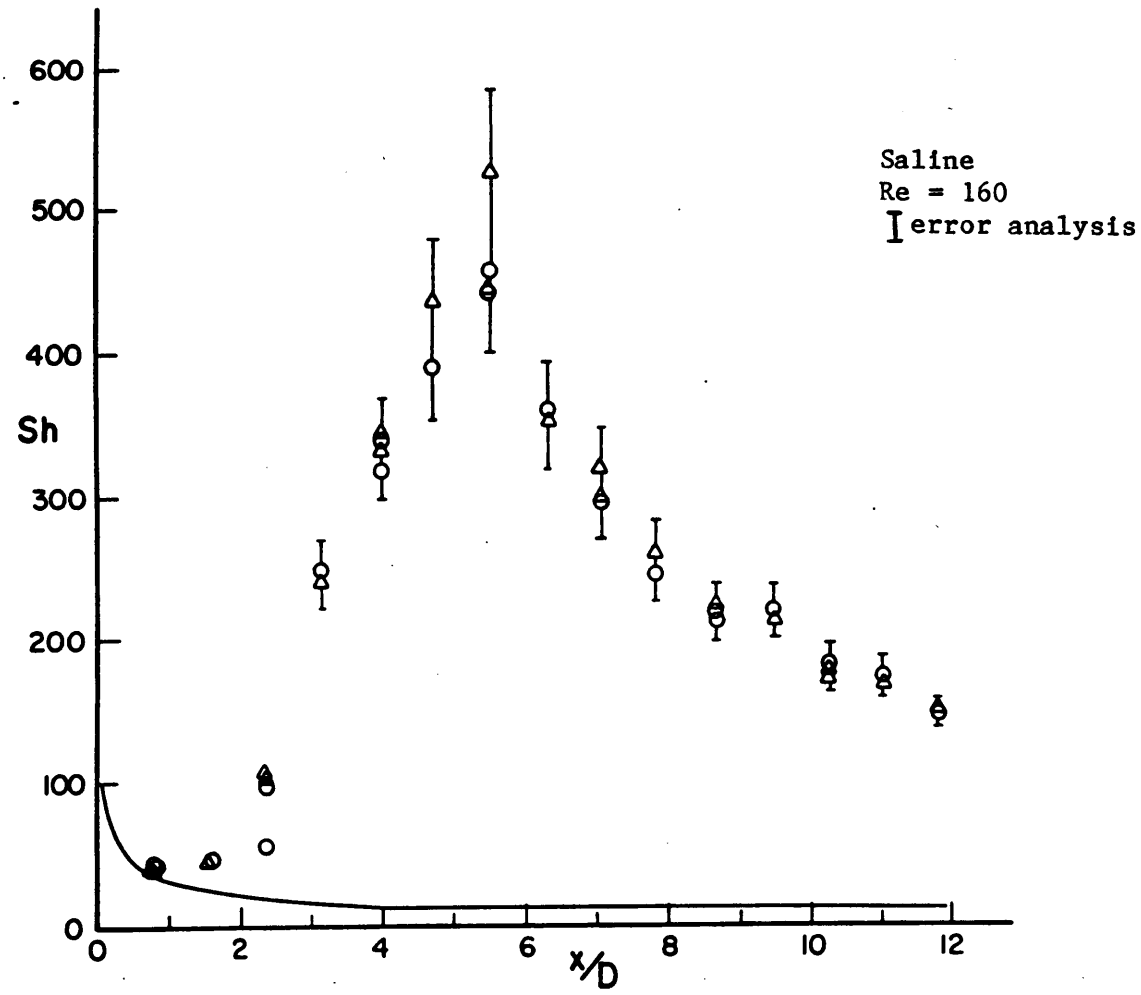

Fig. 10. Experimental Sherwood number obtained for saline due to external error analysis at Re = 160

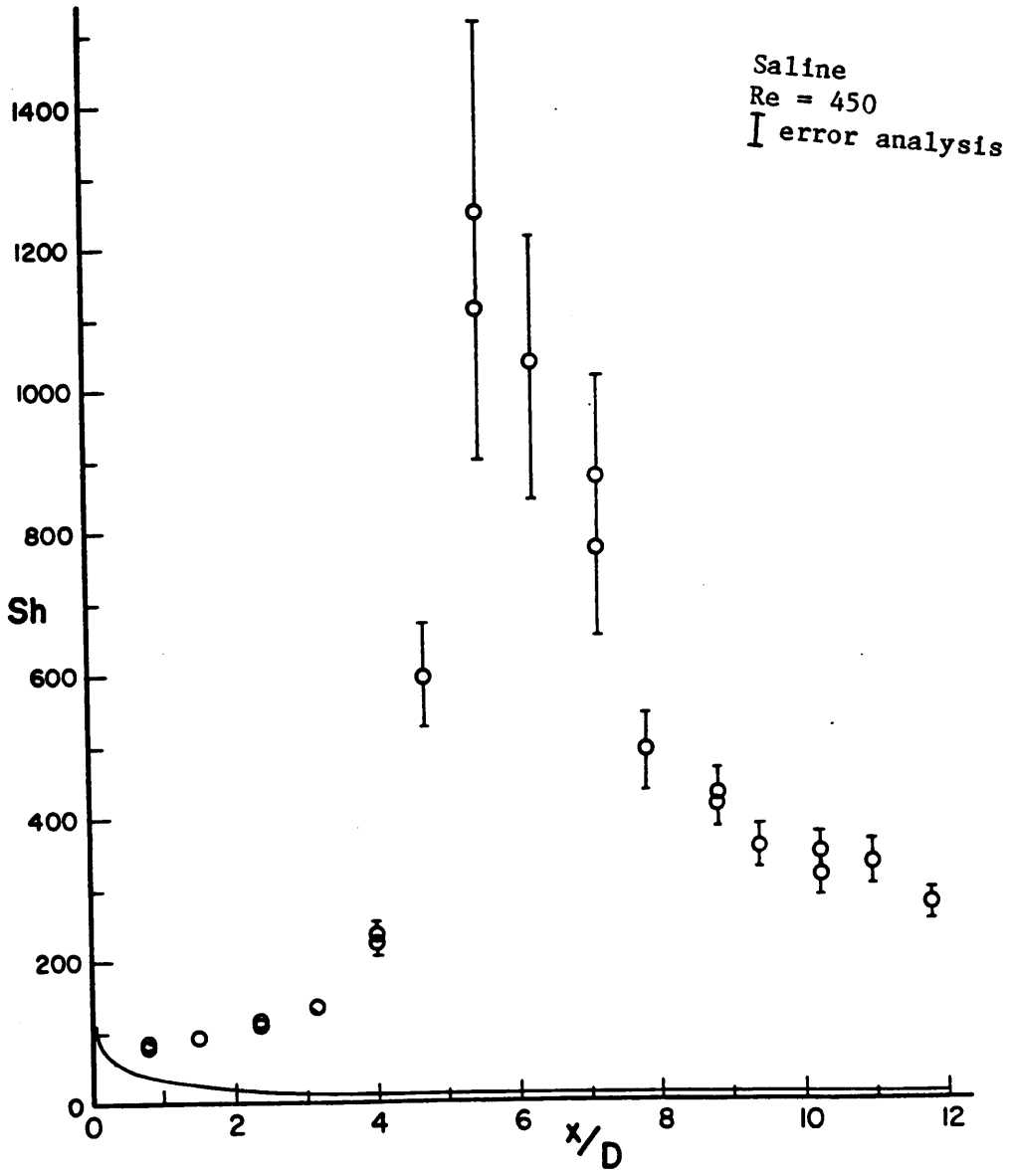

Fig. 11. Experimental Sherwood number obtained for saline due to external error analysis at Re = 450

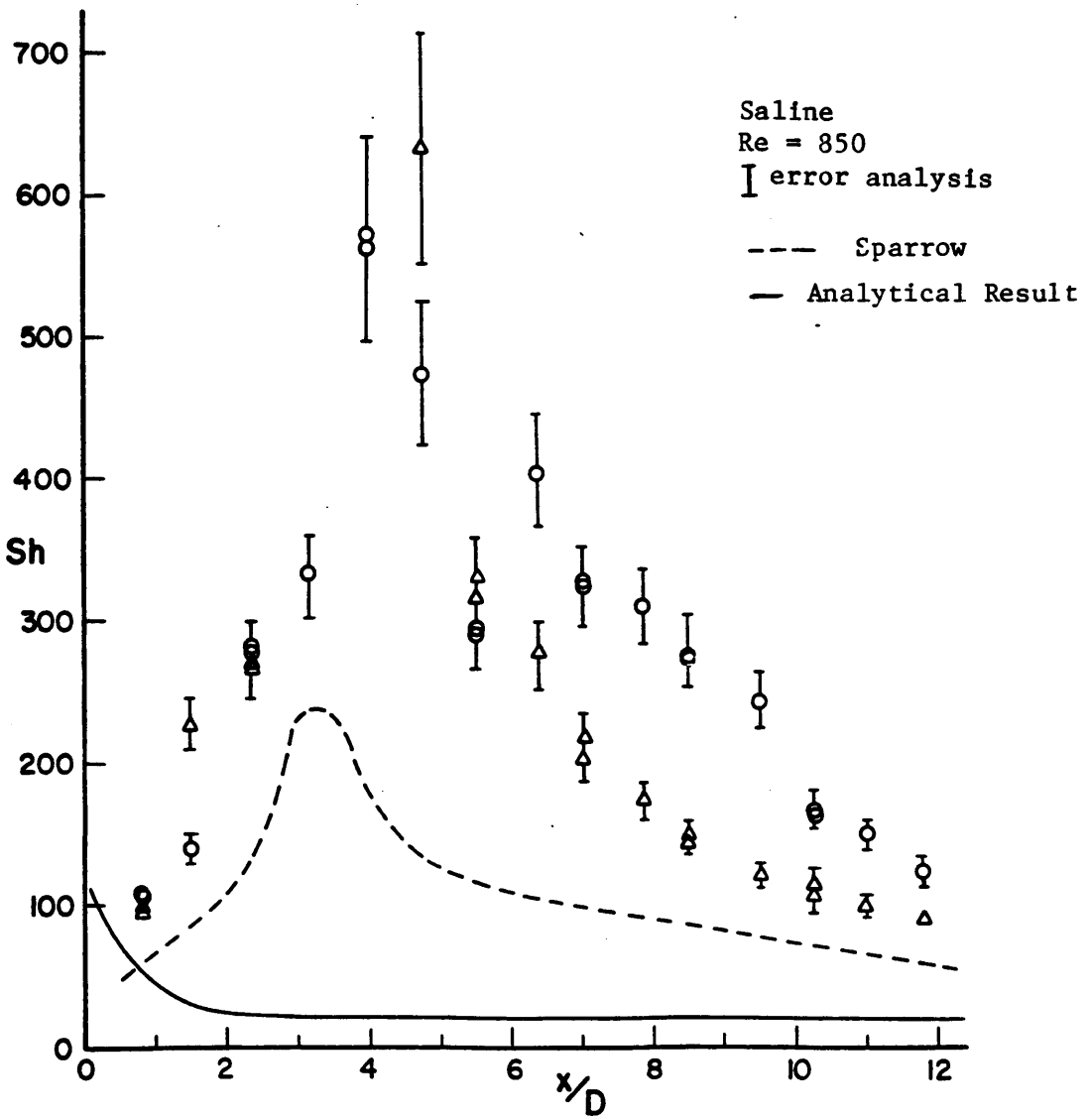

Fig. 12. Experimental Sherwood number obtained for saline due to external error analysis at Re = 850

dimensionalizing x with the channel height, H. The Reynolds number and Sherwood number uses the hydraulic diameter, 2H. These were the only results found at a comparable Reynolds number.

During the measurement of PO_2 by the oxygen electrode, an unexpected result was found. During the experiments with the two higher Reynolds number of 450 and 850, cyclic fluctuations were discovered in the PO_2 level. The maximum amplitude of these fluctuations was found to occur in the recirculating flow region rather than the redeveloping flow area. The fluctuations seem to indicate some type of unsteady flow within the recirculating flow region itself. This result is consistent with the results that Glass [26] found. The maximum amplitude of the fluctuations is represented by the bars in Figs. 13, 14, and 15. Figure 16 shows an actual time record of P_s for saline at x = 1 cm and Re = 850. The corresponding plot of the measured P_s values with bars representing the maximum fluctuations is shown in Fig. 17 for saline with Re = 850. The period is three minutes and the P_s oscillation is 200 mm Hg. The time period of the fluctuations is presented in dimensionless form as fd/u vs. x/d in Fig. 18. The dashed lines show the boundary of the time period of velocity fluctuations measured by Ahmed et al. [12].

A comparison between the experimental and calculated Sherwood numbers is shown in Figs. 19, 20, and 21. The results show that the transfer around the reattachment point is about ten times higher than the analytical values for no step. Plots of this type eliminate from the analysis the effect of the Reynolds number on the transfer for

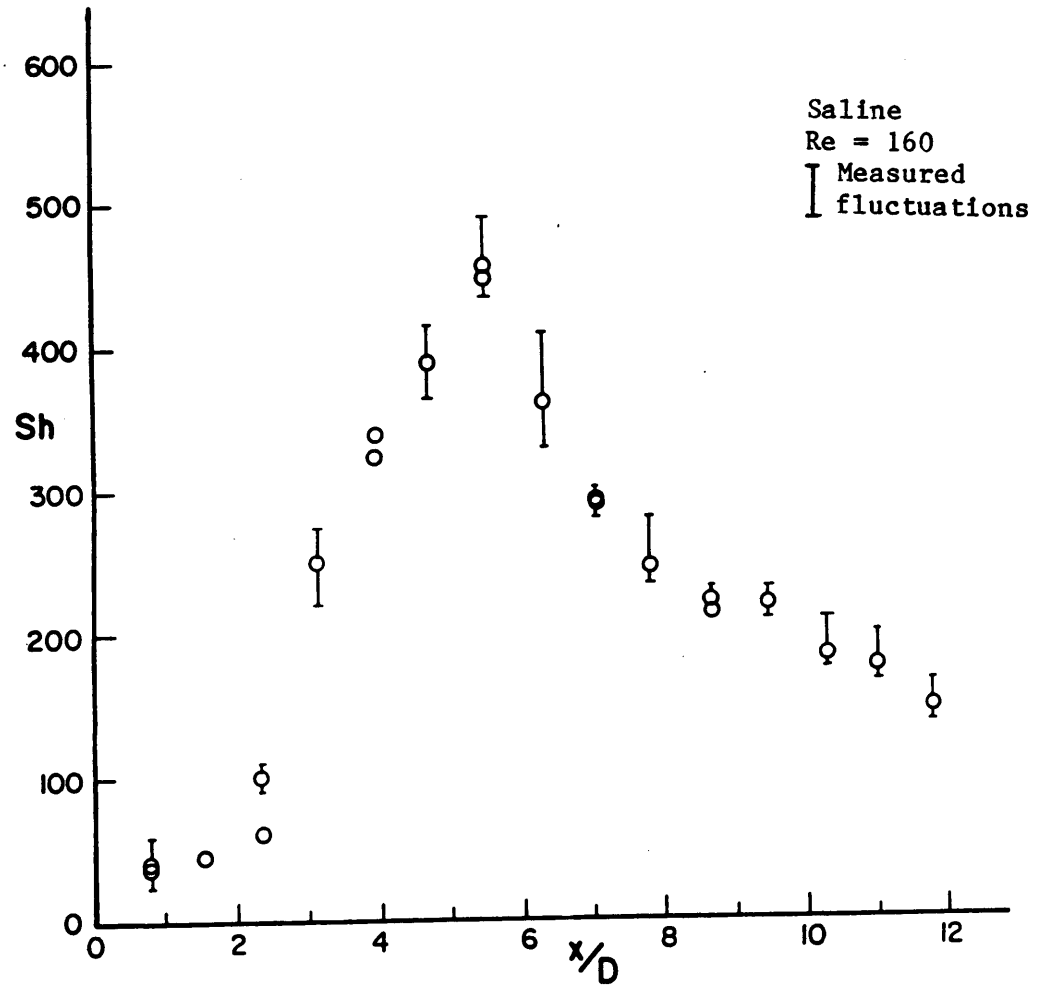

Fig. 13. Variations of experimental Sherwood number obtained for saline at Re = 160

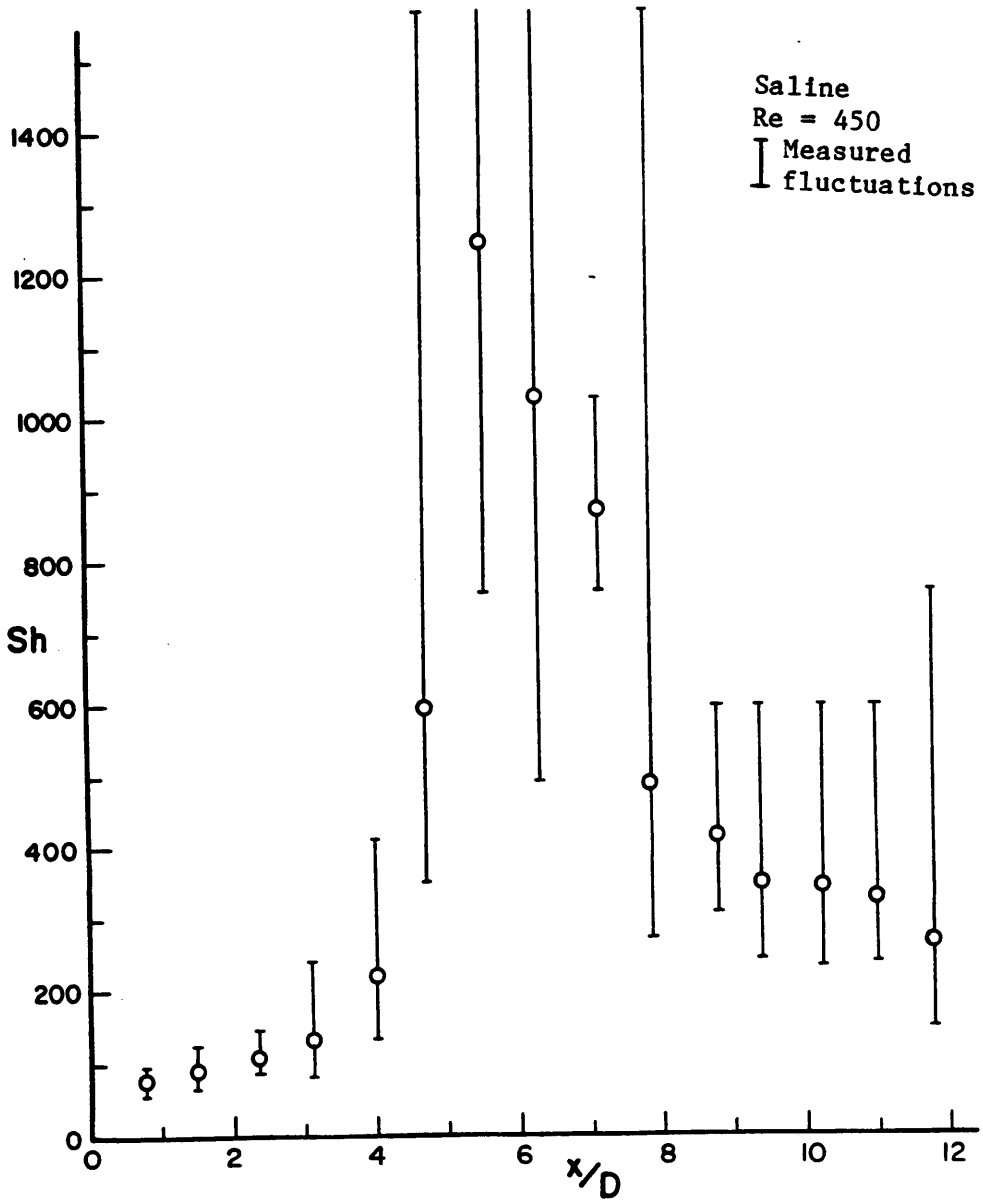

Fig. 14. Variations of experimental Sherwood number obtained for saline at Re = 450

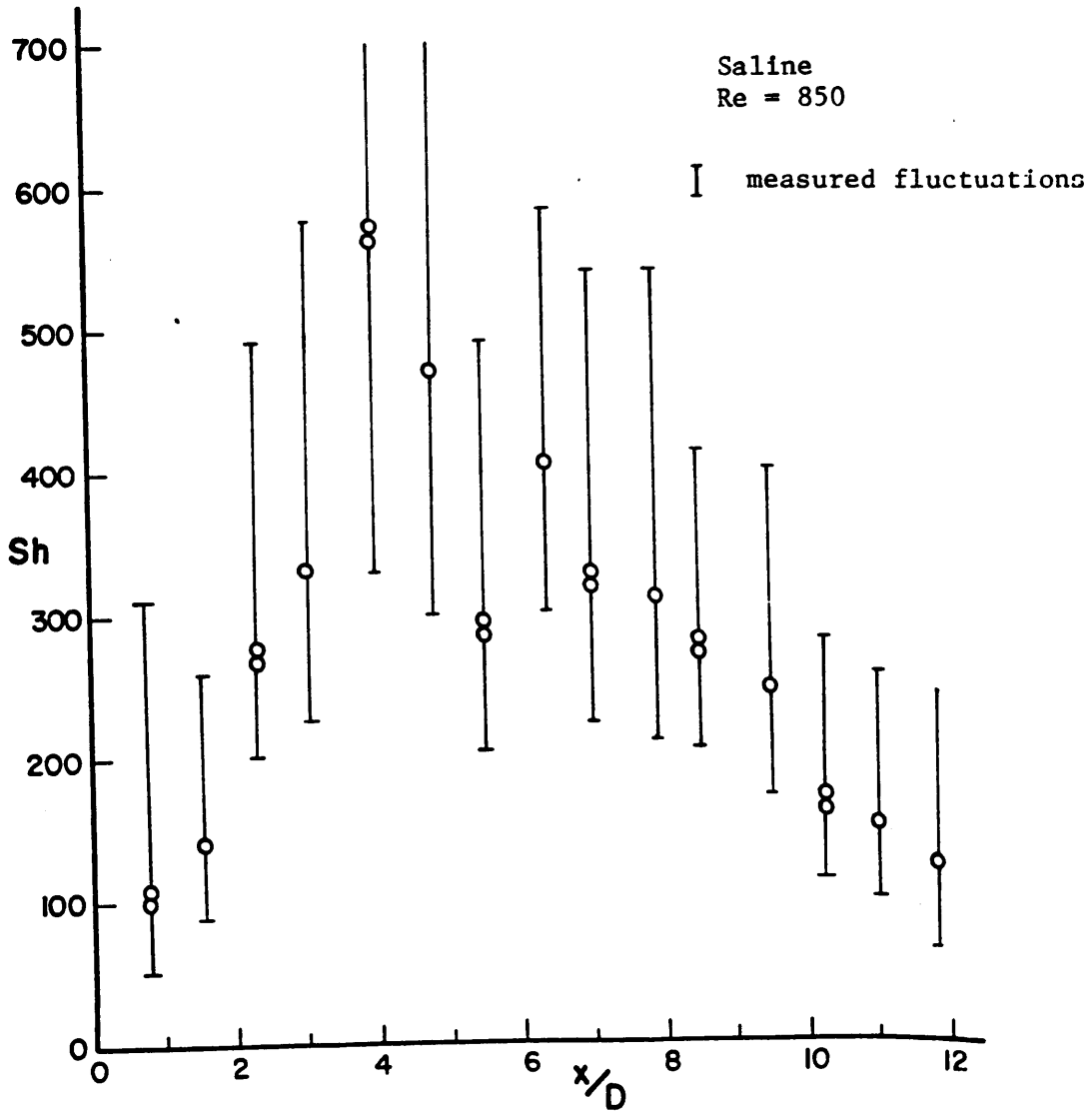

Fig. 15. Variations of experimental Sherwood number obtained for saline at Re = 850

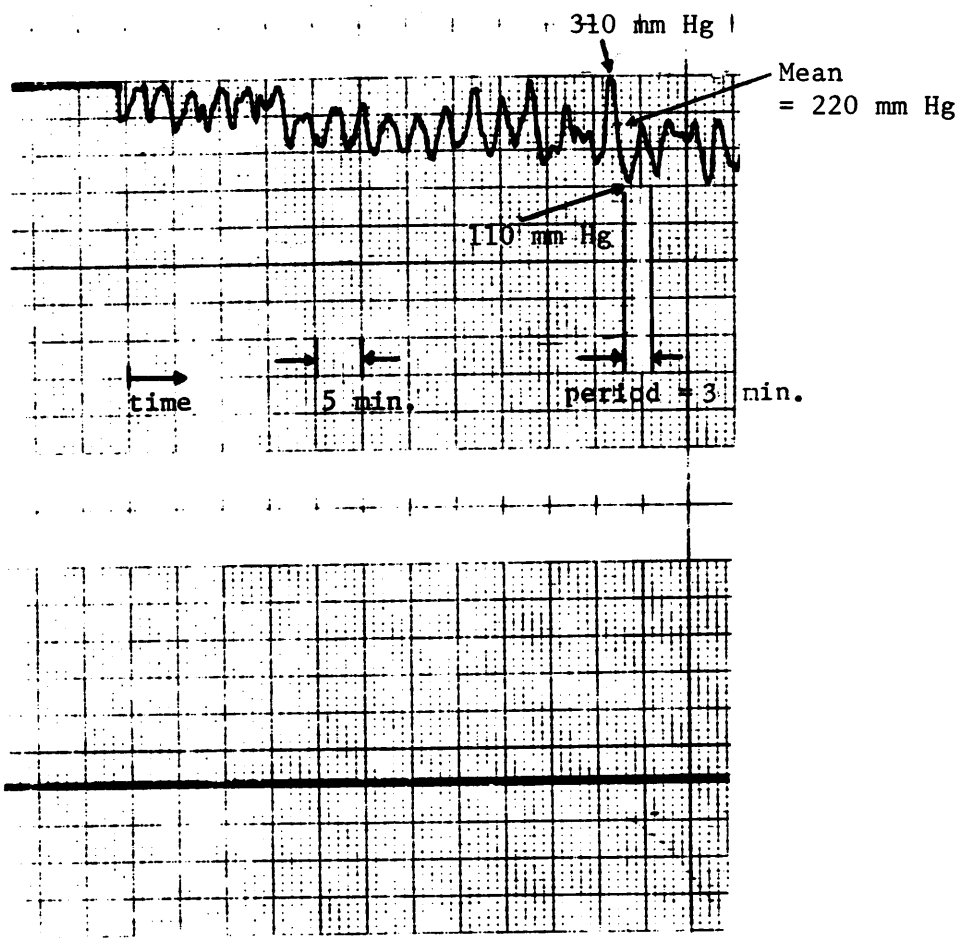

Fig. 16. Fluctuations of measured oxygen partial pressure recorded in a strip-chart recorder

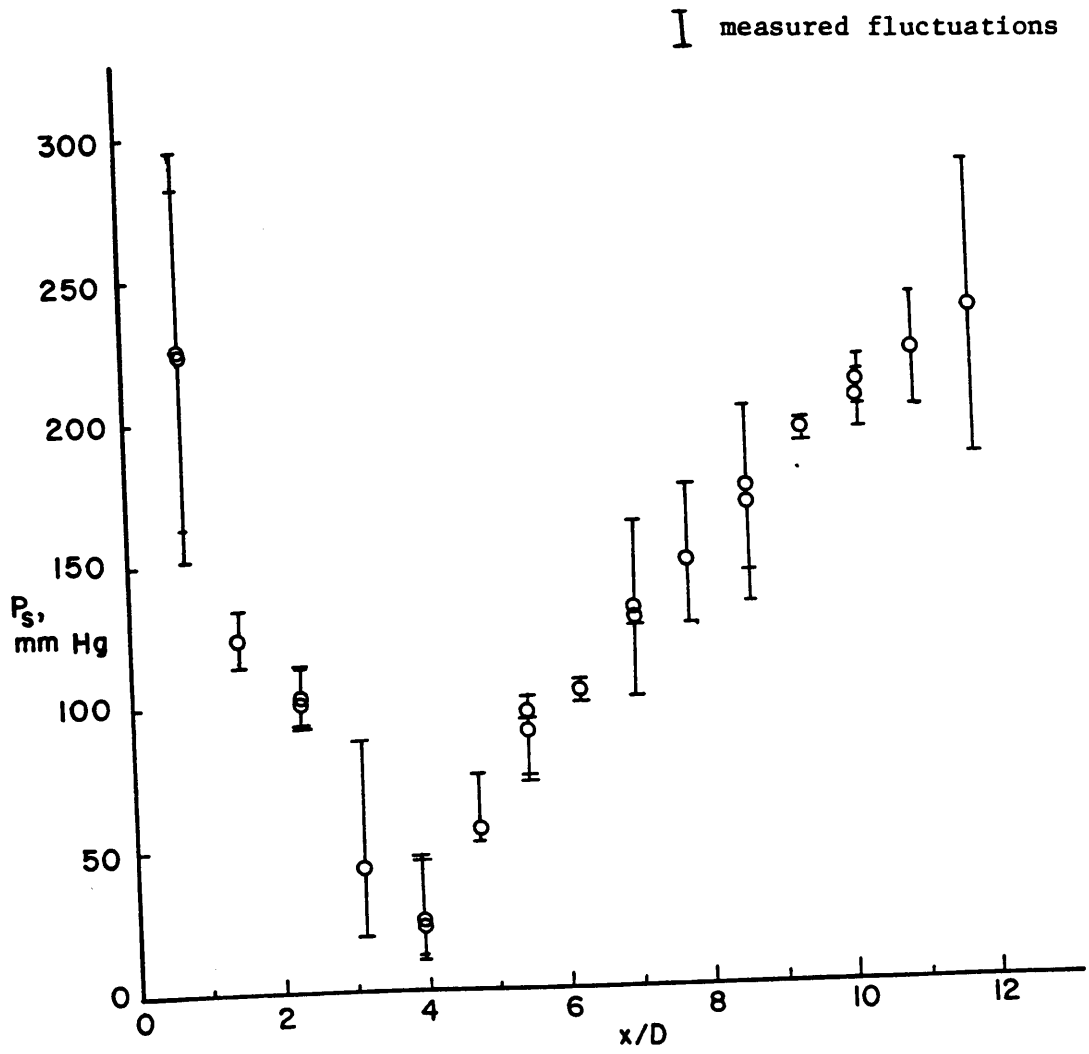

Fig. 17. Fluctuations of measured oxygen partial pressure for saline at Re = 850

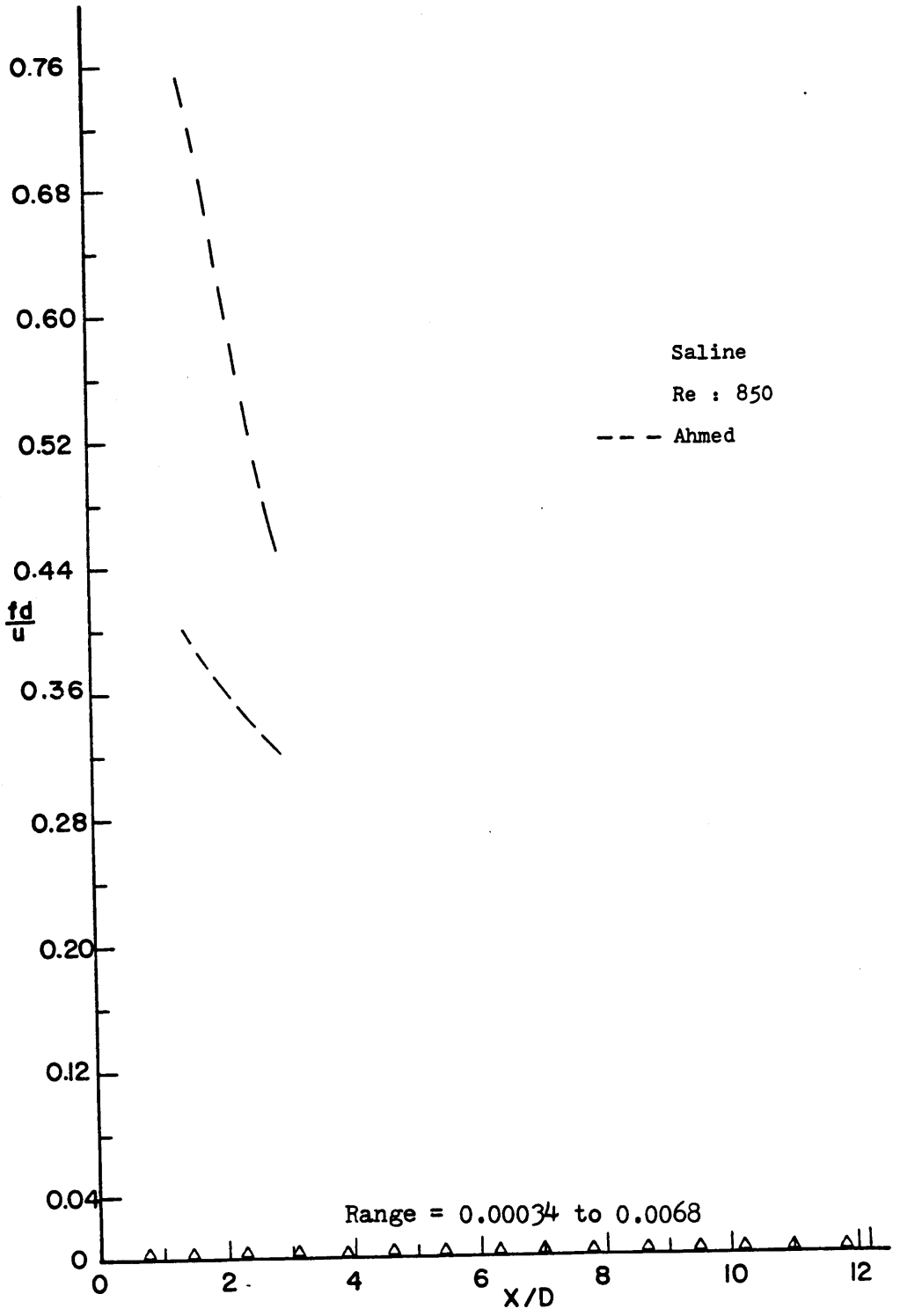

Fig. 18. Frequency of fluctuations vs. dimensionless axial distance

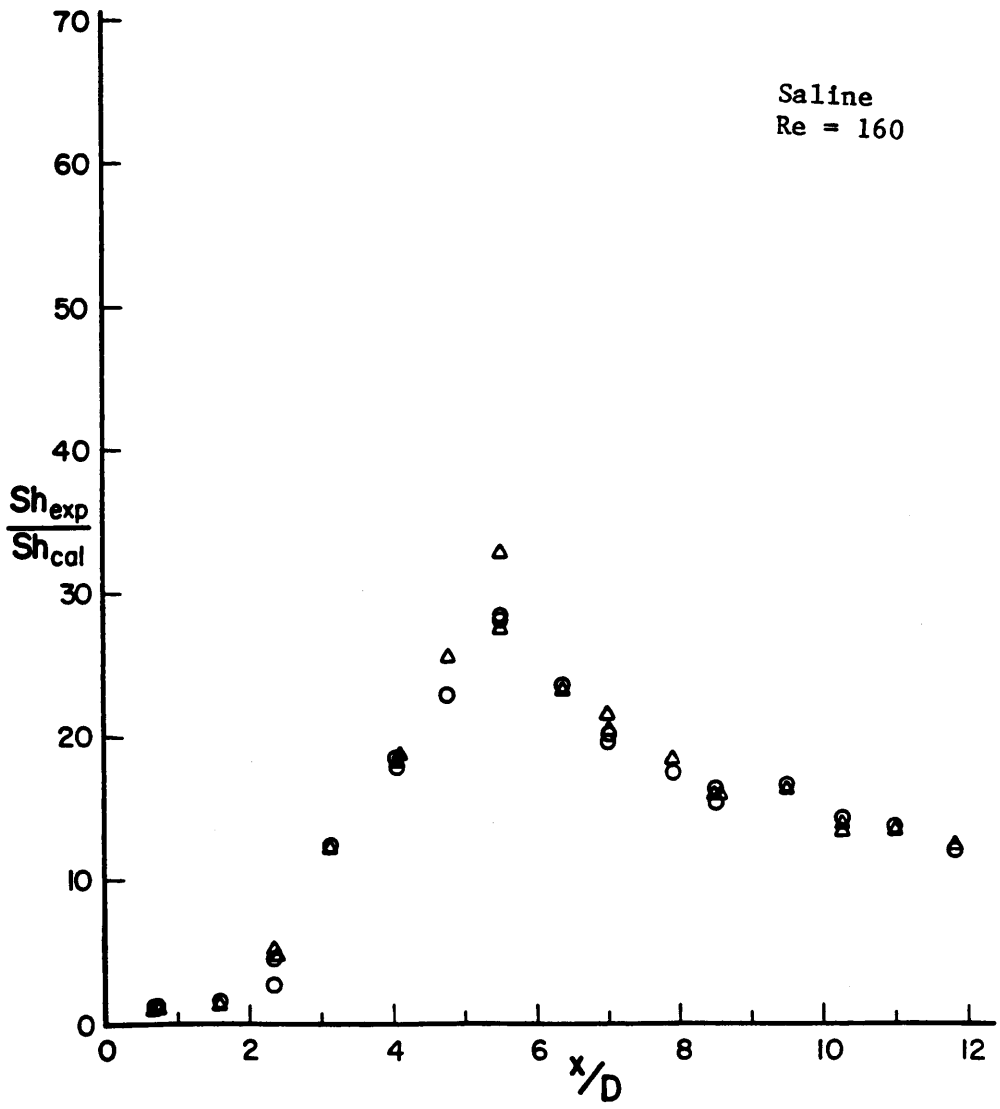

Fig. 19. Comparison of experimental transfer results and calculated transfer results for saline at Re = 160

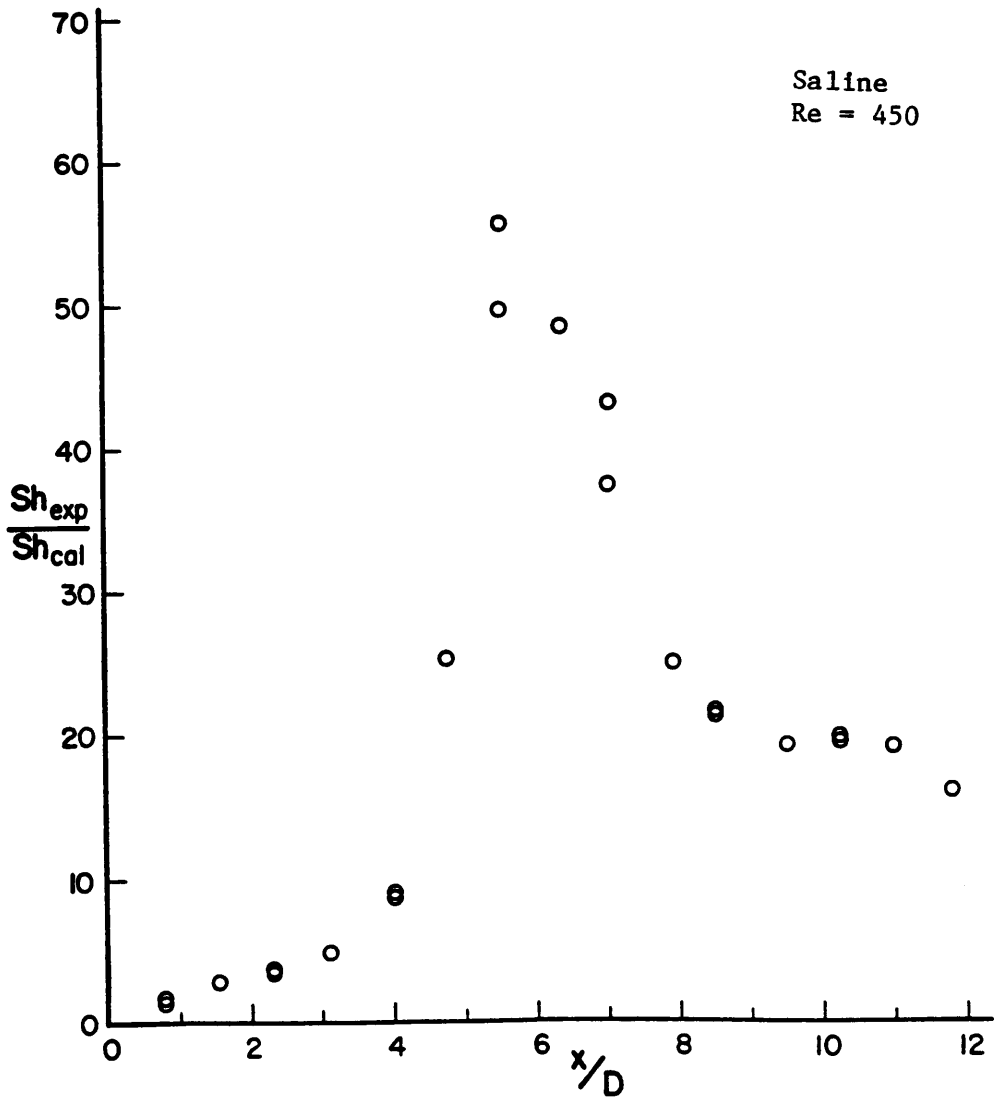

Fig. 20. Comparison of experimental transfer results and calculated transfer results for saline at Re = 450

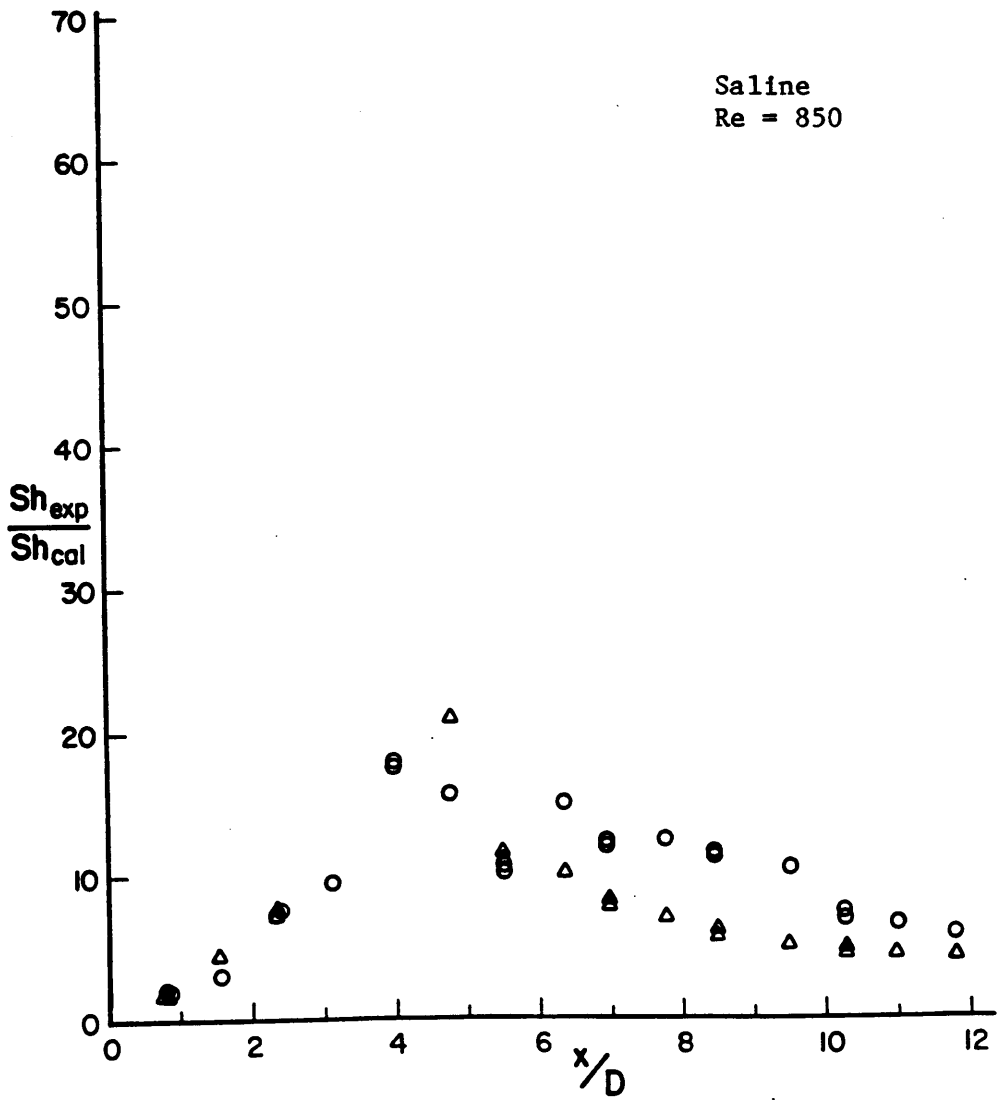

Fig. 21. Comparison of experimental transfer results and calculated transfer results for saline at Re = 850

laminar flow, which allows a more direct comparison for different Reynolds number results.

5.3 Whole Blood Results

The whole blood results for Reynolds number equal to 160 and 450 are presented with the error estimates in the form of Sherwood number versus dimensionless length in Fig. 22 and 23, respectively. Results for a Reynolds number of 850 could not be obtained because of the large amount of hemolysis due to the high flow rates needed to achieve this Reynolds number. The values of the Sherwood number where x/D is between 4 and 5.5 for the Re = 450 case were too large to be measured. For this range the values of the measured oxygen partial pressure at the surface, P_s, were very close (within the measurement accuracy) to the inlet oxygen partial pressure, P_i.

The experimental transfer coefficients for the two Reynolds numbers 160 and 450 with diffusion coefficient equal to 1.5×10^{-5} cm^2/s were compared with the calculated transfer coefficients (computed by the blood program) in Figs. 24 and 25. The diffusion coefficient used is the standard value for whole blood [27]. Except for the first few values, the experimental transfer coefficients were at least nine times higher than the calculated transfer coefficients. To account for possible shear-induced augmentation, a comparison of the experimental Sherwood number to the calculated Sherwood number with diffusivities (2.0×10^{-5} cm^2/s and 3.0×10^{-5} cm^2/s) at Re = 160 and Re = 450 are presented in Fig. 26 and Fig. 27. The higher diffusion coefficients

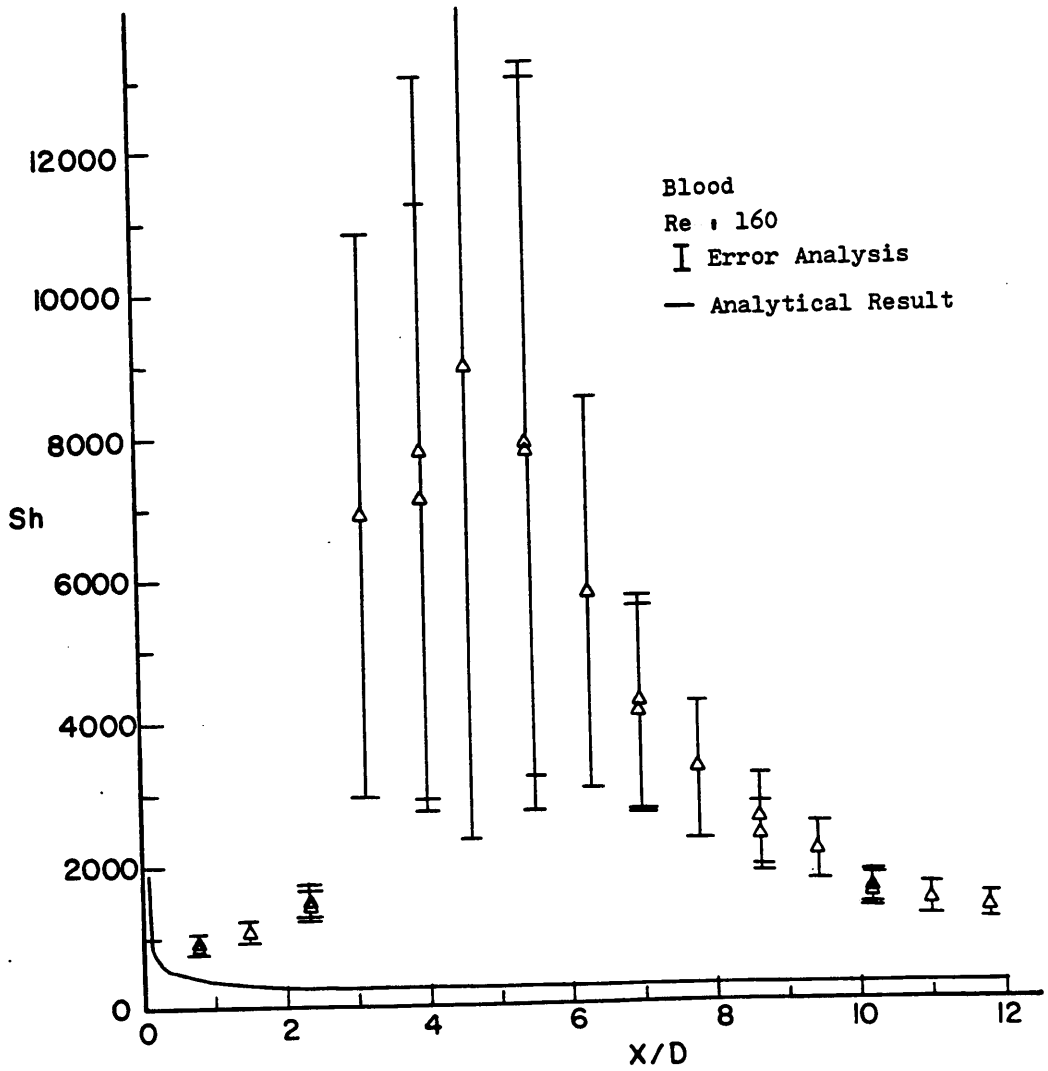

Fig. 22. Experimental Sherwood number obtained for blood calculated from external error analysis at Re = 160

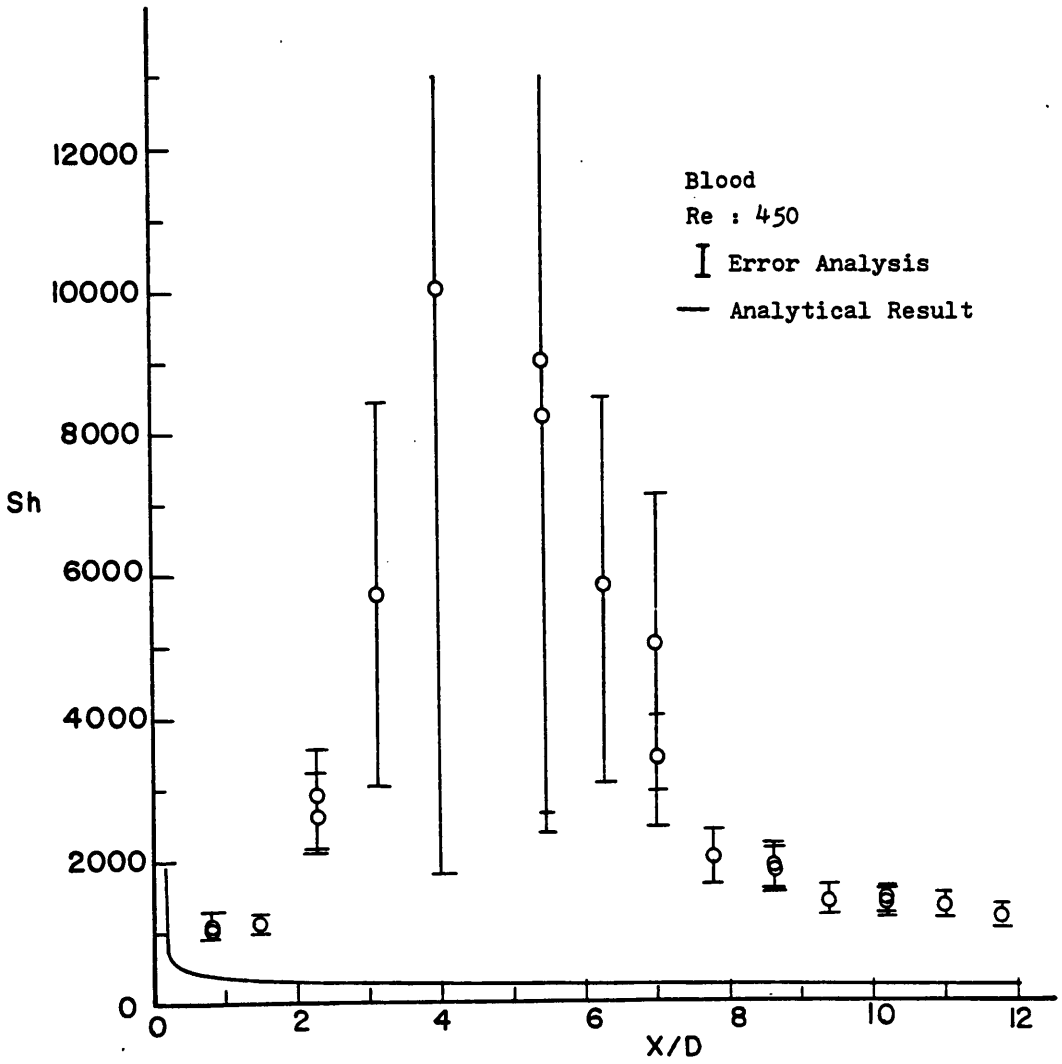

Fig. 23. Experimental Sherwood number obtained for blood calculated from external error analysis at Re = 450

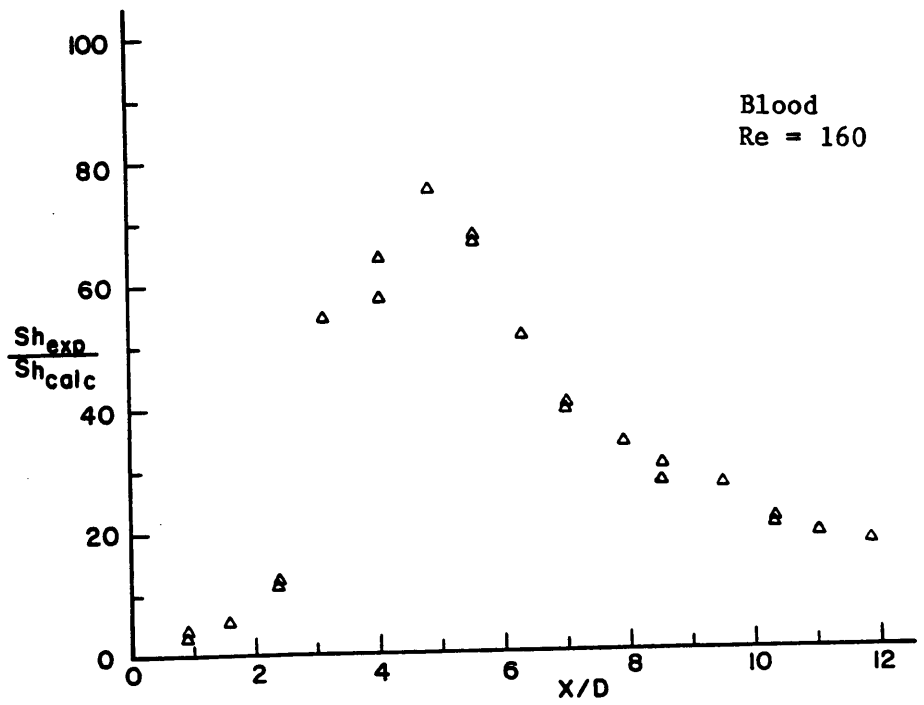

Fig. 24. Comparison of experimental transfer results and calculated transfer results for whole blood with $D_c = 1.5 \times 10^{-5}$ cm^2/s, at Re = 160

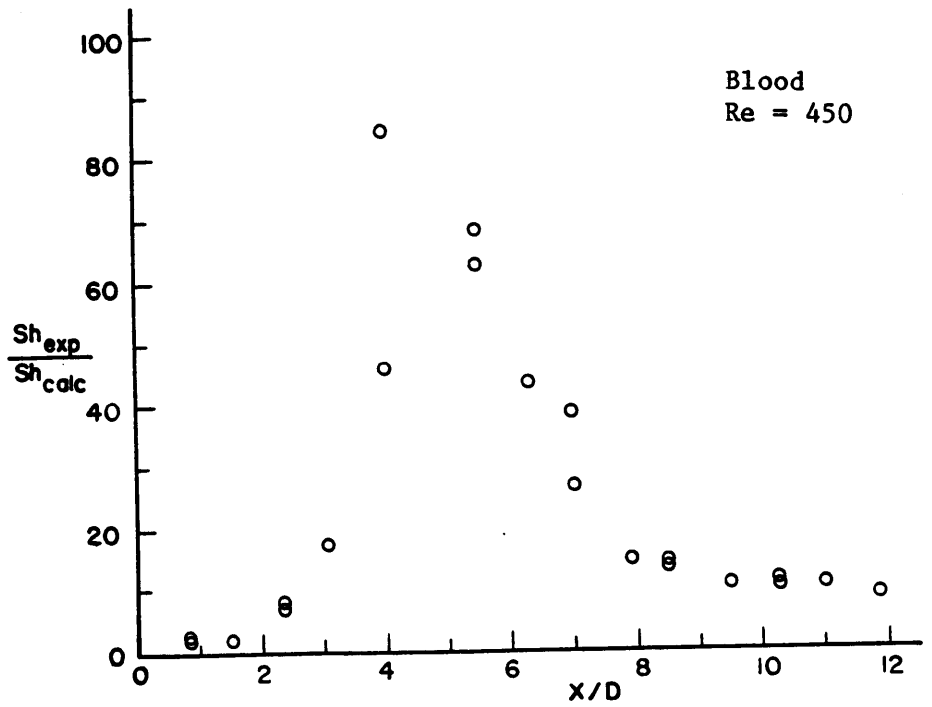

Fig. 25. Comparison of experimental transfer results and calculated transfer results for whole blood with $D_c = 1.5 \times 10^{-5}$ cm^2/s, at Re = 450

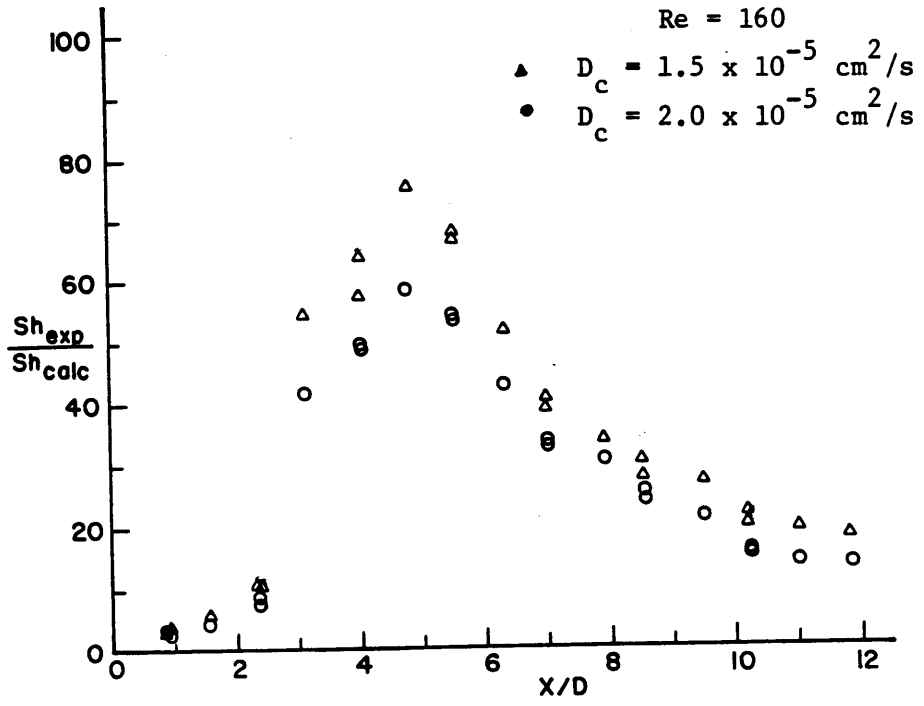

Fig. 26. Comparison of experimental transfer results and calculated transfer results for whole blood with D_c = 1.5 x 10^{-5} cm^2/s and D_c = 2.0 x 10^{-5} cm^2/s, at Re = 160

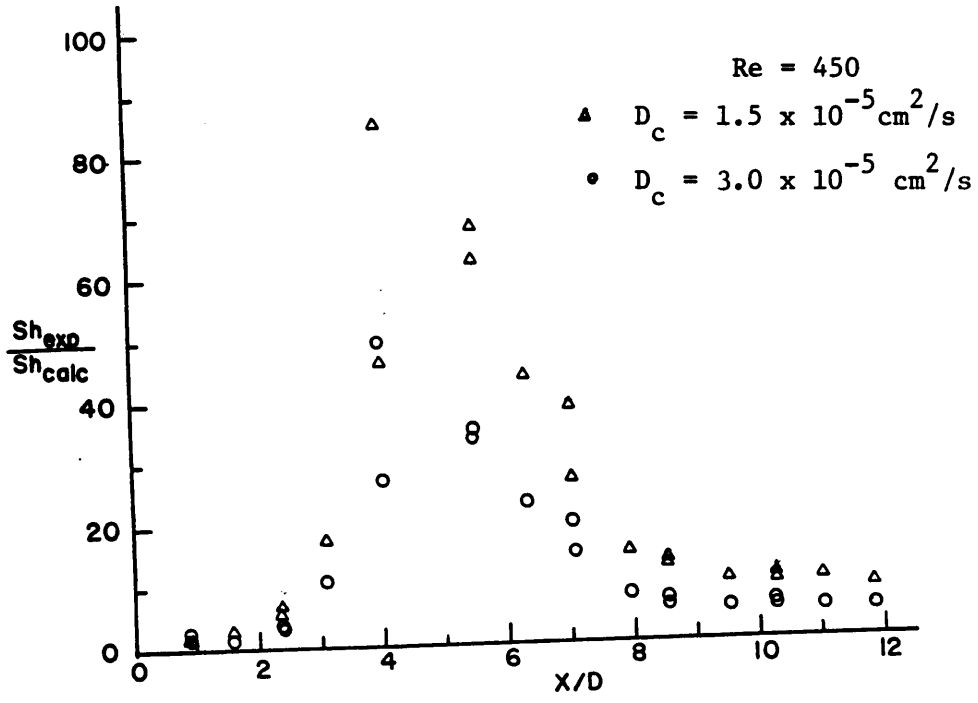

Fig. 27. Comparison of experimental transfer results and calculated transfer results for whole blood with $D_c = 3.0 \times 10^{-5}$ cm^2/s, at Re = 450

listed above, (2.0×10^{-5} cm^2/s, and 3.0×10^{-5} cm^2/s) were based on the augmentation of oxygen transfer due to shear-induced red-cell motion [44].

Figure 28 and 29 shows the range of the Sherwood numbers obtained from the measurements of the cyclic oscillation of oxygen partial pressure during the blood experiments. The region around the reattachment point constituted the maximum range of the Sherwood number oscillations.

In Fig. 30, the position of the peak transfer is compared to the reattachment point taken from Back's results (Fig. 8) for saline and blood solutions. The ratio of these two lengths from the step is plotted as a function of Reynolds number.

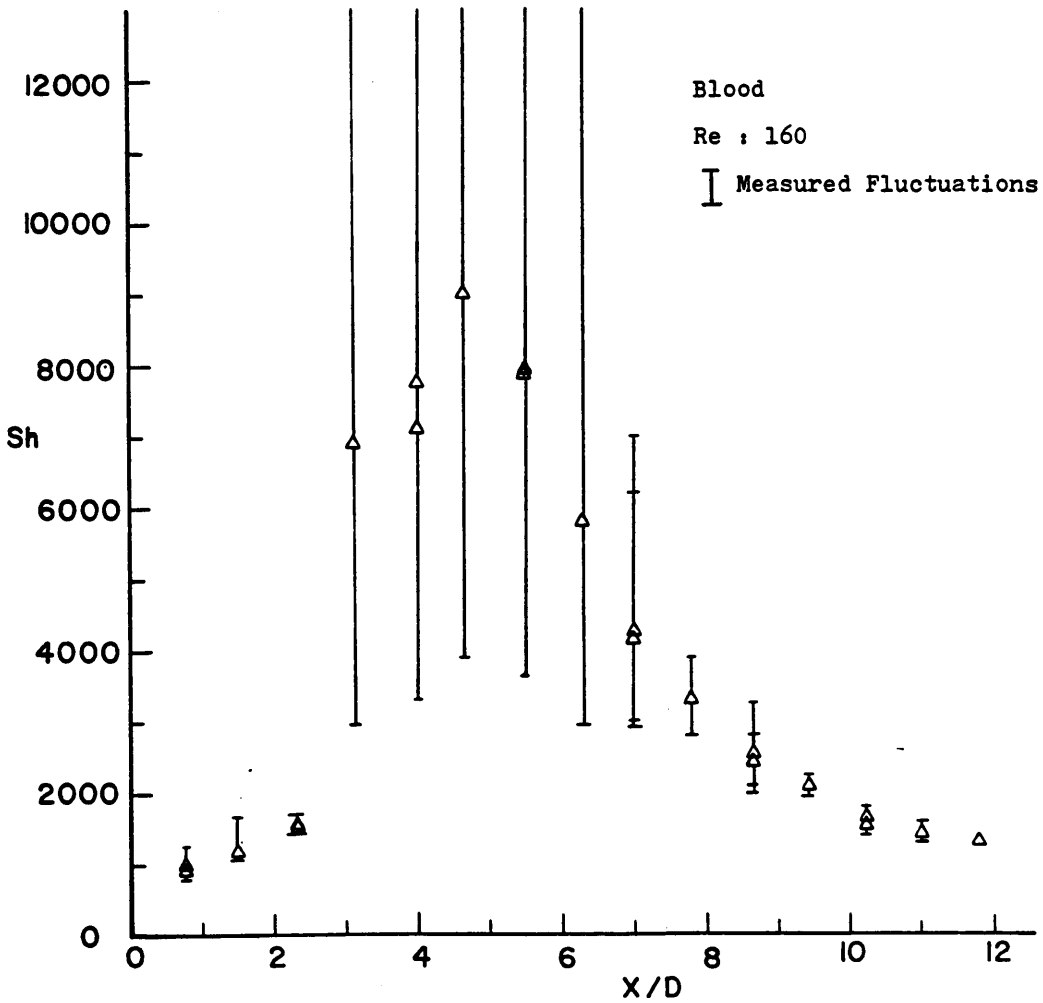

Fig. 28. Variations of experimental Sherwood number obtained for whole blood at Re = 160

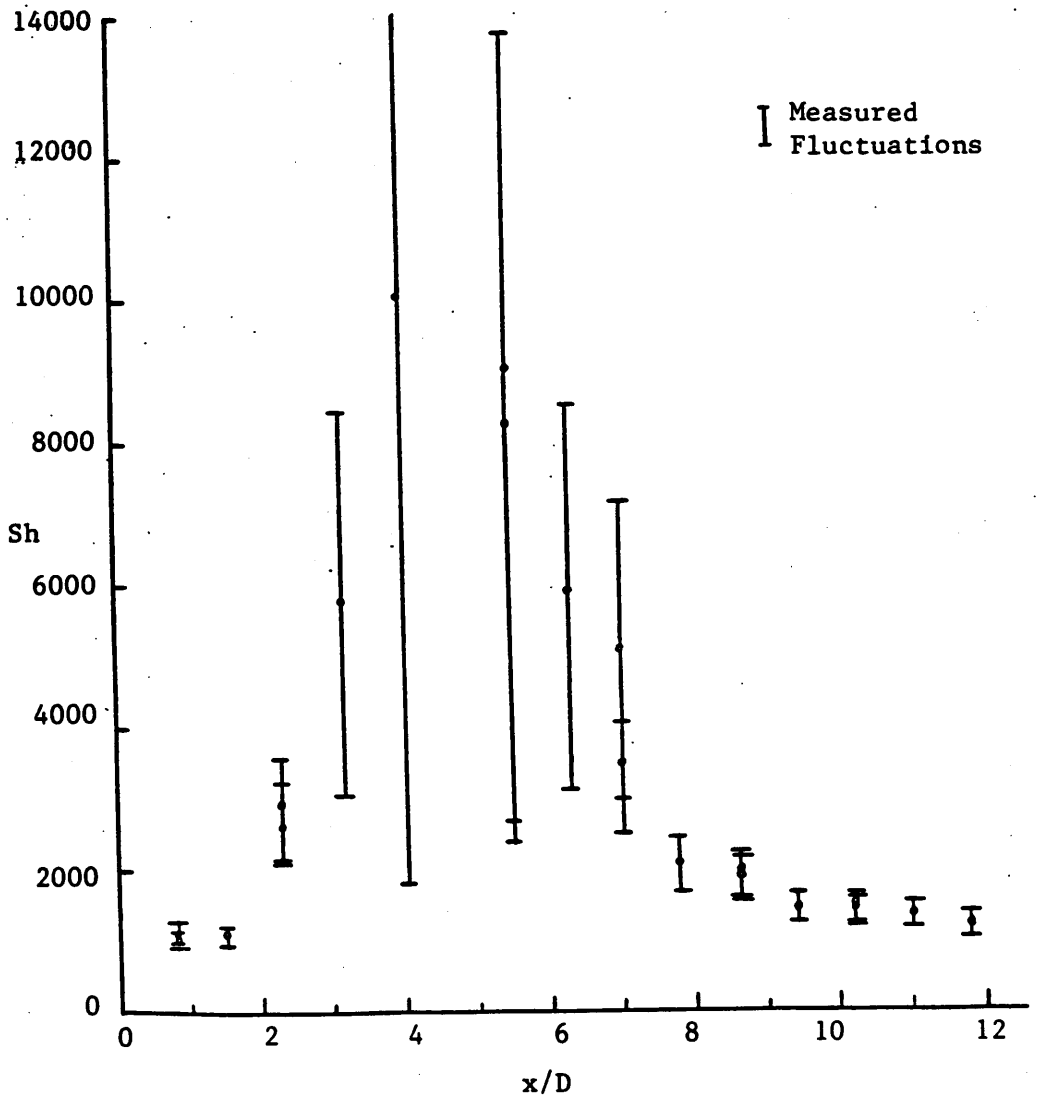

Fig. 29. Variations of experimental Sherwood number obtained for whole blood at Re = 450

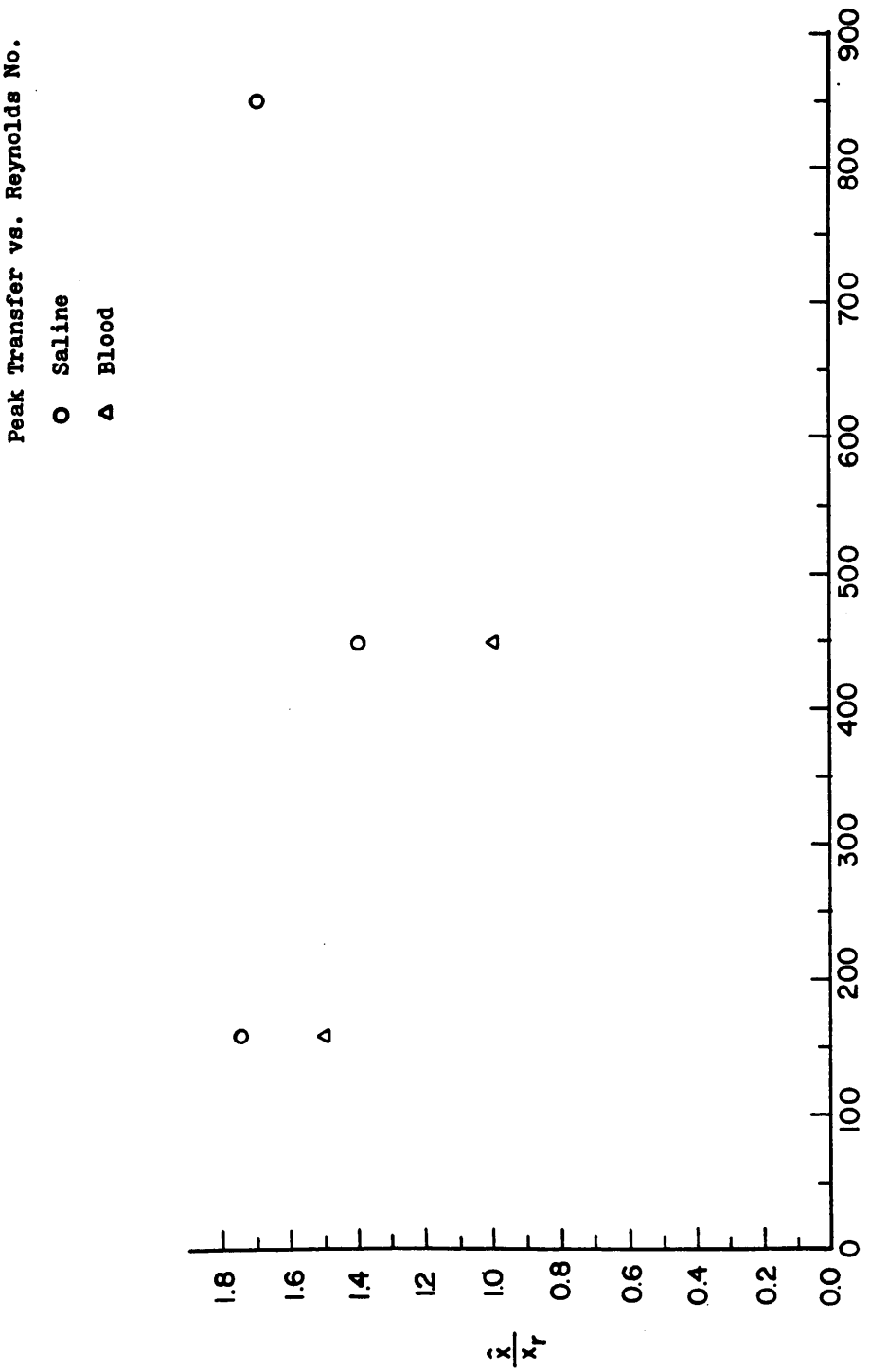

Fig. 30. Peak transfer vs. Reynolds number

6. DISCUSSION

To ensure that the flow was fully developed, a 49.3 cm non-transfer length was provided upstream of the step. This gave at least 100 upstream tube diameters for the velocity profile to develop. All of the experiments were conducted at low Reynolds numbers (< 1000) to ensure that the upstream flow was laminar.

The flow visualization technique used to locate the reattachment point at various Reynolds numbers was only conducted using saline solution and not whole blood because of better visibility. No effort was made to precisely inject the bubble or dye so the radial location when it reached the step probably varied. Although the reattachment point was only estimated by real-time observation, the reattachment points located matched well with those of Back et al. [7], as shown in Fig. 9. The values of s/d and d/D were almost identical to those used by Back et al. [7].

The experimental results of Feuerstein et al. [5] gave much larger reattachment lengths, however. Back et al. [28] suggest that the reason for the much larger reattachment lengths reported by Feuerstein et al. was due to the difference in upstream velocity profiles. The experiments of Back et al. had a nearly-flat profile while that in Feuerstein's case was a parabolic profile. Because the present results had a parabolic profile but matched well with the results of Back et al., they do not support this explanation.

The experimental transfer results for saline and whole blood (Figs. 10, 11, 12, 22 23) show that the Sherwood numbers are lowest inside the

recirculating region and highest beyond the reattachment point (redeveloping region). However, the experimental transfer results are at least ten times higher than the calculated transfer results for most of the recirculation region studied, as shown in Figs. 19, 20, 21, 24 and 25. The presence of the step, therefore, increases transfer for most of the downstream region. Although this result is somewhat surprising, it is consistent with the analytical results of Schneiderman et al. [21] for separated flow in blood (Re < 200). Their transfer results showed a large increase over most of the region downstream of a model stenosis with only a small decrease right after separation.

The inlet partial pressure, P_i was used to calculate the experimental mass transfer coefficient, h_d, as seen in Eq. (3.2). In the analytical solution, however, h_d was calculated using P_{av}. Although P_{av} should have been used instead of P_i when calculating the experimental h_d, P_{av} was not used because the experimental velocity and concentration profiles were not known. Moreover, the experimental vaues of $(P_i - P_s)$ and the analytical value of $(P_{av} - P_s)$ calculated by the computer program (Appendix A or Appendix B) only differed by at most 7 percent.

In the redeveloping region some of the PO_2 values measured at the wall (P_s) were very close to the PO_2 at the step inlet (P_i) and hence the mass transfer coefficient, h_d, and the Sherwood number, Sh, values could not be calculated. The external error analysis further showed that the error is larger than the measurement when the PO_2 at the wall is very close to the PO_2 in the free stream. The longer bars as seen in

Figs. 10, 11 12, 22 and 23 depict the large errors in this region. A thinner-walled membrane tube (lower transfer resistances) would be needed to accurately measure the transfer in these regions.

Two graphs (Figs. 26 and 27) were also plotted to show the effect of shear-induced red blood cell motion on the ratio of the experimental to calculated Sherwood numbers. The augmented diffusivities were based on the upstream shear rate at the tube wall and were taken from the correlations presented by Diller and Mikic [27]. This gave values of 2.0×10^{-5} cm^2/s and 3.0×10^{-5} cm^2/s for the Re = 160 and Re = 450 cases, respectively. The higher diffusivity in the calculation gives a large Sh_{calc}, which correspondingly lowers all of the points. Comparison between the two figures shows a better correlation when using the lower diffusivity of 1.5×10^{-5} cm^2/s. The augmented diffusivities do not give a significant improvement in the match (at the same of value of Re) between the blood results (Figs. 16 and 27) and the saline results (Figs. 19 and 20) either. Therefore, there is no evidence for shear-induced augmentation in these experimental results.

The calculation of the time constant (Appendix D) gives an estimate of the rate that a change in transfer rate equilibrates through the tube membrane. This is helpful to establish an approximate time for the microsensor readings to reach a steady-state and for interpreting the unsteady or transient phenomena observed. The time constant for the P_s response of the system has an estimated value of about 15 minutes. For the system to reach 95 percent of response should, therefore , take about three time constants or about 45 minutes. The experimental

response (Fig. 35) was about 30 minutes, slightly faster than predicted.

Cyclic fluctuations of the measured P_s were observed during the transfer experiments as shown in Fig. 16. At the higher Reynolds numbers (450 and 850), the fluctuations were more pronounced. In addition, the fluctuations appeared to be more intense in the recirculating region than the redeveloping region. Because of the limitation on the time response of the system (Appendix D), oscillations with a period of much less than one minute were difficult to measure. From Fig. 35 the system response to a step input after 2 minutes is about 30 percent. This indicates that significant damping of the probe response would be present even for the periods of two minutes. The fluctuation of the h_d values represented in Figs. 13-15 are calculated from the P_s values based on the assumption of steady-state transfer. Since the main system time lag is in the tube membrane, this is a reasonable assumption.

The reason for these cyclic fluctuations is not completely understood. Flow unsteadiness has been observed by other investigators measuring the velocity distributions downstream of sudden expansions [10,11,12]. Durst et al. [11] concluded that the fluctuations were probably due to small waves in the shear layer. Back [7] saw shear instabilities for upstream Reynolds numbers greater than 250. As seen by Fig. 18, however, the period of the present unsteadiness was about three orders of magnitude larger than that documented by Ahmed at al. [12]. It is possible that the unsteadiness due to the shear layer instability also causes a longer period oscillation.

Some of the time intervals between measurements were as short as 3 minutes for the saline and blood experiments instead of the full response value of 30 minutes shown in Appendix D. This may warrant some questions as to the validity of the results. If the system was not sufficiently responding to the change in P_s caused by the location changes of the step relative to the electrode, however, there would be significant hysteresis in the measured values. As seen in the figures of the results, such a difference in P_s values for measuring and decreasing x values was not measured. This was one of the criteria used for acceptance of a data set. This repeatability of the results (to within 10%) when the step was moved in both directions relative to the electrode during each experiment showed that the results are valid. Moreover, to wait for 15 to 30 minutes between each measurement is too long, especially for the blood experiments since the blood would be hemolyzed before the experiment was done.

Between different data sets of the same Reynolds number for saline, repeatability of the results is better than 10 percent for Reynolds number equal to 160. For Reynolds numbers of 850 some points differ by as much as 20 percent for the two different sets of data measured. No comparison could be made between data sets of Reynolds number equal to 450 for saline and also for blood (Re = 160 and 450) due to the availability of only one data set each.

The time taken for the fluid to complete one circuit through the system during the transfer experiments was

	Re	Circuit time, min.	Period of fluctuation, min.
Saline	160	15.4	0.3
	450	5.4	0.5
	850	2.9	3.0
Blood	160	2.9	0.2
	450	1.0	0.3

The period of fluctuation was small relative to the circuit time in all cases except for saline of Re = 850. As the Reynolds number increased the period of fluctuation also increased. This is the opposite trend of the circuit time which decreased with increasing Reynolds number. Therefore, the cyclic fluctuations do not appear to be caused by an artifact of the flow around the system.

7. CONCLUSIONS

The following conclusions can be made from the findings of this project.

1. The mass transfer of oxygen in saline was measured downstream of a backward-facing step inside a tube with Reynolds number between 160 and 850. The transfer was found to be high throughout the separation and around the reattachment point regions relative to that of a developing boundary layer at the same position downstream. The highest transfer was measured near the reattachment point.
2. The transfer coefficients of blood were much higher than those of saline because of the chemical reaction between oxygen and hemoglobin. However, the ratio of the experimental transfer results to the calculated transfer for blood and saline at the same Reynolds number were nearly the same. This indicates that the transfer process is not affected by the particulate nature of blood.
3. The amplitude and the period of the cyclic fluctuations recorded during the experiments increased with higher Reynolds number. Fluctuations of the measured partial pressure of oxygen were larger in saline than in blood.

8. RECOMMENDATIONS

Although the apparatus used for this project has some limitations, it is still a reliable set-up which can be used to make a number of further studies. More experiments could be done to verify trends. The following are recommended as possibilities for further reserch.

1. Run experiments on whole blood to determine the reattachment point. This can be used to compare the reattachment points obtained using saline solution.
2. Run further transfer tests using blood at higher Reynolds numbers (> 450). This will require using a pump that will do less damage to the red blood cells so that longer tests can be run.
3. Use a more stable oxygen electrode to measure the partial pressure of oxygen.
4. Develop a new experimental apparatus to measure the mass transfer which has a faster response to measure the time-dependent behavior.

REFERENCES

1. Aung, Win, and C. B. Watkins, "Heat Transfer Mechanisms in Separated Forced Convection," Turbulent Forced Convection in Channels and Bundles, ed. by S. Kakas and D. B. Spalding, McGraw-Hill, 1979, pp. 233-257.

2. Goldsmith, H. L., "The Flow of Model Particles and Blood Cells and Its Relation to Thrombogenesis," Progress in Hemostasis and Thrombosis, Ed., T. H. Spaet, Grune and Stratton, N.Y., 1972, p. 97.

3. Goldsmith, H. L., and T. Karino, "Microscopic Considerations: The Motions of Individual Particles," Ann. N.Y. Acad. Sci., Vol. 283, 1977, pp. 241-255.

4. Buerk, D. G., and T. K. Goldstick, "Arterial Wall Oxygen Consumption Rate Varies Spatially," Am. J. Physiol., Vol. 243, 1982, pp. 4948-4958.

5. Feuerstein, I. A., G. K. Pike, and G. F. Round, "Flow in an Abrupt Expansion as a Model for Biological Mass Transfer Experiments," J. Biomechanics, Vol. 8, 1975, pp. 41-51.

6. Cooney, D. O., Biomedical Engineering Principles, Vol. 2, Marcel Dek'ker, Inc., New York, 1976.

7. Back, L. H., and E. J. Roschke, "Shear-Layer Flow Regimes and Wave Instabiities and Reattachment Lengths Downstream of an Abrupt Circular Channel Expansion," J. Appl. Mech., Trans. ASME, Vol. 94, 1972, pp. 677-681.

8. Macagno, E. O., and T. K. Hung, "Computational and Experimental Study of a Captive Annular Eddy," J. Fluid Mech., Vol. 28, 1967, pp. 43-64.

9. Goldstein, R. J., V. L. Eriksen, R. M. Olson, and E. R. G. Eckert, "Laminar Separation, Reattachment and Transition of the Flow Over a Downstream-Facing Step," J. Basic Engineering, Trans. ASME, Dec. 1970, pp. 732-741.

10. Denham, M. K., and M. A. Patrick, "Laminar Flow Over a Downstream Facing Step in a Two-Dimensional Flow Channel," Trans. Inst. Chem. Engrs., Vol. 52, 1974, pp. 361-367.

11. Durst, F., A. Melling, and J. H. Whitelaw, "Low Reynolds Number Flow Over a Plane Symmetric Sudden Expansion," J. Fluid Mech., Vol. 64, Part 1, 1974, pp. 111-128.

12. Ahmed, S. A., and D. P. Giddens, "Flow Disturbance Measurements Through a Constricted Tube at Moderate Reynolds Numbers," J. Biomechanics, Vol. 1b, No. 12, 1983, pp. 955-963.

13. Armaly, B. F., F. Durst, J. C. Pereira, and B. Schonnung, "Experimental and Theoretical Investigation of Backward-Facing Step Flow," J. Fluid Mech, Vol. 127, 1983, pp. 473-496.

14. Mueller, T. J., and R. A. O'Leary, "Physical and Numerical Experiments in Laminar Incompressible Separating and Reattaching Flows," AIAA Paper No. 70-763, July, 1970.

15. Sparrow, E. M., and J. P. Kalejs, "Local Convective Transfer Coefficients in a Channel Downstream of a Partially Constricted Inlet," Int. J. Heat Mass Transfer, Vol. 20, 1077, pp. 1241-1249.

16. Back, L. H., P. F. Massier, and E. J. Roschke, "Partially Ionized Gas Flow and Heat Transfer in the Separation, Reattachment and Redevelopment Regions Downstream of an Abrupt Circular Channel Expansion," J. Heat Transfer, Trans. ASME, February 1972, pp. 119-127.

17. Runchal, A. K., "Mass Transfer Investigation in Turbulent Flow Downstream of Sudden Enlargement of a Circular Pipe for Very High Schmidt Numbers," Int. J. Heat Mass Trasnfer, Vol. 14, 1971, pp. 781-792.

18. Zukauskas, A., A Slancianskas, and A. Pedisius, Heat Transfer, Vol. 3, eds. U. Grigull, E. Hanhne, K. Stephan and J. Straub, Hemisphere Pub. Co., 1982, pp. 217-221.

19. Larson, H. K., "Heat Transfer in Separated Flows," J. Aerosciences, Nov. 1959, pp. 731-738.

20. Sparrow, E. M., and J. E. O'Brien, "Heat Transfer Coefficients on the Downstream Face of an Abrupt Enlargement or Inlet Constriction in a Pipe," Trans ASME, Vol. 102, August 1980, pp. 408-414.

21. Schneiderman, G., C. E. Ellis, and T. E., Goldstick, "Mass Transport to Walls of Stenosed Arteries: Variation with Reynolds Number and Blood Flow Separation," J. Biomechanics, Vol. 12, 1979, pp. 869-877.

22. Chilcott, R. E., "A Review of Separated and Reattaching Flows with Heat Transfer, Int. J. Heat Mass Transfer, Vol. 10, 1967, pp. 783-797.

23. Pattantyus, I. A., "Carrier-Facilitated Oxygen Transport in Flowing Blood," M.S. Thesis, Virginia Polytechnic Institute and State University, Blacksburg, Virginia, 1982.

24. Diller, T. E., "Oxygen Diffusion Through Flowing Blood," Sc.D. Thesis, M.I.T., Cambridge, 1977.

25. Shah, R. K., and A. L. London, Laminar Flow Forced Convection in Ducts, Ed., T. F. Irvine, Jr., and J. P. Hartnett, Academic Press, 1978.

26. Glass, J. M., "Measurement of Oxygen Transfer in Separated Blood Flow," B.S. Senior Project Report, Virginia Polytechnic Institute and State University, Blacksburg, Virginia, 1984.

27. Diller, T. E., and B. B. Mikic, "Oxygen Diffusion in Blood: A Translational Model of Sher-Induced Augmentation," Trans. ASME, Vol. 105, Nov. 1983, pp. 346-352.

28. Roschke, E. J., and L. H. Back, "The Influence of Upstream Conditions On Flow Reattachment Lengths Downstream of an Abrupt Circular Channel Expansion," J. Biomechanics, Vol. 9, 1976, pp. 481-483.

29. Middleman, S., Transport Phenomena in the Cardiovascular System, Wiley-Interscience, New York, 1972.

30. Nerem, R. M., and J. F. Cornhill, "The Role of Fluid Mechanics in Atherogenesis," J. Biomechanical Engineering, Trans. ASME, Vol. 120, 1980, pp. 181-189.

31. Britts, W. C., II, "Oxygen Transfer in Pulsating Laminar Flow," M.S. Thesis, Virginia Polytechnic Institute and State University, Blacksburg, Virginia, 1982.

32. Cho, Y. Z., L. H. Back, and D. W. Crawford, "Prssure Difference-Flow Rate Variation in a Femoral Artery Branch Casting of Man for Steady Flow," J. Biomechanical Enginering, Trans. ASME, Vol. 105, 1983, pp. 258-262.

33. Lutz, R. J., J. N. Cannon, K. B. Bischoff, R. L. Dedrick, R. K. Stiles, and D. L. Fry, "Wall Shear Stress Distribution in a Model Canine Artery During Steady Flow," Circ. Res., Vol. 41, No. 3, 1977, pp. 391-399.

34. Seki, N., N. Fujusako, and T. Hirata, "Effect of Stall Length on Heat Transfer in Reattachment Region Behind a Double Step at Entrance to an Enlarged Flat Duct," Int. J. Heat Mass Transfer, Vol. 19, 1976, pp. 700-702.

35. Caton, J. A., "The Use of a Simple Heat Trasnfer Model for Separated Flows in Tubes," Trans. ASME, Vol. 105, Nov. 1983, pp. 928-931.

36. Zemanick, P. P., and R. S. Dougall, "Local Heat Transfer Downstream of Abrupt Circular Channel Expansion," J. Heat Trasnfer, Trans. ASME, Feb. 1970, pp. 53-60.

37. Holman, J. P., Heat Transfer, 4th Edition, McGraw-Hill Book Company, Inc., 1976.

38. Vogel, J. C., J. K. Eaton, and E. W. Adams, "Combined Heat Trasnfer and Fluid Dynamic Measurements Behind a Backward-Facing Step," ASME, 83-WA/HT-11, pp. 1-8.

39. Aung, W., "An Experimental Study of Laminar Heat Transfer Downstream of Backsteps," J. Heat Transfer, Trans. ASME, Vol. 105, 1983, pp. 823-829.

40. Kumar, A., and K. S. Yajnik, "Internal Separated Flows at Large Reynolds Number," J. Fluid Mech., Vol. 97, Part 1, 1980, pp. 27-51.

41. Carnahan, B., H. A. Luther, and J. O. Wilkes, Applied Numerical Methods, John Wiley & Sons, Inc., N.Y., 1969, pp. 441-442.

42. Colton, C. K., and R. F. Drake, "Effect of Boundary Conditions on Oxygen Transport to Blood Flowing in a Tube," Chemical Engineering Symposium Series, Vol. 67, No. 114, 1971, pp. 88-95.

43. Levenberg, K., "A Method for the Solution of Certain Non-Linear Problems in Least Squares,"Quart. Appl. Math., 1944, pp. 164-168.

44. Marquardt, D. W., "An Algorithm for Least Squares Estimation of Nonlinear Parameters," J. SIAM, 1963.

45. Von Rosenberg, D. V., Methods for the Numerical Solution of Partial Differential Equations, Am. Elsevier Pub. Co., N.Y., 1969.

46. Diller, T. E., B. B. Mikic, and P. A. Drinker, "Shear-Induced Augmentation of Oxygen Transfer in Blood," J. Biomechanical Engineering, Trans. ASME, Vol. 102, February 1980, pp. 67-72.

APPENDIX A

SALIN3, a Computer Program for Calculating Sherwood Number of Water

The actual numerical solution is partly derived from the program used by Pattantyus [23]. This solution utilizes a half step Crank-Nicholsen Finite Difference technique. Since water does not contain hemoglobin, there is no saturation and the governing transfer equations are linear. No iterations in the program are needed.

The entire program operates on partial pressures. Most of the variable names are listed and defined to make it easier to follow and understand.

Variables for Programs

RR1 - inside radius of silicone membrane tube, cm.

BP - barometric pressure, mm Hg.

Q - flow rate of fluid, cc/min.

ALPHA0 - α_o, solubility of O_2 in fluid, cc O_2/cc blood-atm.

HIO2C - high oxygen concentration, percentage in decimal form

KI - k, constant in Margaria equation

MI - m, constant in Margaria equation

WALL - Sh_w, oxygen transfer resistance of the membrane tube wall; does not include diffusivity of fluid

DX - initial axial step size, cm.

LI - transfer length, cm.

SI - saturation at the beginning of the entry length, percentage in decimal form.

PINTL - oxygen partial pressure at the beginning of the entry length, mm Hg.

THB - total hemoglobin, percent

COHB - carboxyhemoglobin, percent

METHB - methemoglobin, percent

F - number of radial steps

H - F + 1

STEP - number of time steps executed before step size is changed

DE - $\partial\eta$

PI - π

PPO - partial pressure of high oxygen content gas, corrected for vapor pressure of water

DINT - diffusivity multiplied by 10^5

CTE - C_T, experimental hemoglobin concentration

SATI - entrance saturation based on hemoglobin available for saturation

PINT - see PINTL

POUT - see PPO

SP - multiplier containing constants and conversion factors

SIP - exponential term in Margaria equation

SINT - saturation calculated based on PINT

SOUT - saturation calculated based on POUT

CT - denominator of nondimensionalized transfer, θ

TERM1, TERM2 - intermediate variables used for calculating transfer and sink strength

M - sink strength of fluid

XLO - nondimensional transfer length

MF - term used to check nonlinearity of PHI(I)

DX - step size based on sink strength of fluid

XL - nondimensional transfer length divided by diffusivity

TH(I) - nondimensionalizing term for the finite difference equations

DE1, DE2 - constants used in finite difference equations

DX1 - inverse of axial step size

DSDP- - $\frac{\partial s}{\partial p}$, slope of the saturation curve expressed in terms of the Margaria equation

PO(I) - nondimensional pressure, 1/2 step behind P(I)

A1(I), A2(I), A3(I), B1(I), B2(I), B3(I), D(I) - tridiagonal matrices

PHI(I) - slope of the saturation curve

SH - wall Sherwood number

HS1, HS2 - boundary values based on wall Sherwood number

X - axial location of the numerical solution

THETA - nondimensionalized transfer

BETA(I), GAMMA(I) - arrays used in the tridiagonal matrix solution

PI(I) - nondimensional pressure, 1/2 step ahead of P(I)

FI(I) - nondimensionalized slope of the saturation curve

KOU - counter for nonlinear iterations

P(I) - radial partial pressure distribution

S(I) - radial saturation distribution

HD1 - mass transfer coefficient, cm/s.

SHWN - Sherwood number

AL - characteristic length, cm

PHIM - tube permeability, $(cm^2\ cc/cc)/(atm\text{-}s)$

DC - diffusion coefficient, cm^2/s.

APPENDIX B

BLOOD, a Computer Program for Calculating Sherwood Number of Whole Blood

This program is an extended version of SALIN3. The actual numerical solution is also partly derived from the program used by Pattantyus [10]. This solution utilizes a half step Crank-Nicholsen finite difference technique to solve the following governing transfer equations for the partial pressure distribution:

$$(1 - \eta^2)\left(1 + \frac{\psi_B}{\partial_A}\right)\frac{\partial \hat{P}}{\partial x^+} = \frac{1}{\eta}\frac{\partial}{\partial \eta}\left(\eta \frac{\partial \hat{P}}{\partial \eta}\right)$$

Unlike water, whole blood does contain hemoglobin and thus has a chemical reactions. The Crank-Nicholsen method of solutions allows an accurate representation of the non-linear term and generally has good stability characteristics. Since the transfer equations are non-linear, iterations in the program are required.

The entire program also operates on partial pressures. All the experimental parameters are read into the program and the Sherwood numbers along the entire test section are then calculated.

```
JOB WATFIVBLOODFLW,P=50,T=20
C      PROGRAM FOR THE SALINE EXPERIMENTS
       INTEGER F, H , J, STEP
       REAL M,N,SH,LI,KI,MI,PS,TXL,XL,XLO
       REAL HD,SHN,AL,PHIM,DC,SHWN,HD1
       DIMENSION A1(100), A2(0), A3(100), B1(101), B2(101),
      X D(101), P0(101), P1(101), GAMMA(101), BETA(101),
      X TH(100), E(100), FI(100), S(100), P(102),
      X PHI(100),B3(101)
       F=30
       H=F+1
       DE=1.0/30.0
       STEP=40
C
C      .....INPUT EXPERIMENTAL PARAMETERS.....
C
       READ(5,*) BP,Q,HIO2C
       READ(5,*) WALL,DX0
       PI=3.141592654
       PP0=(BP-47.)*HIO2C
       DC=2.85E-5
       PB=0.0
       RO=0.3389
       RI=0.2465
       ALPHAO=0.0239
       PO=660.0
       RRI=0.635
       PHIM=5.32E-6
       AL=1.27
       WRITE(6,52)BP,Q,WALL,HIO2C
   52  FORMAT (2X,'BP=',F5.1,2X,'Q=',F5.1,2X,'WALL=',F5.1,
      +2X,'HIO2C=',F3.1,/)
C
C      .....BEGIN SOLUTION LOOP FOR ONE DATA POINT.....
C
   81  READ(5,*) LI
       WRITE(6,53)LI,DX0
53     FORMAT(2X,'LI=',F4.1,2X,'DX0=',E15.8/)
       DINT=2.85
C
C      .....CALCULATE BULK TRANSFER FROM EXPERIMENTAL
C      .....VALUES
C
       POUT=PP0
       PINT=0.0
       POUT=PP0
       CT=1.0
       SP=POUT-PINT
       SINT=0.0
       M=1.
       DO 12 I=1,H
```

```
        P(I)=PINT
12      PO(I)=(P(I)-PINT)/(POUT-PINT)
C
C       .....DEFINE VALUES FOR NUMERICAL METHOD.....
C
        XLO=(PI*LI*60.)/(2.*10.**5*Q)
        DX=DXO*M
        XL=XLO*DINT
        E(1)=DE/2.0
        TH(1)=E(1)*(1.0-E(1)**2)*4.0*DE/CT
        DO 570 I=2,F
          E(I)=E(I-1)+DE
570       TH(I)=E(I)*(1.0-E(I)**2)*4.0*DE/CT
C  MATRIX INITIALIZATION
10      DE1=1.0/(4.0*DE)
        DE2=1.0/(DE**2)
20      DX=DXO*M
        XL=XLO*DINT
        DX1=1.0/DX
        PHI(1)=0.0
        A3(1)=DE2
        B3(1)=DE2
15      DO 17 I=2,F
        PHI(I)=PHI(I-1)
        A1(I)=DE2/2.0-DE1/E(I)
        B1(I)=A1(I)
        A3(I)=DE2/2.0+DE1/E(I)
17      B3(I)=A3(I)
        SH=WALL/DINT
        WRITE(6,119)SH
119     FORMAT(2X,'SHERWOOD NUMBER=',F10.6)
        HS1=0.5-2.0/(SH*DE)
        HS2=0.5+2.0/(SH*DE)
        J=1
        X=0.0
        THETA=0.0
        I=H
          B1(I)=HS1
          B2(I)=HS2
          CH=1.0
C START SOLUTION
50        X=X+DX
C    SET MATRIX B2,A2
100     DO 150 I=1,F
          AB=(1.0-E(I)**2)*(1.0+PHI(I))*DX1
          A2(I)=AB-DE2
150       B2(I)=-AB-DE2
C    SET MATRIX D
200       D(1)=-A2(1)*PO(1)-A3(1)*PO(1)
        DO 250 I=2,F
250     D(I)=-A1(I)*PO(I-1)-A2(I)*PO(I)-A3(I)*PO(I+1)
```

```
      D(H)=CH
C   TRIDIAGONAL MATRIX SOLVER
400   BETA(1)=B2(1)
      GAMMA(1)=D(1)/BETA(1)
      DO 405 I=2,H
        BETA(I)=B2(I)-B1(I)*B3(I-1)/BETA(I-1)
405     GAMMA(I)=(D(I)-B1(I)*GAMMA(I-1))/BETA(I)
      P1(H)=GAMMA(H)
      DO 410 L=1,F
        I=H-L
410     P1(I)=GAMMA(I)-B3(I)*P1(I+1)/BETA(I)
C CHECK PHI
C CALCULATE THETA
      THETA=0.0
      DO 530 I=1,F
      P(I)=PINT+(POUT-PINT)*P1(I)
      S(I)=0.0
      C=S(I)-SINT+(P(I)-PINT)/SP
530   THETA=THETA+C*TH(I)
C END CHECK
      PS=(P1(H)+P1(H-1))/2.0
      HD=SH*DC*(1.0-PS)/(2.0*RRI*PS)
      SHN=HD*AL/DC
      HD1=2.0*DC*(P1(H-1)-P1(H))/(DE*RRI*(2.0*THETA-P1(H)
     &-P1(H-1)))
      SHWN=HD1*AL/DC
      TXL=3.0*XL
      WRITE(6,888)X,PS,THETA,HD,SHN,HD1,SHWN
888   FORMAT(2X,'X=',F8.6,2X,'PS=',F7.5,2X,'THETA=',F7.5,
     +2X,'HD=',F6.4,2X,'SHN=',F10.6,2X,'HD1=',F10.8,2X,
     +'SHWN=',F10.6,/)
      IF(J-STEP)33,610,610
610     DX=2.0*DX
        DX1=1.0/DX
        J=0
33    DO 670 I=1,H
670    P0(I)=P1(I)
       J=J+1
      IF(X.GT.TXL)GO TO 111
      GO TO 50
 111  WRITE(6,*) (P1(I),I=1,H)
      STOP
      END
ENTRY
```

```
JOB WATFIV   BLOODFLW,P=50,T=20
C      BLOOD PROGRAM 7
       INTEGER F, STEP, J, H
       REAL M,N,SH,LI,KI,MI,MF,CO,METHB,PS,TXL,XL,XLO,
      +DC,SHWN,HD1,ALPHA0,HD,SHN,AL,PHIM
       DIMENSION A1(150), A2(150), A3(150), B1(151), B2(151),
      X D(151), P0(151), P1(151), GAMMA(151), BETA(151),
      X TH(150), E(150), FI(150), S(150), P(152),
      X PHI(150),B3(151)
       F=100
       H=F+1
       STEP=40
       DE=1.0/100.0
C
C      .....INPUT EXPERIMENTAL PARAMETERS.....
C
       READ(5,*) BP,Q,ALPHA0,HIO2C
       READ(5,*) KI,MI,WALL,DX0
       PI=3.141592654
       PP0=(BP-47.)*HIO2C
       DC=1.5E-5
       RRI=0.635
       PHIM=5.32E-6
       AL=1.27
       WRITE(6,52)BP,Q,WALL,ALPHA0,HIO2C
   52  FORMAT (2X,'BP=',F5.1,2X,'Q=',F5.1,2X,'WALL=',F5.1,
      +2X,'ALPHA0=',E15.8,2X,'HIO2C=',F3.1,/)
   81  READ(5,*) LI,SI,PINTL,THB,COHB,METHB
       WRITE(6,53)LI,DX0,PINTL,KI,MI
53     FORMAT(2X,'LI=',F4.1,2X,'DX0=',E15.8,2X,'PINTL=',
      +F4.1,2X,'KI=',E15.8,2X,'MI=',F5.1,/)
       DINT=1.5
C
C      .....CALCULATE BULK TRANSFER FROM EXPERIMENTAL
C      .....VALUES.....
C
       CTE=1.39*THB/100.
       SATI=SI*(1.-(COHB+METHB)/100.)
       PINT=PINTL
       POUT=PP0
       SP=(CTE/ALPHA0)*760.
       SIP=(1.0+KI*PINT)/(KI*PINT)
       SINT=(SIP**3+MI-1.0)/(SIP**4+MI-1.0)
       SIP=(1.0+KI*POUT)/(KI*POUT)
       SOUT=(SIP**3+MI-1.0)/(SIP**4+MI-1.0)
       CT=(SOUT-SINT)+(POUT-PINT)/SP
       S0=SOUT
       TERM1=CTE*(S0-SATI)
       TERM2=ALPHA0*(PP0-PINTL)/760.
       M=1.+TERM1/TERM2
       WRITE(6,40)PP0,CTE,SATI,S0,TERM1,TERM2
```

```
40     FORMAT(2X,'PPO=',E13.7,2X,'CTE=',E13.7,2X,'SATI=',
      +E13.7,2X,'SO=',E13.7,2X,'TERM1=',E13.7,2X,
      +'TERM2=',E13.7,/)
C
C      .....DEFINE VALUES FOR NUMERICAL METHOD.....
C
       CO=COHB
       XLO=(PI*LI*60.)/(2.*10.**5*Q)
       MF=M*0.02
       WRITE(6,57)
   57  FORMAT (' ',4X,'THB',8X,'COHB',5X,'METHB')
       WRITE(6,58) THB,COHB,METHB
   58  FORMAT (3F10.2,/)
       WRITE(6,59)M,MF,SI
59     FORMAT(2X,'M=',E14.7,2X,'MF=',E14.7,2X,'SI=',
      +E14.7,/)
       E(1)=DE/2.0
       TH(1)=E(1)*(1.0-E(1)**2)*4.0*DE/CT
       DO 570 I=2,F
         E(I)=E(I-1)+DE
570      TH(I)=E(I)*(1.0-E(I)**2)*4.0*DE/CT
C  MATRIX INITIALIZATION
10     DE1=1.0/(4.0*DE)
       DE2=1.0/(DE**2)
20     DX=DXO
       XL=XLO*DINT
       DX1=1.0/DX
       SIP=(1.0+KI*PINT)/(KI*PINT)
       DSDP=(SIP**6+MI*(4.0*SIP**3-3.0*SIP*SIP))/
      X (((SIP**4+MI)**2)*KI*PINT*PINT)
       PHI(1)=DSDP*SP
11     DO 12 I=1,H
       P(I)=PINT
       PO(I)=(P(I)-PINT)/(POUT-PINT)
   12  CONTINUE
       A3(1)=DE2
       B3(1)=DE2
15     DO 17 I=2,F
       PHI(I)=PHI(I-1)
       A1(I)=DE2/2.0-DE1/E(I)
       B1(I)=A1(I)
       A3(I)=DE2/2.0+DE1/E(I)
17     B3(I)=A3(I)
       SH=WALL/DINT
       WRITE(6,119)SH
119    FORMAT(2X,'SHERWOOD NUMBER= ',F10.6,//)
       HS1=0.5-2.0/(SH*DE)
       HS2=0.5+2.0/(SH*DE)
       J=1
       X=0.0
       THETA=0.0
```

```
      I=H
        B1(I)=HS1
        B2(I)=HS2
        CH=1.0
C START SOLUTION
50      X=X+DX
      KOU=0
C   SET MATRIX B2,A2
100   DO 150 I=1,F
        AB=(1.0-E(I)**2)*(1.0+PHI(I))*DX1
        A2(I)=AB-DE2
150     B2(I)=-AB-DE2
C   SET MATRIX D
200     D(1)=-A2(1)*PO(1)-A3(1)*PO(1)
      DO 250 I=2,F
250   D(I)=-A1(I)*PO(I-1)-A2(I)*PO(I)-A3(I)*PO(I+1)
      D(H)=CH
C   TRIDIAGONAL MATRIX SOLVER
400   BETA(1)=B2(1)
      GAMMA(1)=D(1)/BETA(1)
      DO 405 I=2,H
        BETA(I)=B2(I)-B1(I)*B3(I-1)/BETA(I-1)
405     GAMMA(I)=(D(I)-B1(I)*GAMMA(I-1))/BETA(I)
      P1(H)=GAMMA(H)
      DO 410 L=1,F
        I=H-L
        P1(I)=GAMMA(I)-B3(I)*P1(I+1)/BETA(I)
       IF((P1(I).GT.1.0E-60).AND.(P1(I).LT.1.0E75))
     + GO TO 410
        P1(I)=0.0
410     CONTINUE
C CHECK PHI
      DO 459 I=1,F
      P(I)=PINT+(POUT-PINT)*(PO(I)+P1(I))/2.0
      SIP=(1.0+KI*P(I))/(KI*P(I))
      DSDP=(SIP**6+MI*(4.0*SIP**3-3.0*SIP*SIP))/
     X (((SIP**4+MI)**2)*KI*P(I)*P(I))
      FI(I)=SP*DSDP
459     CONTINUE
      DO 460 I=1,F
        IF (ABS(PHI(I)-FI(I))-MF)    460,460,462
460   CONTINUE
      GO TO 500
462   DO 465 I=1,F
465   PHI(I)=FI(I)
      KOU=KOU+1
C     END CHECK
      IF (KOU-20) 100,90,90
C CALCULATE THETA
500   THOLD=THETA
      THETA=0.0
```

```
      DO 530 I=1,F
      P(I)=PINT+(POUT-PINT)*P1(I)
      SIP=(1.0+KI*P(I))/(KI*P(I))
      S(I)=(SIP**3+MI-1.0)/(SIP**4+MI-1.0)
      C=S(I)-SINT+(P(I)-PINT)/SP
530   THETA=THETA+C*TH(I)
C CALCULATE MASS TRANSFER COEFFICIENT AND SHERWOOD NUMBER
      PS=(P1(H)+P1(H-1))/2.0
      HD=SH*DC*(1.0-PS)/(2.0*RRI*PS)
      SHN=HD*AL/DC
      HD1=2.0*DC*(P1(H-1)-P1(H))/(DE*RRI*(2.0*THETA-P1(H)
     &-P1(H-1)))
      SHWN=HD1*AL/DC
      TXL=10.0*XL
      XOM=X/M
      WRITE(6,888)X,XOM,PS,THETA,HD,SHN,HD1,SHWN
888   FORMAT(2X,'X=',F10.8,2X,'XOM=',F10.8,2X,'PS=',
     +F7.5,2X,'THETA=',F7.5,2X,'HD=',F6.4,2X,'SHN=',
     +F11.6,2X,'HD1=',F10.8,2X,'SHWN=',F10.6,/)
C TIME STEP
C  CHANGE DX
600   IF (J-STEP) 650,610,610
610     DX=2.0*DX
        DX1=1.0/DX
        J=0
C  RESET P0 & PHI
      I=1
      P0(I)=P1(I)+DX*(P1(I+1)-P1(I))*(1.0/(2.0*DE*E(I))
     X +DE2)/(2.0*(1.0-E(I)**2))*(1.0+PHI(I))
      DO 630 I=2,F
630   P0(I)=P1(I)+DX*((P1(I+1)-P1(I-1))/(2.0*DE*E(I))
     X +(P1(I+1)-2.0*P1(I)+P1(I-1))*DE2)/
     X (2.0*(1.0-E(I)**2))*(1.0+PHI(I))
      DO 640 I=1,F
      P(I)=PINT+(POUT-PINT)*P0(I)
      SIP=(1.0+KI*P(I))/(KI*P(I))
      DSDP=(SIP**6+MI*(4.0*SIP**3-3.0*SIP*SIP))/
     X (((SIP**4+MI)**2)*KI*P(I)*P(I))
640   PHI(I)=SP*DSDP
650   DO 670 I=1,H
670     P0(I)=P1(I)
C   COUNTER
      J=J+1
C   END CHECK
      IF(X.GT.TXL)GO TO 111
      GO TO 50
90    WRITE(6,900)
900   FORMAT(5X,'PHI IS UNSTABLE')
111   WRITE(6,*)(P1(I),I=1,H)
      STOP
      END
```

APPENDIX C

External Error Analysis

The external error analysis applied to the measurement of oxygen transfer in separated flow is detailed in this appendix. Many possible sources of error exist in the data collection method and data collection equipment. The basic formula for external error of a function Z(a,b,c,d) is

$$E_E^2 = \frac{e^2 E}{Z^2} = e_a^2 \left(\frac{\partial Z}{\partial a}\right)^2 + e_b^2 \left(\frac{\partial Z}{\partial b}\right)^2 \quad \text{(C.1)}$$
$$e_c^2 \left(\frac{\partial Z}{\partial c}\right)^2 + e_d^2 \left(\frac{\partial Z}{\partial d}\right)^2$$

Estimates, based on experience, judgement, or actual measurement are made for e_a, e_b, etc. and E_E is calculated.

The result of each measurement is the mass transfer coefficient,

$$h_d = \underbrace{\frac{\phi_m}{\alpha_b r_i \ln (r_o/r_i)}}_{\text{Bias Error}} \cdot \underbrace{\frac{P_s - P_o}{P_i - P_s}}_{\text{Repeatability Error}}$$

Errors in the values of ϕ_m, α_b, r_i, r_o, P_s, P_o, and P_b are considered. The partial derivatives with respect to each variable are:

$$\frac{\partial h}{\partial \phi_m} = \frac{1}{\alpha_b r_i \ln (r_o/r_i)} \cdot \frac{P_s - P_o}{P_i - P_s} \quad \text{(C.2)}$$

$$\frac{\partial h}{\partial \alpha_b} = \frac{\phi_m}{r_i \ln (r_o/r_i)} \cdot \frac{P_s - P_o}{P_i - P_s} \cdot \left(\frac{-1}{\alpha_b^2}\right) \tag{C.3}$$

$$\frac{\partial h}{\partial r_i} = \frac{\phi_m}{\alpha_b} \cdot \frac{P_s - P_o}{P_i - P_s} \cdot \left[\frac{-\{r_o/r_i) - 1\}}{\{r_i \ln (r_o/r_i)^2\}}\right] \tag{C.4}$$

$$\frac{\partial h}{\partial r_o} = \frac{\phi_m}{\alpha_b r_i} \cdot \frac{P_s - P_o}{P_i - P_s} \cdot \left[\frac{-1/r_o}{\{\ln (r_o/r_i)\}^2}\right] \tag{C.5}$$

$$\frac{\partial h}{\partial P_s} = \frac{\phi_m}{\alpha_b r_i \ln (r_o/r_i)} \cdot \left[\frac{P_i - P_o}{(P_i - P_s)^2}\right] \tag{C.6}$$

$$\frac{\partial h}{\partial P_o} = \frac{\phi_m}{\alpha_b r_i (r_o/r_i)} \cdot \left(\frac{-1}{P_i - P_s}\right) \tag{C.7}$$

$$\frac{\partial h}{\partial P_b} = \frac{\phi_m}{\alpha_b r_i (r_o/r_i)} \cdot \frac{P_o - P_s}{(P_i - P_s)^2} \tag{C.8}$$

The estimated errors associated with each measurement are as follows:

$e_{P_s} = 5$ mm Hg ; accuracy limit of microsensor readout

$e_{\phi_m} = 2.66 \times 10^{-7} \frac{cm^2}{atm-5}$; resistance of the tube membrane (±5 percent)

$e_{\alpha_b} = 4.46 \times 10^{-4} \frac{cm^3}{cm^3-atm}$; solubility of blood in oxygen. (±2 percent)

$e_{r_i} = 0.005$ cm ; accounts for 0.8 percent of the internal radius of tubing

e_{r_o} = 0.005 cm ; accounts for 0.6 percent of the external radius of tubing

e_{P_i} = 1 mm Hg ; accuracy of oxygen concentration obtained from gas tank

e_{P_o} = 1 mm Hg ; accuracy of oxygen concentration obtained from gas tank

The partial derivatives in Eqs. (C.2) to (C.8) and these values of error are substituted into Eq. (C.1) and an error estimate is produced.

Figure 31 shows how the estimated bias error and repeatability error vary with the mass transfer coefficient for saline and blood, while Fig. 32 shows how the bias error and repeatability error vary with the difference in partial pressures for saline and blood.

The repeatability error represents the errors due to the partial pressures (P_i, P_s, P_o) since these values were measured druing every experiment. The bias error represents the errors due to the uncertainty in the physical and geometric constants which were not varied from experiment to experiment.

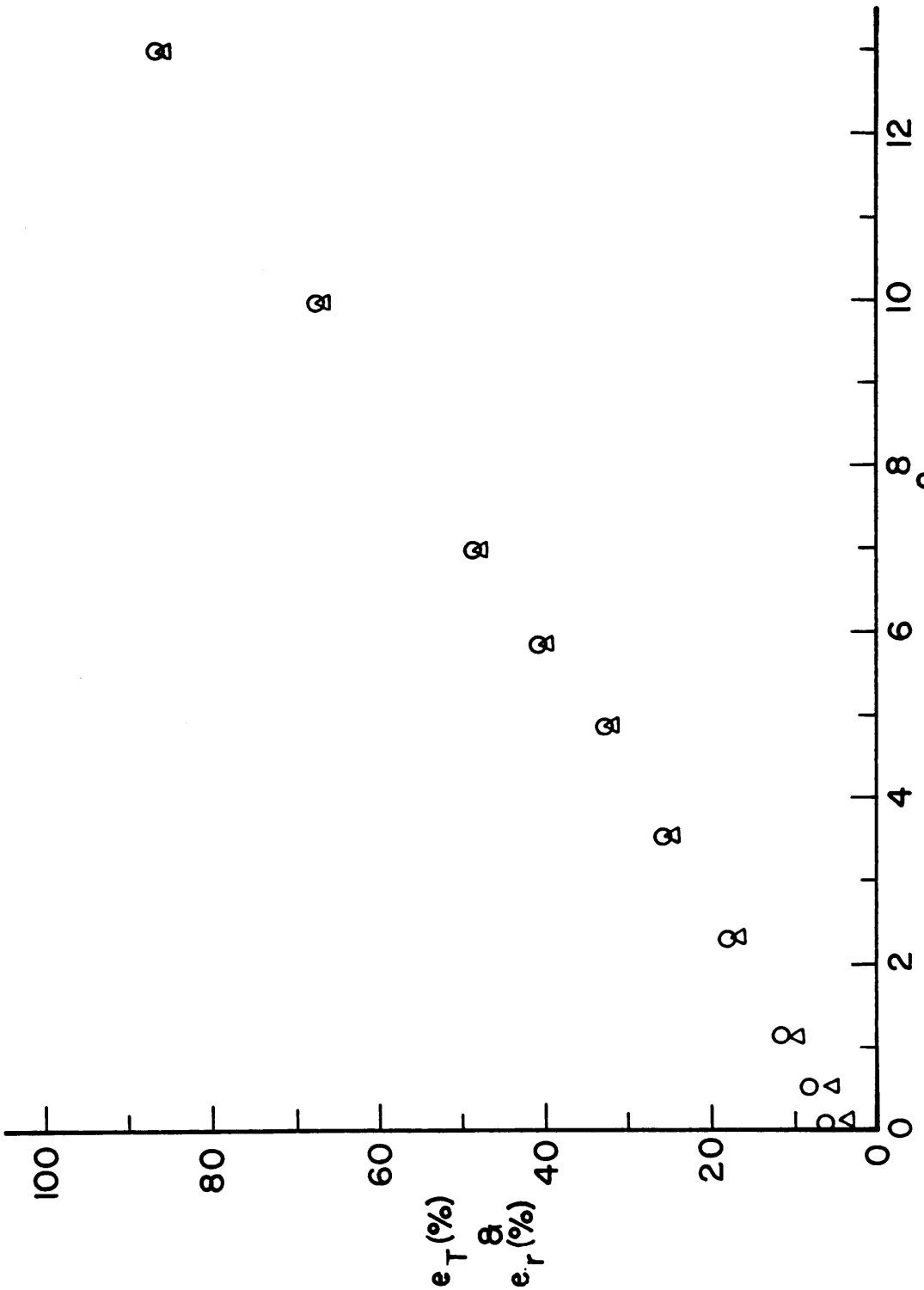

Fig. 31. Total error vs. mass transfer coefficient for saline and blood

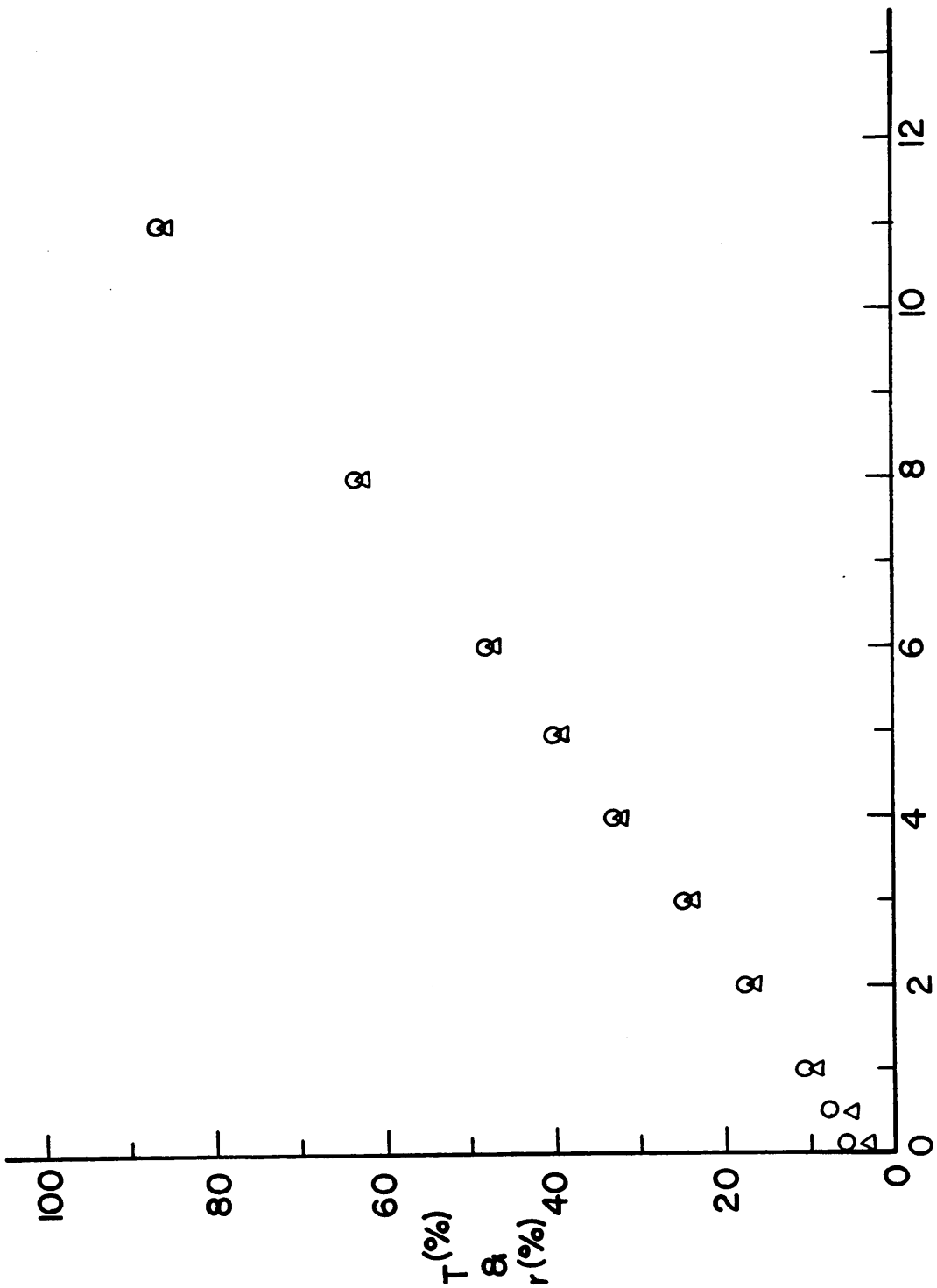

Fig. 32. Total error vs. difference in partial pressure for saline and blood

APPENDIX D

Time Constant Calculations

Two models are presented in detail to determine how the partial pressure of oxygen measured, P_s, varies with time. The outside partial pressure is maintained at some initial partial pressure P_i. It is then suddenly changed from P_i to P_o. An expression for the measured partial pressure, P_s, as a function of time can then be obtained. The two models are described as follows.

Model 1

The approximate time taken for gas to diffuse through the silicon membrane is calculated assuming a lumped resistance and capacitance across the membrane.

Applying the transient mass conservation for a control volume around the membrane in Fig. 33.

$$J = \frac{C_o - C}{R} = V a_s \frac{dp}{dt}$$

$$\frac{(P_o - P)a_s}{\frac{\ln (r_o/r_i)}{2\pi D_m L}} = V a_s \frac{dp}{dt}$$

$$\frac{dp}{dt} + \frac{2\pi D_m L(P-P_o)}{V \ln(r_o/r_i)} = 0 \quad (D.1)$$

$$\therefore \quad \tau = \frac{V \ln (r_o/r_i)}{2\pi D_m L}$$

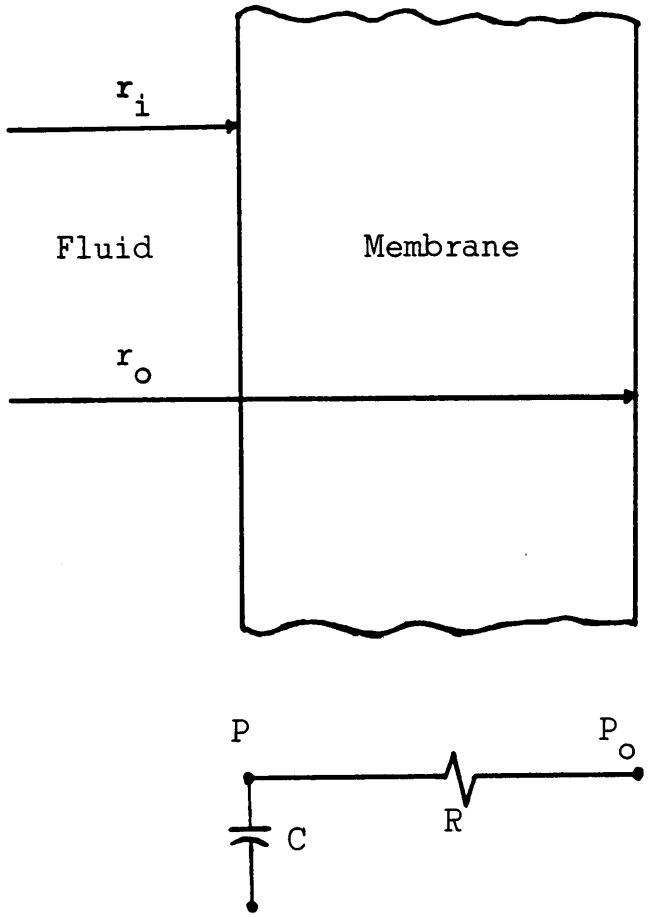

Fig. 33. Diffusion of gas through membrane with membrane resistance only

$$\tau = \frac{(r_o^2 - r_i^2) \ln (r_o/r_i)}{2D_m}$$

For the silicon rubber tube used the values of the parameters to evaluate the time constant are:

$r_o = 0.873125$ cm

$r_i = 0.635$ cm

$D_m = 1.6 \times 10^{-5}$ cm^2/s

$\therefore \quad \tau = 3570$ s.

The time constant is therefore approximately one hour for the change in tube concentration. Since the capacitance is placed at the inside surface of the tube, this is an overestimate of the time constant.

Model 2

Figure 34 shows a more detailed model of the complete transfer process in the tube wall and fluid for a sudden change of P_o surrounding the membrane. The capacitance is moved to the center of the tube wall and the resistance in the fluid is added. As the gas diffuses through the membrane, the storage term, P_m, is "charged." Gas also diffuses from P_m through the membrane and into the fluid. The factor α_b/α_m (the partition coefficient) is multiplied with the resistance term R_1 to account for the different solubilities of the fluid and the membrane.

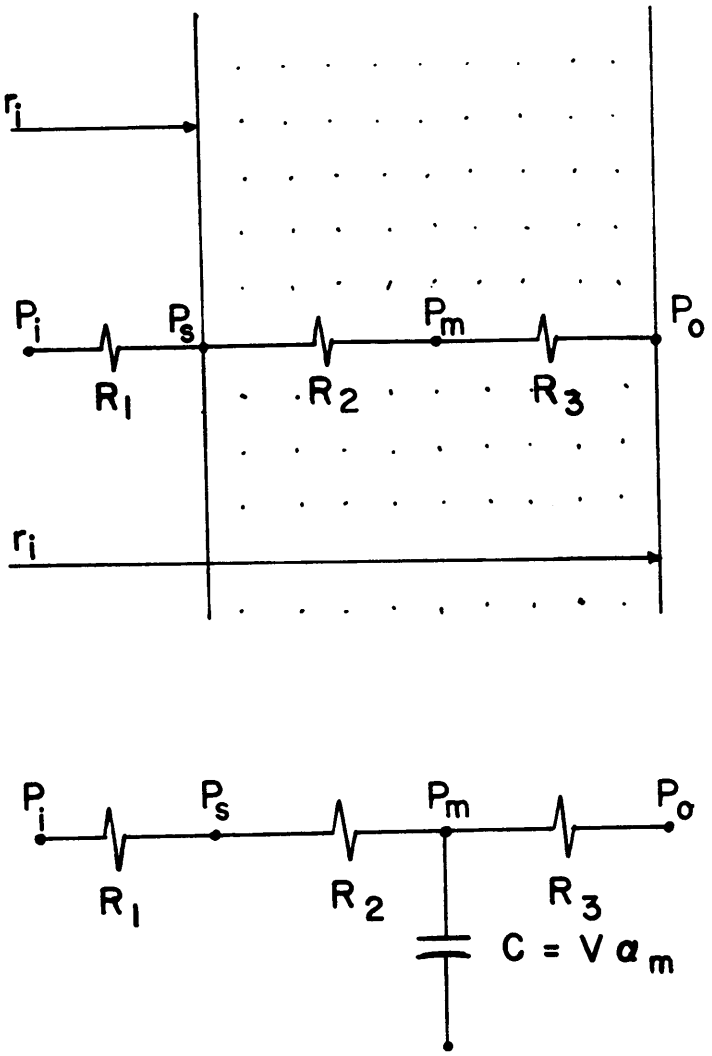

Fig. 34. Diffusion of gas through membrane with membrane and convective resistances

$$J_1 = \frac{C_i - C_m}{R_1 + R_2} \qquad J_2 = \frac{C_o - C_m}{R_3}$$

Mass conservation for a control volume around node P_m gives

$$J = J_1 + J_2 = V\alpha_m \frac{dP_m}{dt}$$

Substituting for J_1 and J_2 gives

$$\frac{C_i - C_m}{R_1 + R_2} + \frac{C_o - C_m}{R_3} = V\alpha_m \frac{dP_m}{dt}$$

$$C = \alpha_m P$$

$$\frac{P_i - P_m}{R_1 + R_2} + \frac{P_o - P_m}{R_3} = V \frac{dP_m}{dt}$$

where

$$R_1 = \frac{1}{h_d \; 2\pi r_i L \; (\alpha_b/\alpha_m)}$$

$$R_2 = \frac{\ln\{(r_i + \frac{r_o - r_i}{2})/\; r_i\}}{2\;\pi\; D_m\; L}$$

$$R_2 = \frac{\ln\;(\frac{r_o + r_i}{2r_i})}{2\;\pi\; D_m\; L} = \frac{\ln\;\frac{1}{2}\;(1 + r_o/r_i)}{2\;\pi\; D_m\; L}$$

$$R_3 = \frac{\ln \left\{ r_o / \left(r_i + \frac{r_o - r_i}{2} \right) \right\}}{2 \pi D_m L}$$

$$R_3 = \frac{\ln \left(\frac{2r_o / r_i}{1 + r_o / r_i} \right)}{2 \pi D_m L}$$

Solving for P_m gives

$$\frac{dP_m}{dt} + \frac{1}{V} \left[\frac{1}{R_1 + R_2} + \frac{1}{R_3} \right] P_m = \frac{P_i}{V(R_1 + R_2)} + \frac{P_o}{VR_3} \qquad (D.2)$$

$$\left[\frac{dP_m}{dt} + \frac{1}{\tau} P_m = P_i A + P_o B \right] \qquad (D.3)$$

where,

$$A = \frac{1}{V} \left(\frac{1}{R_1 + R_2} \right) \quad , \quad B = \frac{1}{VR_3}$$

$$\frac{1}{\tau} = \frac{1}{V} \left[\frac{1}{R_1 + R_2} + \frac{1}{R_3} \right] = A + B$$

The general solution is

$$\therefore P_m = \tau A P_i + \tau B P_o + A_1 e^{-t/\tau}$$

with A_1 to be determined from the initial condition

$$\text{I.C. @ } t = 0 \quad P_m = P_{mo}$$

$$A_1 = P_{mo} - \tau AP_i - \tau BP_o$$

The solution for P_m is then

$$P_m = P_{mo}\, e^{-t/\tau} + (1 - e^{-t/\tau})\ \frac{AP_i + BP_o}{A + B}$$

or in terms of the resistances,

$$p_m = P_{mo}e^{-t/\tau} + (1 - e^{-t/\tau}) \cdot \frac{P_i/(R_1 + R_2) + P_o/R_3}{1/(R_1 + R_2) + 1/R_3} \qquad (D.4)$$

Having found the expression for the storage term, P_m, the next step is to obtain an expression for P_s.

Conservation of mass flux around the node P_s yields

$$\frac{P_m - P_s}{R_2} + \frac{P_i - P_s}{R_1} = 0$$

Solving for P_s gives

$$P_s = \frac{R_1}{R_1 + R_2}\ P_m + \frac{R_2}{R_1 + R_2}\ P_i$$

and substituting the expression for P_m yields

$$P_s = \frac{R_1}{R_1 + R_2} \cdot P_{mo}e^{-t/\tau} + \frac{R_1}{R_1 + R_2}\ (1 - e^{-t/\tau})$$

$$\cdot \left[\frac{\frac{P_i}{R_1 + R_2} + \frac{P_o}{R_3}}{\frac{1}{R_1 + R_2} + \frac{1}{R_3}}\right] + \frac{R_2}{R_1 + R_2} P_i \qquad (D.5)$$

For the limit of $t \to \infty$, $e^{-t/\tau} \to 0$ and

This reduces to Eq. (D.6) for the steady-state case.

$$P_s(\infty) = \frac{R_1}{R_1 + R_2} \left[\frac{\frac{P_i}{R_1 + R_2} + \frac{P_o}{R_3}}{\frac{1}{R_1 + R_2} + \frac{1}{R_3}}\right] + \frac{R_2}{R_1 + R_2} P_i \qquad (D.6)$$

This matches with Eq. (3.1) for steady-state transfer.
Sample Calculation:

Comparison of model response with experiments using blood data of August 3,

Re = 160	r_o = 0.873125 cm
P_i = 20 mm Hg	r_i = 0.635 cm
P_o = 661 mm Hg	α_b = 0.0223 cc/cc-atm
h_d = 0.0113 cm/s	α_m =0.31 cc/cc-atm

$$R_1 = \frac{1}{2\pi r_i \, h_d \, L \, (\alpha_b/\alpha_m)} = \frac{308.3}{L} \left[\frac{s}{cc}\right]$$

$$R_2 = \frac{\ln \left\{(r_i + \frac{r_o + r_i}{2})/r_i\right\}}{2\pi \, D_m \, L} = \frac{1709.5}{L} \left[\frac{s}{cc}\right]$$

$$R_3 = \frac{\ln \left\{ r_o / \left(r_i + \frac{r_o - r_i}{2} \right) \right\}}{2\pi D_m L} = \frac{1458.3}{L} \left[\frac{s}{cc} \right]$$

$$\frac{1}{\tau} = \frac{1}{\pi (r_o^2 - r_i^2) L} \left[\frac{1}{R_1 + R_2} + \frac{1}{R_3} \right]$$

$$\rightarrow \quad \tau = 955 \text{ s}$$

$$P_s = \frac{R_1}{R_1 + R_2} (1 - e^{-t/\tau}) \left[\frac{\frac{P_i}{R_1 + R_2} + \frac{P_o}{R_3}}{\frac{1}{R_1 + R_2} + \frac{1}{R_3}} \right] + \frac{R_2}{R_1 + R_2} P_i$$

Substitution of the resistance gives the relation between the measured partial pressure of oxygen, P_s, and the time, t.

$$P_s = 80 - 63\, e^{-t/\tau} \text{ mm Hg.} \qquad \text{(D.7)}$$

Figure 35 shows the comparison of the measured values of P_s with that of the P_s values obtained from Eq. (D.7). The experimental response was about 30 minutes.

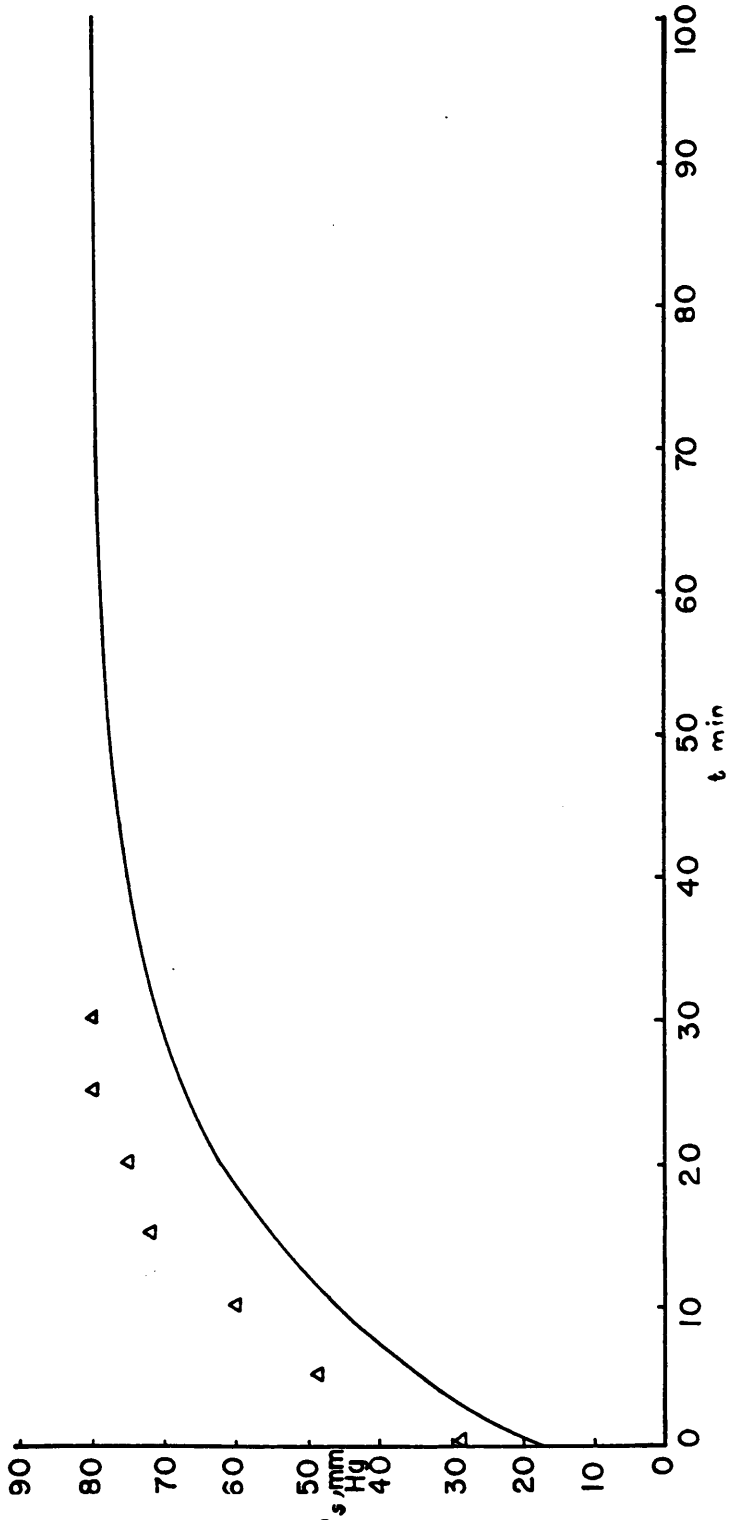

Fig. 35. Comparison of measured P_s with those of P_s obtained from Equation (D.7)

APPENDIX E

Tabulation of Calculated Mass Transfer Coefficients from Experiments

The data presented in this appendix show the results of the calculated mass transfer coefficients from experimental values.

Table 2. Calculated Mass Transfer Results for Saline at Re = 160, 7/14/84

Date: 7/14/84
Barometric pressure: 707 mm Hg
Mean flow rate: 0.03 ℓ/min.
Reynolds number: 160
Transfer gases: 100% O_2 and 100% N_2

x (cm)	x/D	Time	t (min)	Measured P_s (mm Hg)	Δ (mm Hg)	Corrected P_s (mm Hg)	$\frac{P_s - P_o}{P_i - P_s}$	h_d (cm/s)	Sh
1	0.79	2:50	142	350	-2.85	353	0.9	0.00099	44.3
2	1.57	3:10	162	340	-1.98	342	0.9	0.0011	46.9
3	2.36	3:13	165	220	-1.85	222	2.0	0.0022	99.6
4	3.15	3:15	167	110	-1.77	112	5.0	0.0056	250.8
5	3.94	3:18	170	85	-1.64	86	6.7	0.0076	339.8
6	4.72	3:25	177	75	-1.33	76	7.7	0.0088	390.9
7	5.51	3:29	181	65	-1.16	66	9.7	0.010	457.9
8	6.30	3:32	184	80	-1.03	81	7.0	0.0081	361.7
9	7.09	3:34	186	95	-0.94	96	6.1	0.0066	296.1
10	7.81	3:38	190	110	-0.77	111	5.9	0.0056	247.9
11	8.66	3:41	193	120	-0.64	121	4.9	0.0050	223.2
12	9.45	3:44	196	120	-0.51	121	4.5	0.0049	221.7
13	10.24	3:46	198	140	-0.42	140	3.7	0.0041	183.8
14	11.00	3:48	200	145	-0.34	145	3.6	0.0039	175.0
15	11.80	3:50	202	165	-0.25	165	3.0	0.0033	147.3
13	10.24	3:52	204	140	-0.16	140	3.7	0.0041	182.7
11	8.66	3:54	206	124	-0.076	124	4.3	0.0048	213.9
9	7.09	3:56	208	94	-0.011	94	6.0	0.0066	294.1
7	5.51	3:58	210	65	0.097	65	9.1	0.010	448.7
5	3.94	4:00	212	88	0.184	88	6.5	0.0072	320.8
3	2.36	4:02	214	300	0.27	300	1.2	0.0013	57.9
1	0.79	4:04	216	360	0.36	360	0.8	0.00091	40.6

Table 3. Calculated Mass Transfer Results for saline at Re = 160, 7/31/84

Date: 7/31/84
Barometric pressure: 707 mm Hg
Mean flow rate: 0.03 ℓ/min.
Reynolds number: 160
Transfer gases: 100% O_2 and 100% N_2

x (cm)	x/D	Time (min)	t (min)	Measured P_s (mm Hg)	Δ (mm Hg)	Corrected P_s (mm Hg)	$\frac{P_s - P_o}{P_i - P_s}$	h_d (cm/s)	Sh
1	0.79	12:50	120	380	-4.6	385	0.7	0.00083	36.4
2	1.57	12:53	123	343	-4.5	348	0.9	0.0010	46.7
3	2.36	12:57	127	211	-4.3	215	2.1	0.0024	106.5
4	3.15	1:01	131	116	-4.2	120	5.	0.0050	240.6
5	3.94	1:05	135	87	-4.0	91	6.3	0.0070	339.8
6	4.72	1:10	140	69	-3.8	73	8.1	0.0090	436.7
7	5.51	1:13	143	59	-3.7	63	9.5	0.011	525.3
8	6.30	1:16	146	84	-3.6	88	6.5	0.0070	354.4
9	7.09	1:20	150	90	-3.5	94	6.0	0.0070	320.9
10	7.87	1:23	153	105	-3.4	108	5.1	0.0060	262.5
11	8.66	1:26	156	123	-3.3	126	2.	0.0046	220.2
12	9.45	1:28	158	125	-3.2	128	2.	0.0046	215.8
13	10.24	1:31	161	144	-3.1	147	5.	0.0040	179.4
14	11.02	1:34	164	147	-3.0	150	4.	0.0037	175.0
15	11.81	1:37	167	165	-2.8	168	3.0	0.0033	148.7
13	10.24	1:40	170	146	-2.7	149	4.	0.0037	176.5
11	8.66	1:43	173	124	-2.6	127	2.	0.0046	216.6
9	7.09	1:46	176	95	-2.5	98	5.7	0.0063	300.3
7	5.51	1:48	178	68	-2.4	70	8.4	0.010	442.9
5	3.94	1:52	182	87	-2.3	89	4.	0.0070	330.3
3	2.36	1:55	185	215	-2.2	217	0	0.0022	102.9
1	0.79	1:58	188	370	-2.1	372	0.8	0.00080	38.8

Table 4. Calculated Mass Transfer Results for Saline at Re = 450, 8/24/84

Date: 8/24/84
Barometric pressure: 707 mm Hg
Mean flow rate: 0.073 ℓ/min.
Reynolds number: 450
Transfer gases: 100% O_2 and 100% N_2

x (cm)	x/D	Actual P_s (mm Hg)	$\frac{P_s - P_o}{P_i - P_s}$	h_d (cm/s)	Sh
1	0.79	245	1.69	0.0019	83.1
2	1.57	225	1.93	0.0021	94.8
3	2.36	195	2.38	0.0026	116.9
4	3.15	175	2.77	0.0030	135.9
5	3.94	120	4.50	0.0049	220.2
6	4.72	50	12.20	0.013	597.9
7	5.51	25	25.40	0.023	1245.5
8	6.30	30	21.00	0.023	1029.7
9	7.09	35	17.86	0.019	876.5
10	7.87	60	10.00	0.011	490.0
11	8.66	70	8.43	0.0093	412.7
12	9.45	80	7.25	0.0080	355.9
13	10.24	82	7.05	0.0078	345.7
14	11.02	85	6.77	0.0075	332.5
15	11.81	100	5.60	0.0062	274.2
13	10.24	80	7.25	0.0080	355.6
11	8.66	70	8.43	0.0093	413.5
9	7.09	40	15.50	0.017	762.0
7	5.51	28	22.57	0.025	1105.1
5	3.94	120	4.50	0.0049	220.6
3	2.36	205	2.22	0.0024	108.7
1	0.79	245	1.69	0.0019	82.9

Table 5. Calculated Mass Transfer Results for Saline at Re = 850, 8/14/84

Dage: 8/14/84
Barometric pressure: 707 mm Hg
Mean flow rate: 0.14 ℓ/min.
Reynolds number: 850
Transfer gases: 100% O_2 and 100% N_2

(cm)	x/D	Time	Actual P_s (mm Hg)	$\frac{P_s - P_o}{P_i - P_s}$	h_d (cm/s)	Sh
1	0.79	3:30	210	2.14	0.0024	105.4
2	1.57	3:33	172	2.84	0.0031	140.0
3	2.36	3:35	100	5.60	0.0062	270.0
4	3.15	3:30	85	6.76	0.0074	331.3
5	3.94	3:42	52	11.7	0.013	573.3
6	4.72	3:45	62	9.65	0.011	473.8
7	5.51	3:49	94	6.02	0.0066	294.2
8	6.30	3:53	71	8.30	0.0091	407.2
9	7.09	3:56	87	6.59	0.0073	323.8
10	7.87	3:59	90	6.33	0.0070	310.3
11	8.66	7:02	98	5.73	0.0063	281.6
12	9.45	4:05	110	5.00	0.0055	245.3
13	10.24	4:08	147	3.49	0.0038	170.3
14	11.02	4:11	162	3.07	0.0034	150.1
15	11.81	4:14	184	2.59	0.0029	126.5
13	10.24	4:17	149	3.43	0.0038	167.8
11	8.66	4:20	100	5.6	0.0062	274.0
9	7.09	4:24	87	6.59	0.0073	323.8
7	5.51	4:27	95	5.95	0.0066	291.7
5	3.94	4:30	53	11.45	0.013	561.5
3	2.36	4:33	53	5.6	0.0062	274.0
1	0.79	4:37	210	2.14	0.0024	105.4

Table 6. Calculated Mass Transfer Results for Saline at Re = 850, 8/16/84

Date: 8/16/84
Barometric pressure: 707 mm Hg
Mean flow rate: 0.14 ℓ/min.
Reynolds number: 850
Transfer gases: 100% O_2 and 100% N_2

x (cm)	x/D	Time (min.)	t (min.)	Measured P_s (mm Hg)	Δ (mm Hg)	Corrected P_s (mm Hg)	$\frac{P_s - P_o}{P_i - P_s}$	h_d (cm/s)	Sh
1	0.79	3:55	175	220	-3.2	223	2.0	0.0023	100.3
2	1.57	3:59	179	120	-3.0	123	4.4	0.0051	227.6
3	2.36	4:04	184	100	-2.9	103	5.4	0.0064	268.1
4	3.15	4:09	189	40	-2.7	43	15.0	0.018	817.0
5	3.94	4:12	192	18	-2.6	21	31.0	0.034	2057.2
6	4.72	4:15	195	50	-2.5	53	11.5	0.0142	633.2
7	5.51	4:19	199	88	-2.4	90	6.3	10.0074	329.7
8	6.30	4:21	201	102	-2.3	104	5.3	0.0062	275.7
9	7.09	4:25	205	124	-2.2	126	4.2	0.0049	217.5
10	7.87	4:29	209	147	-2.0	149	3.4	0.0039	173.7
11	8.66	4:33	213	165	-1.9	167	3.0	0.0034	150.1
12	9.45	4:34	214	192	-1.9	194	2.4	0.0027	121.4
13	10.24	4:35	215	208	-1.8	210	2.2	0.0024	107.9
14	11.02	4:36	216	219	-1.8	221	2.0	0.0023	100.3
15	11.81	4:37	217	232	-1.8	234	1.8	0.0021	91.9
13	10.24	4:40	220	200	-1.7	202	2.3	0.0026	114.6
11	8.66	4:43	223	170	-1.6	172	2.9	0.0032	143.3
9	7.09	4:45	225	130	-1.5	132	4.1	0.0013	202.3
7	5.51	4:47	227	90	-1.4	91	6.3	0.0071	316.2
5	3.94	4:49	229	20	-1.36	21	30.4	0.038	1692.1
3	2.36	4:50	230	100	-1.3	101	5.6	0.0063	278.2
1	0.79	4:53	233	221	-1.2	222	2.0	0.0022	97.8

APPENDIX F

Tabulation of the Variations of the Partial Pressures for Saline

The data presented in this appendix show the minimum and maximum Sherwood numbers obtained from the partial pressures recorded during the experiment.

Table 7. Tabulation of the Variations of the Partial Pressures Recorded During Saline Experiment, 7/14/84

Re = 160 P_b = 0 mm Hg $D_o = 2.85 \times 10^{-5}$ cm^2/s

P_o = 660 mm Hg

x (cm)	x/D	P_s (mm Hg)	$\frac{P_s - P_o}{P_b - P_s}$	h_d (cm/s)	Max. Sh	P_s (mm Hg)	$\frac{P_s - P_o}{P_b - P_s}$	h_d (cm/s)	Min. Sh
1	0.79	303	1.2	1.3E-3	59	438	0.5	5.7E-4	25
2	1.57	322	1.01	1.1E-3	52	362	0.8	9.1E-4	40
3	2.36	202	2.3	2.5E-3	113	232	1.8	1.6E-3	92
4	3.15	102	5.5	6.1E-3	275	122	4.4	4.9E-3	221
5	3.94	84	7.05	7.7E-3	346	90	6.3	7.1E-3	319
6	4.72	70	8.5	9.4E-3	421	79	7.4	8.2E-3	366
7	5.51	61	10.0	1.1E-2	492	68	8.7	9.7E-3	436
8	6.30	71	8.3	9.2E-3	413	86	6.7	7.4E-3	331
9	7.09	93	6.1	6.7E-3	303	99	5.7	6.3E-3	281
10	7.81	99	5.7	6.3E-3	281	116	4.7	5.2E-3	233
11	8.66	116	4.7	5.2E-3	233	126	4.2	4.7E-3	210
12	9.45	116	4.7	5.2E-3	233	126	4.2	4.7E-3	210
13	10.24	125	4.2	4.4E-3	210	145	3.5	3.9E-3	174
14	11.0	130	4.0	4.4E-3	201	150	3.4	3.7E-3	167
15	11.8	150	3.4	3.7E-3	167	175	2.7	3.0E-3	136
13	10.24	130	4.0	4.4E-3	201	150	3.4	3.7E-3	167
11	8.66	118	4.5	5.0E-3	225	130	4.08	4.4E-3	201
9	7.09	90	6.3	6.9E-3	130	98	5.73	6.3E-3	281
7	5.51	63	9.4	1.0E-2	446	67	8.85	9.4E-3	436
5	3.94	86	6.6	7.3E-3	327	90	6.33	6.9E-3	311
3	2.36	250	1.6	7.3E-3	807	350	0.89	9.8E-4	44
1	0.79	280	1.3	1.4E-3	66	440	0.5	5.5E-4	25

Table 8. Tabulation of the Variations of the Partial Pressures Recorded During Saline Experiment, 7/14/84

Re = 160 P_b = 0 mm Hg $D_o = 2.85 \times 10^{05}$ cm^2/s

P_o = 660 mm Hg

x (cm)	x/D	P_s (mm Hg)	$\frac{P_s - P_o}{P_b - P_s}$	h_d (cm/s)	Max. Sh	P_s (mm Hg)	$\frac{P_s - P_o}{P_b - P_s}$	h_d (cm/s)	Min. Sh
1		305	1.2	1.3E-3	58	455	0.5	5.1E-4	23
2		335	1.0	1.1E-3	49	385	0.7	8.1E-4	36
3		204	2.2	2.5E-3	111	234	1.8	2.0E-3	89
4		104	5.4	6.1E-3	272	119	4.5	5.2E-3	232
5		84	7.0	7.9E-3	352	94	6.0	6.9E-3	307
6		69	9.0	1.0E-2	446	74	8.0	9.2E-3	410
7		59	10.0	1.2E-2	535	64	9.3	1.1E-2	490
8		74	8.0	9.2E-3	410	94	6.0	6.9E-3	307
9		74	8.0	9.2E-3	410	104	5.3	6.1E-3	272
10		103	5.4	6.1E-3	272	113	4.8	5.5E-3	245
11		123	4.4	4.9E-3	218	128	4.2	4.7E-3	209
12		123	4.4	4.9E-3	218	153	3.3	3.7E-3	165
13		123	4.4	4.9E-3	218	173	2.8	3.1E-3	138
14		123	4.4	4.9E-3	218	173	2.8	3.1E-3	138
15		133	4.0	4.4E-3	196	183	2.6	2.9E-3	129
13		125	4.3	4.8E-3	214	173	2.8	3.1E-3	138
11		121	4.5	5.0E-3	223	133	4.0	4.4E-3	196
9		93	6.1	6.9E-3	307	103	5.4	6.1E-3	272
7		67	9.0	1.0E-3	446	73	8.0	9.1E-3	406
5		80	7.3	8.2E-3	365	90	6.3	7.1E-3	316
3		182	2.6	2.9E-3	129	252	1.6	1.8E-3	80
1		292	1.3	1.4E-3	62	452	0.5	5.1E-3	227

Table 9. Tabulation of the Variations of the Partial Pressures Recorded During Saline Experiment, 8/24/84

Re = 450 P_b = 0 mm Hg $D_o = 2.85 \times 10^{-5}$ cm^2/s

P_o = 660 mm Hg

x (cm)	x/D	P_s (mm Hg)	$\frac{P_s - P_o}{P_b - P_s}$	h_d (cm/s)	Max. Sh	P_s (mm Hg)	$\frac{P_s - P_o}{P_b - P_s}$	h_d (cm/s)	Min. Sh
1	0.79	200	2.0	2.2E-3	98	290	1.2	1.4E-3	63
2	1.57	180	2.6	2.9E-3	131	270	1.4	1.5E-3	71
3	2.36	160	3.1	3.4E-3	153	230	1.8	2.0E-3	92
4	3.15	110	5.0	5.0E-3	245	240	1.7	1.9E-3	86
5	3.94	70	8.4	9.2E-3	413	170	2.8	3.1E-3	141
6	4.72	20	32.0	3.5E-2	1570	80	7.2	7.9E-3	356
7	5.51	10	65.0	7.2E-2	3188	40	15.5	1.7E-2	759
8	6.30	0	∞	∞	∞	60	10.0	1.1E-2	492
9	7.09	30	21.0	2 3E-2	1030	40	15.5	1.7E-2	759
10	7.81	20	32.0	3.5E-2	1570	100	5.6	6.1E-3	275
11	8.66	50	12.2	3.5E-2	598	90	6.3	6.9E-3	311
12	9.45	50	12.2	1.3E-2	598	110	5.0	5.5E-3	245
13	10.24	50	12.2	1.3E-2	598	114	4.7	5.2E-3	235
14	11.0	50	12.2	1.3E-2	598	120	4.5	4.9E-3	221
15	11.8	40	15.5	1.8E-2	760	160	3.1	3.4E-3	153
13	10.24	50	12.2	1.3E-2	597	110	5.0	5.5E-3	245
11	8.66	51	11.9	1.3E-2	584	89	6.4	7.0E-3	315
9	7.09	30	21.0	2.3E-2	1030	50	32.0	3.5E-2	1560
7	5.51	10	65.0	7.2E-2	3188	46	13.3	1.5E-2	668
5	3.94	70	8.4	9.2E-3	413	170	2.8	3.1E-3	141
3	2.36	150	3.4	3.7E-3	167	260	1.5	1.7E-3	76
1	0.79	200	2.0	2.2E-3	98	290	1.2	1.4E-3	63

Table 10. Tabulation of the Variations of the Partial Pressures Recorded During Saline Experiment, 8/14/84

Re = 850 P_b = 0 mm Hg $D_o = 2.85 \times 10^{-5}$ cm^2/s

P_o = 660 mm Hg

x (cm)	x/D	P_s (mm Hg)	$\frac{P_s - P_o}{P_b - P_s}$	h_d (cm/s)	Max. Sh	P_s (mm Hg)	$\frac{P_s - P_o}{P_b - P_s}$	h_d (cm/s)	Min. Sh
1		110	5.0	5.5E-3	245	310	1.1	1.2E-3	55
2		106	5.2	5.7E-3	257	238	1.7	1.9E-3	87
3		70	8.4	9.2E-3	414	130	4.0	4.4E-3	200
4		52	11.7	1.2E-2	575	118	4.5	5.5E-3	225
5		25	25.4	2.8E-2	1248	79	7.3	8.0E-3	361
6		31	20.3	2.2E-2	994	93	6.0	6.7E-3	299
7		60	10.0	1.1E-2	490	128	4.1	4.5E-3	204
8		51	11.9	1.3E-2	584	91	6.2	6.8E-3	307
9		61	9.8	1.0E-2	481	113	4.8	5.3E-3	238
10		55	11.0	1.2E-2	539	125	4.2	4.7E-3	210
11		70	8.43	9.2E-3	414	126	4.2	4.6E-3	208
12		72	8.1	8.9E-3	401	148	3.4	3.8E-3	170
13		113	4.8	5.3E-3	238	181	2.6	2.9E-3	130
14		106	5.2	5.7E-3	257	218	2.0	2.2E-3	99
15		110	5.0	5.5E-3	245	258	1.5	1.7E-3	77
13		98	5.7	6.3E-3	281	200	2.3	2.5E-3	113
11		72	8.1	8.9E-3	401	128	4.1	4.5E-3	204
9		55	11.0	1.2E-2	539	119	4.5	5.0E-3	223
7		63	9.4	1.0E-2	463	127	4.2	4.6E-3	206
5		20	32.0	3.5E-2	1569	86	6.6	7.3E-3	327
3		60	10.0	1.1E-2	490	140	3.7	4.0E-3	182
1		90	6.3	6.9E-3	310	330	1.0	1.1E-3	49

Table 11. Tabulation of the Variations of the Partial Pressures Recorded During Saline Experiment. 8/16/84

Re = 850 P_b = 0 mm Hg $D_o = 2.85 \times 10^{-5}$ cm^2/s
P_o = 660 mm Hg

x (cm)	x/d	P_s (mm Hg)	$\frac{P_s - P_o}{P_b - P_s}$	h_d (cm/s)	Max. Sh	($mm P_s$ Hg)	$\frac{P_s - P_o}{P_b - P_s}$	($cm h_d$/s)	Min. Sh
1	0.79	163	3.0	3.4E-3	154	283	1.3	1.5E-3	67
2	1.57	113	4.8	5.5E-3	245	133	4.0	4.4E-3	200
3	2.35	93	6.1	6.9E-3	311	113	5.0	5.5E-3	245
4	3.15	18	35.7	4.7E-2	2094	88	6.5	7.4E-3	332
5	3.94	10	65.0	7.0E-2	3208	43	14.5	1.7E-2	758
6	4.72	53	11.5	1.3E-2	579	73	8.0	9.2E-3	414
7	5.51	72	8.2	9.2E-3	412	92	6.2	6.9E-3	311
8	6.30	102	5.5	6.1E-3	274	106	5.2	5.8E-3	262
9	7.09	102	5.5	6.1E-3	274	126	4.2	4.7E-3	212
10	7.81	126	4.2	4.7E-3	212	172	2.8	3.1E-3	141
11	8.66	132	4.0	4.4E-3	200	202	2.3	2.5E-3	113
12	9.45	190	2.5	2.7E-3	123	198	2.3	2.6E-3	116
13	10.24	202	2.3	2.5E-3	113	218	2.0	2.2E-3	101
14	11.0	202	2.3	2.5E-3	113	240	1.7	1.9E-3	87
15	11.8	182	2.6	2.9E-3	131	286	1.3	1.4E-3	65
13	10.24	192	2.5	2.7E-3	121	212	2.1	2.3E-3	105
11	8.66	142	3.6	4.0E-3	182	202	2.3	2.5E-3	113
9	7.09	102	5.5	6.1E-3	274	162	3.1	3.4E-3	153
7	5.51	81	7.1	7.9E-3	356	101	5.6	6.1E-3	153
5	3.94	13	50.0	5.8E-2	2629	45	14.0	1.5E-2	668
3	2.36	91	6.3	6.9E-3	311	111	5.0	5.5E-3	245
1	0.79	151	3.4	3.7E-3	167	293	1.2	1.3E-3	62

APPENDIX G

Comparison Between Experimental Sherwood Numbers and Calculated Sherwood Numbers for Saline

The experimental Sherwood numbers in this appendix were obtained from the measured partial pressures while the calculated Sherwood numbers were obtained from the computer programs in Appendix A.

Table 12 Comparison between experimental Sherwood numbers and calculated Sherwood numbers for saline at Re=160, 7/14/84

Date: 7/14/84
Barometric pressure: 707 mm Hg
Mean flow rate: 0.03 l/min
Downstream tubing diameter: 1.27 cm
Reynolds number: 160
D_c: 2.85E-5 cm^2/s
Transfer gases: 100% O_2 and 100% N_2

x(cm)	x^+	Sh_{exp}	Sh_{calc}	(Sh_{exp}/Sh_{calc})
1	8.95E-5	44.3	33.0	1.3
2	1.79E-4	46.9	25.5	1.8
3	2.69E-4	99.6	22.0	4.5
4	3.58E-4	250.8	19.8	12.7
5	4.48E-4	339.8	18.3	18.6
6	5.37E-4	391.0	17.1	22.9
7	6.27E-4	458.0	16.1	28.5
8	7.16E-4	361.7	15.4	23.5
9	8.06E-4	296.1	14.8	20.0
10	8.95E-4	247.9	14.2	17.5
11	9.85E-4	223.2	13.7	16.3
12	1.07E-3	221.7	13.3	16.7
13	1.16E-3	183.8	12.9	14.3
14	1.25E-3	175.0	12.6	13.9
15	1.34E-3	147.3	12.3	11.9
13	1.16E-3	182.7	12.9	14.2
11	9.85E-4	213.9	13.7	15.6
9	8.06E-4	294.1	14.8	19.9
7	6.27E-4	448.7	16.1	27.9
5	4.48E-4	320.8	18.3	17.6
3	2.69E-4	57.9	22.0	2.6
1	8.95E-5	40.6	33.0	1.2

Table 13 Comparison between experimental Sherwood numbers and calculated Sherwood numbers for saline at Re=160, 7/31/84

Date: 7/31/84
Barometric pressure: 707 mm Hg
Mean flow rate: 0.03 l/min
Downstream tubing diameter: 1.27 cm
Reynolds number: 160
D_c: 2.85E-5 cm^2/s
Transfer gases: 100% O_2 and 100% N_2

x(cm)	x^+	Sh_{exp}	Sh_{calc}	(Sh_{exp}/Sh_{calc})
1	8.95E-5	36.4	33.0	1.1
2	1.79E-4	46.7	25.5	1.8
3	2.69E-4	106.5	22.0	4.8
4	3.58E-4	240.6	19.8	12.2
5	4.48E-4	339.8	18.3	18.6
6	5.37E-4	436.7	17.1	25.5
7	6.27E-4	525.3	16.1	32.6
8	7.16E-4	354.4	15.4	23.0
9	8.06E-4	320.9	14.8	21.7
10	8.95E-4	262.5	14.2	18.5
11	9.85E-4	220.2	13.7	16.1
12	1.07E-3	215.8	13.3	16.2
13	1.16E-3	179.4	12.9	13.9
14	1.25E-3	175.0	12.6	13.9
15	1.34E-3	148.7	12.3	12.1
13	1.16E-3	176.5	12.9	13.7
11	9.85E-4	216.6	13.7	15.8
9	8.06E-4	300.3	14.8	20.3
7	6.27E-4	442.9	16.1	27.5
5	4.48E-4	330.5	18.3	18.1
3	2.69E-4	102.9	22.0	4.7
1	8.95E-5	38.8	33.0	1.2

Table 14 Comparison between experimental Sherwood numbers and calculated Sherwood numbers for saline at Re=450, 8/24/84

Date: 8/24/84
Barometric pressure: 707 mm Hg
Mean flow rate: 0.073 l/min
Downstream tubing diameter: 1.27 cm
Reynolds number: 450
D_c: 2.85E-5 cm^2/s
Transfer gases: 100% O_2 and 100% N_2

x(cm)	x^+	Sh_{exp}	Sh_{calc}	(Sh_{exp}/Sh_{calc})
1	3.68E-5	83.1	49.0	1.7
2	7.36E-5	94.8	35.5	2.7
3	1.10E-4	116.9	30.6	3.8
4	1.47E-4	135.9	27.4	4.9
5	1.84E-4	220.2	25.2	8.7
6	2.21E-4	597.9	23.7	25.2
7	2.58E-4	1245.5	22.3	55.9
8	2.94E-4	1029.7	21.2	48.6
9	3.31E-4	876.5	20.3	43.2
10	3.68E-4	490.0	19.6	25.0
11	4.05E-4	412.7	18.9	21.8
12	4.42E-3	355.9	18.4	19.4
13	4.78E-3	345.7	17.8	19.4
14	5.15E-3	332.5	17.3	19.2
15	5.52E-3	274.2	16.9	16.2
13	4.78E-3	355.6	17.8	20.0
11	4.05E-4	413.5	18.9	21.9
9	3.31E-4	762.0	20.3	37.5
7	2.58E-4	1105.1	22.3	49.6
5	1.84E-4	220.6	25.2	8.8
3	1.10E-4	108.7	30.6	3.6
1	3.68E-5	82.9	49.0	1.7

Table 15 Comparison between experimental Sherwood numbers and calculated Sherwood numbers for saline at Re=850, 8/14/84

Date: 8/14/84
Barometric pressure: 707 mm Hg
Mean flow rate: 0.14 l/min
Downstream tubing diameter: 1.27 cm
Reynolds number: 850
D_c: 2.85E-5 cm^2/s
Transfer gases: 100% O_2 and 100% N_2

x(cm)	x^+	Sh_{exp}	Sh_{calc}	(Sh_{exp}/Sh_{calc})
1	1.92E-5	105.4	65.0	1.6
2	3.84E-5	140.0	47.0	3.0
3	5.76E-5	274.0	39.0	7.0
4	7.67E-5	331.3	35.0	9.5
5	9.59E-5	573.3	32.0	18.0
6	1.15E-4	473.8	30.1	15.7
7	1.34E-4	294.2	28.4	10.4
8	1.53E-4	407.2	27.0	15.1
9	1.73E-4	323.8	26.0	12.4
10	1.92E-4	310.3	24.8	12.5
11	2.11E-4	281.6	24.1	11.7
12	2.30E-3	245.3	23.3	10.5
13	2.49E-3	170.3	22.6	7.5
14	2.69E-3	150.1	21.9	6.9
15	2.88E-3	126.5	21.4	5.9
13	2.49E-3	167.8	22.6	7.4
11	2.11E-4	274.0	24.1	11.4
9	1.73E-4	323.8	26.0	12.5
7	1.34E-4	291.7	28.4	10.3
5	9.59E-5	561.5	32.0	17.5
3	5.76E-5	274.0	39.0	7.0
1	1.92E-5	105.4	65.0	1.6

Table 16 Comparison between experimental Sherwood numbers and calculated Sherwood numbers for saline at Re=850, 8/16/84

Date: 8/16/84
Barometric pressure: 707 mm Hg
Mean flow rate: 0.14 l/min
Downstream tubing diameter: 1.27 cm
Reynolds number: 850
D_c: 2.85E-5 cm^2/s
Transfer gases: 100% O_2 and 100% N_2

x(cm)	x^+	Sh_{exp}	Sh_{calc}	(Sh_{exp}/Sh_{calc})
1	1.92E-5	100.3	65.0	1.5
2	3.84E-5	227.6	47.0	4.8
3	5.76E-5	268.1	39.0	6.9
4	7.67E-5	817.0	35.0	23.3
5	9.59E-5	2057.2	32.0	64.3
6	1.15E-4	633.2	30.1	21.0
7	1.34E-4	329.7	28.4	11.6
8	1.53E-4	275.7	27.0	10.2
9	1.73E-4	275.7	26.0	8.4
10	1.92E-4	217.5	24.8	7.0
11	2.11E-4	173.7	24.1	6.2
12	2.30E-3	121.4	23.3	5.2
13	2.49E-3	107.9	22.6	4.8
14	2.69E-3	100.3	21.9	4.6
15	2.88E-3	91.9	21.4	4.3
13	2.49E-3	114.6	22.6	5.1
11	2.11E-4	143.3	24.1	5.9
9	1.73E-4	202.3	26.0	7.8
7	1.34E-4	316.2	28.4	11.1
5	9.59E-5	1692.1	32.0	52.9
3	5.76E-5	278.2	39.0	7.1
1	1.92E-5	97.8	65.0	1.5

APPENDIX H

Calculated Mass Transfer Results for Whole Blood

This appendix shows the mass transfer results obtained from the measured values of the partial pressures obtained during the experiments.

Table 17. Calculated Mass Transfer Results for Whole Blood with $D_c = 1.5 \times 10^{-5}$ cm^2/s at Re = 160

Date: 8/3/84
Barometric pressure: 707 mm Hg
Mean flow rate: 0.14 ℓ/min.
Reynolds number: 160
Transfer gases: 100% O_2 and 3% O_2

X (cm)	X/D	Time (min.)	t (mm Hg)	P_s (mm Hg)	Δ (mm Hg)	Actual P_s (mm Hg)	$\frac{P_s - P_o}{P_i - P_s}$	h_d (cm/s)	Sh
1	0.79	12:58	38	43	-37.4	80.4	9.6	0.011	970
2	1.57	1:02	42	35	-37.3	72.3	11.2	0.013	1109
3	2.36	1:08	48	22	-37.2	59.2	15.3	0.018	1524
4	3.15	1:16	56	-8	-37.1	29.1	69.3	0.082	6925
5	3.94	1:19	59	-9	-37.0	28.0	79.0	0.093	7897
6	4.72	1:22	62	-10	-37.0	27.0	90.4	0.11	9034
7	5.51	1:28	68	-9	-36.9	27.9	80.0	0.094	7981
8	6.30	1:32	72	-6	-36.8	30.8	58.3	0.069	5819
9	7.09	1:36	76	-2	-36.7	34.7	42.5	0.050	4240
10	7.87	1:40	80	2	-36.7	38.7	33.2	0.039	3325
11	8.66	1:46	86	7	-36.6	43.6	26.1	0.31	2608
12	9.45	1:50	90	12	-36.5	48.5	21.5	0.025	2147
13	10.24	1:54	94	21	-36.4	57.4	16.1	0.019	1607
14	11.02	1:58	98	25	-36.7	61.3	14.5	0.017	1449
15	11.81	2:04	104	28	-36.2	64.2	13.5	0.016	1350
13	10.24	2:08	108	22	-36.2	58.2	15.8	0.019	1579
11	9.66	2:12	112	10	-36.1	46.1	23.5	0.028	2347
9	7.09	2:16	116	-1	-36.0	35.0	41.7	0.049	4157
7	5.51	2:21	121	-8	-36.0	28.0	79.0	0.093	7897
5	3.94	2:25	125	-7	35.9	28.9	70.9	0.084	7094
3	2.36	2:29	129	25	-35.8	60.8	14.7	0.017	1469
1	0.79	2:37	137	44	-35.7	79.7	9.7	0.011	970

Table 18. Calculated Mass Transfer Results for Whole Blood with $D_c = 1.5 \times 10^{-5}$ cm^2/s at Re = 450.

Date: 8/20/84
Barometric pressure: 707 mm Hg.
Mean flow rate: 0.40 ℓ/min.
Reynolds number: 450
Transfer gases: 100% O_2 and 3% O_2

x (cm)	x/D	Time	t (min.)	P_s (mm Hg)	Δ (mm Hg)	Actual P_s (mm Hg)	$\frac{P_s - P_o}{P_i - P_s}$	h_d (cm/s)	Sh
1	0.79	1:40	40	62.0	-14.2	76.2	10.4	0.012	1040
2	1.57	1:45	45	60.0	-13.8	73.8	10.9	0.013	1089
3	2.36	1:48	48	30.0	-13.6	43.6	26.1	0.031	2610
4	3.15	1:50	50	17.5	-13.5	30.9	57.5	0.068	5739
5	3.94	1:52	52	13.0	-13.3	26.3	100.4	0.12	10031
6	4.72	1:54	54	9.0	-13.2	22.2	293.9	0.35	29359
7	5.51	1:56	56	14.0	-13.0	27.0	90.0	0.11	9006
8	6.30	1:59	59	18.0	-12.8	30.8	58.2	0.069	5819
9	7.09	2:04	64	20.0	-12.5	32.5	50.4	0.059	5031
10	7.87	2:07	67	38.0	-12.3	50.3	20.2	0.024	2023
11	8.66	2:10	70	40.0	-12.0	52.0	18.9	0.022	1884
12	9.45	2:12	72	48.0	-11.9	59.9	15.0	0.018	1442
13	10.24	2:14	74	50.0	-11.8	61.8	14.3	0.017	1431
14	11.02	2:17	77	53.0	-11.5	64.5	13.4	0.016	1335
15	11.81	2:21	81	58.0	-11.3	69.3	11.9	0.014	1191
13	10.24	2:23	83	53.0	-11.1	64.1	13./5	0.016	1357
11	8.66	2:25	85	42.0	-10.9	52.9	18.4	0.022	1829
9	7.09	2:27	87	27.0	-10.8	37.8	34.9	0.041	3485
7	5.51	2:29	89	17.0	-10.7	27.7	82.3	0.097	8230
5	3.94	2:32	92	13.0	-10.5	23.5	183.4	0.22	18316
3	2.36	2:35	95	31.0	-10.3	41.3	29.1	0.034	2910
1	0.79	2:38	98	61.0	-10.1	71.1	11.5	0.014	1153

APPENDIX I

Comparison Between Experimental Sherwood Numbers and Calculated Sherwood Numbers for Whole Blood

In this appendix a comparison between the experimental Sherwood numbers and the calculated Sherwood numbers (Appendix B) for whole blood are presented for $D_c = 1.5 \times 10^{-5}$ cm^2/s, $D_c = 2.0 \times 10^{-5}$ cm^2/s and $D_c = 3.0 \times 10^{-5}$ cm^2/s.

Table 19 Comparison of experimental Sherwood number and calculated Sherwood numbers for blood at Re=160 and D_c=1.5E-5 cm_2/s

Date: 8/3/84
Barometric pressure: 707 mm Hg
Mean flow rate: 0.14 l/min
Downstream tubing diameter: 1.27 cm
Reynolds number: 160
D_c: 1.5E-5 cm^2/s
Transfer gases: 100% O_2 and 3% O_2

x(cm)	x^+	Sh_{exp}	Sh_{calc}	(Sh_{exp}/Sh_{calc})
1	1.01E-5	970	343.7	2.8
2	2.02E-5	1109	212.4	5.2
3	3.03E-5	1524	132.5	11.5
4	4.04E-5	6925	126.5	54.7
5	5.05E-5	7897	123.3	64.1
6	6.06E-5	9034	120.2	75.2
7	7.07E-5	7981	116.7	68.4
8	8.08E-5	5819	112.0	52.0
9	9.09E-5	4240	105.3	40.3
10	1.01E-4	3325	95.4	34.9
11	1.11E-4	2608	84.6	30.8
12	1.21E-4	2147	78.9	27.2
13	1.31E-4	1607	77.0	20.9
14	1.41E-4	1449	76.1	19.0
15	1.51E-4	1350	75.5	17.9
13	1.31E-4	1579	77.0	20.5
11	1.11E-4	2347	84.6	27.7
9	9.09E-5	4157	105.3	39.5
7	7.07E-5	7897	116.7	67.7
5	5.05E-5	7094	123.3	57.5
3	3.03E-5	1469	132.5	11.1
1	1.01E-5	970	343.7	2.8

Table 20 Comparison of experimental Sherwood numbers and calculated Sherwood numbers for blood at Re=450 and D_c=1.5E-5 cm_2/s

Date: 8/20/84
Barometric pressure: 707 mm Hg
Mean flow rate: 0.40 l/min
Downstream tubing diameter: 1.27 cm
Reynolds number: 450
D_c: 1.5E-5 cm^2/s
Transfer gases: 100% O_2 and 3% O_2

x(cm)	x^+	Sh_{exp}	Sh_{calc}	(Sh_{exp}/Sh_{calc})
1	3.53E-6	1040	390.0	2.7
2	7.07E-6	1089	369.2	3.0
3	1.06E-5	2610	346.5	7.5
4	1.41E-5	5739	318.8	18.0
5	1.77E-5	10031	214.6	46.7
6	2.12E-5	29359	131.5	223.3
7	2.47E-5	9006	130.3	69.1
8	2.83E-5	5819	130.3	44.8
9	3.18E-5	5031	129.0	39.0
10	3.53E-5	2023	128.0	15.8
11	3.89E-5	1884	127.0	14.8
12	4.24E-5	1442	126.0	11.4
13	4.59E-5	1442	125.0	11.5
14	4.95E-5	1335	124.0	10.8
15	5.30E-5	1191	123.0	9.7
13	4.59E-5	1357	125.0	10.9
11	3.89E-5	1829	127.0	14.4
9	3.18E-5	3485	129.0	27.0
7	2.47E-5	8230	130.3	63.2
5	1.77E-5	18316	214.6	85.4
3	1.06E-5	2910	346.5	8.4
1	3.53E-6	1153	390.0	3.0

Table 21. Comparison of Experimental Sherwood Number with $D_c = 1.5 \times 10^{-5}$ cm^2/s and calculated Sherwood Numer with $D_c = 2.0 \times 10^{-5}$ cm^2/s for Whole Blood at Re = 160

Re = 160 Q = 0.14 ℓ/min $\gamma_w = 198\ s^{-1}$
$D_c = 2.0 \times 10^{-5}$ cm^2/s

x (cm)	s^+	Sh_{exp}	Sh_{calc}	Sh_{exp}/Sh_{calc}
1	1.32E-5	970	428.9	2.3
2	2.69E-5	1109	241.6	4.6
3	4.05E-5	1524	170.0	8.9
4	5.39E-5	6925	165.3	41.9
5	6.73E-5	7897	160.0	49.4
6	8.08E-5	9034	154.7	58.4
7	9.42E-5	7981	148.0	53.9
8	1.08E-4	5819	137.3	42.4
9	1.21E-4	4240	125.3	33.8
10	1.35E-4	3325	110.5	30.1
11	1.48E-4	2608	104.0	25.1
12	1.62E-4	2147	101.3	21.2
13	1.75E-4	1607	100.0	16.0
14	1.88E-4	1449	99.1	14.6
15	2.02E-4	1350	98.0	13.8
13	1.75E-4	1579	100.2	15.8
11	1.48E-4	2347	104.0	22.6
9	1.21E-4	4157	125.3	33.2
7	9.42E-5	7897	148.0	53.4
5	6.73E-5	7094	160.0	44.3
3	4.04E-5	1469	170.0	8.6
1	1.35E-5	970	428.9	2.3

Table 22. Comparison of Experimental Sherwood Number with $D_c = 1.5 \times 10^{-5}$ cm^2/s and Calculated Sherwood Number with $D_c = 3.0 \times 10^{-5}$ cm^2/s at Re = 450

Re = 450 Q = 0.41 ℓ/min. $\gamma_w = 568\ s^{-1}$

$D_c = 3.0 \times 10^{-5}$ cm^2/s

x (cm)	x^+	Sh_{exp}	Sh_{calc}	Sh_{exp}/Sh_{calc}
1	7.07E-6	1040	732.0	1.4
2	1.41E-5	1089	661.6	1.7
3	2.12E-5	2610	587.0	4.5
4	2.83E-5	5739	494.4	11.6
5	3.53E-5	10031	368.0	27.3
6	4.24E-5	29359	270.0	108.7
7	4.95E-5	9006	256.0	35.2
8	5.65E-5	5819	252.0	23.1
9	6.36E-5	5031	250.0	20.1
10	7.07E-5	2023	246.0	8.2
11	7.78E-5	1884	242.0	7.8
12	8.48E-5	1442	240.0	6.0
13	9.19E-5	1442	236.0	6.1
14	9.90E-5	1335	232.0	5.8
15	1.06E-4	1191	228.0	5.2
13	9.19E-5	1357	236.0	5.8
11	7.78E-5	1829	242.0	7.6
9	6.36E-5	3485	250.0	13.9
7	4.95E-5	8230	256.0	32.1
5	3.53E-5	18316	368.0	49.8
3	2.12E-5	2910	587.0	5.0
1	7.07E-6	1153	732.0	1.6

APPENDIX J

Tabulation of the Variations of the Partial Pressures for Whole Blood

The data presented in this appendix show the minimum and maximum Sherwood numbers obtained from the partial pressures recorded during the experiments.

Table 23. Tabulation of the Variations of the Partial Pressures Recorded During Whole Blood Experiment at Re = 160

Re = 160 P_b = 0 mm Hg P_o = 660 mm Hg $D_o = 1.5 \times 10^{-5}$ cm^2/s

x (cm)	x/D	P_s (mm Hg)	$\frac{P_s - P_o}{P_b - P_s}$	h_d (cm/s)	Max. Sh	P_s (mm Hg)	$\frac{P_s - P_o}{P_b - P_s}$	h_d (cm/s)	Min. Sh
1		67	12.62	1.49E-2	1262	93	7.77	9.17E-3	776
2		69	12.06	1.42E-2	1202	75	10.64	1.26E-2	1067
3		57	16.30	1.92E-2	1626	61	14.61	1.72E-2	1456
4		17	∞	∞	∞	41	29.48	3.48_2	2946
5		17	∞	∞	∞	39	32.68	3.86E-2	3268
6		18	∞	∞	∞	36	39.00	4.60E-2	3895
7		19	∞	∞	∞	37	36.65	4.32E-2	3658
8		21	639.00	7.5E-1	63500	41	29.48	3.49E-2	2946
9		29	70.11	8.27E-2	7002	41	29.48	3.48E-2	2946
10		36	39.00	4.60E-2	3895	42	28.09	3.31E-2	2802
11		39	32.68	3.86E-2	3268	49	21.07	2.49E-2	2108
12		47	22.70	2.68E-2	2269	51	19.65	3.32E-2	1964
13		54	17.82	2.10E-2	1778	60	25.00	1.77E-2	1499
14		57	16.30	1.92E-2	1626	65	13.22	1.56E-2	1321
15		61	14.61	1.76E-2	1490	67	12.62	1.52E-2	1287
13		53	18.39	2.17E-2	1837	63	13.88	1.64E-2	1389
11		42	18.09	3.31E-2	2802	51	19.65	2.32E-2	1964
9		30	63.00	7.43E-2	6291	40	31.00	3.66E-2	3099
7		20	∞	∞	∞	36	39.00	4.60E-2	3895
5		18	∞	∞	∞	40	31.00	3.66E-2	3099
3		56	16.78	1.98E-2	1676	66	12.91	1.52E-2	1287
1		66	12.91	1.52E-2	1287	94	7.65	9.02E-3	764

Table 24. Tabulation of the Variations of the Partial Pressures Recorded During Whole Blood Experiment at Re = 450

Re = 450 P_b = 0 mm Hg P_o = 660 mm Hg $D_o = 1.5 \times 10^{-5}$ cm^2/s

x (cm)	x/D	P_s (mm Hg)	$\frac{P_s - P_o}{P_b - P_s}$	h_d (cm/s)	Max. Sh	P_s (mm Hg)	$\frac{P_s - P_o}{P_b - P_s}$	h_d (cm/s)	Min. Sh
1		55	17.29	1.04E-2	1727	97	7.31	8.62E-3	730
2		64	13.55	1.60E-2	1355	84	9.00	1.06E-2	897
3		24	159.00	1.88E-1	15971	64	13.55	1.60E-3	1355
4		18	∞	∞	∞	43	26.83	3.17E-2	2684
5		14	∞	∞	∞	38	34.56	3.08E-2	3454
6		13	∞	∞	∞	31	57.18	6.75E-2	5715
7		13	∞	∞	∞	41	29.48	3.48E-2	2946
8		23	212.33	2.50E-1	21167	39	32.68	3.86E-2	3268
9		23	212.33	2.50E-1	21167	43	26.83	3.17E-2	1684
10		42	28.09	3.31E-2	2802	58	15.84	1.87E-2	1583
11		40	31.00	3.66E-2	3099	64	13.55	1.60E-2	1355
12		50	20.33	2.40E-2	2032	70	11.80	1.39E-2	1177
13		42	28.09	3.31E-2	2802	82	9.32	1.10E-2	931
14		49	21.07	2.49E-2	2108	81	9.49	1.12E-2	948
15		51	19.65	2.32E-2	1964	87	8.55	1.01E-2	855
13		52	19.00	2.24E-2	1897	76	10.43	1.23E-2	1041
11		40	31.00	3.66E-2	3099	66	12.91	1.52E-2	1287
9		24	159.00	1.88E-1	15917	52	19.00	2.24E-2	1897
7		23	212.33	2.50E-1	21167	33	48.23	5.69E-2	4818
5		20	∞	∞	∞	25	127.00	1.50E-1	12700
3		35	41.77	3.92E-2	4166	46	23.62	2.79E-2	2362
1		44	25.67	3.03E-2	2565	97	7.31	8.62E-3	7298

APPENDIX K

Tabulation of Unprocessed Data

The data presented in this appendix is the unprocessed data recorded during the experiments.

Table 25 Tabulation of unprocessed data for saline at Re=160, 7/14/84

Date: 7/14/84
Barometric pressure: 707 mm Hg
Mean flow rate: 0.03 l/min
Downstream tubing diameter: 1.27 cm
Reynolds number: 160
Transfer gases: 100% O_2 and 100% N_2

Time	x(cm)	Microsensor reading (mm Hg)	pH	pO_2 (mm Hg)	pCO_2 (mm Hg)
2:50	1	300-435	6.948	10.4	0.6
3:10	2	320-360			
3:13	3	200-230	6.070	8.9	2.0
3:15	4	100-120			
3:18	5	82-88	6.050	8.0	2.2
3:25	6	69-78			
3:29	7	60-67	6.120	7.9	2.0
3:32	8	70-85			
3:34	9	92-98	6.220	8.5	1.8
3:38	10	98-115			
3:41	11	115-125			
3:44	12	115-125			
3:46	13	125-145			
3:48	14	130-150			
3:50	15	150-175			
3:52	13	130-150			
3:54	11	118-130			
3:56	9	90-98			
3:58	7	63-67	6.520	8.8	2.2
4:00	5	86-90			
4:02	3	250-350			
4:04	1	280-440	6.643	8.1	2.3

Table 26 Tabulation of unprocessed data for saline at Re=160, 7/31/84

Date: 7/31/84
Barometric pressure: 707 mm Hg
Mean flow rate: 0.03 l/min
Downstream tubing diameter: 1.27 cm
Reynolds number: 160
Transfer gases: 100% O_2 and 100% N_2

Time	x(cm)	Microsensor reading (mm Hg)	pH	pO_2 (mm Hg)	pCO_2 (mm Hg)
12:50	1	300-450	6.750	8.8	1.0
12:53	2	330-380			
12:57	3	200-230	6.785	9.0	0.9
1:01	4	100-115			
1:05	5	80-90	6.635	9.5	1.1
1:10	6	65-70			
1:13	7	60-67	6.765	8.5	1.0
1:16	8	70-90			
1:20	9	70-100	6.220	8.5	1.8
1:23	10	100-110			
1:26	11	120-125			
1:28	12	120-150			
1:31	13	120-170			
1:34	14	120-170			
1:37	15	130-180			
1:40	13	122-170			
1:43	11	118-130			
1:46	9	90-100	6.780	8.7	1.2
1:48	7	65-71			
1:52	5	78-88			
1:55	3	180-250	6.800	8.5	0.9
1:58	1	290-450	6.780	8.2	1.0

Table 26 Tabulation of unprocessed data for saline at Re=450, 8/24/84

Date: 8/24/84
Barometric pressure: 707 mm Hg
Mean flow rate: 0.073 l/min
Downstream tubing diameter: 1.27 cm
Reynolds number: 450
Transfer gases: 100% O_2 and 100% N_2

Time	x(cm)	Microsensor reading (mm Hg)	pH	pO_2 (mm Hg)	pCO_2 (mm Hg)
12:05	1	200-290	6.700	12.0	1.5
12:11	2	180-270			
12:15	3	160-230			
12:19	4	110-240	6.750	10.0	1.4
12:22	5	70-170			
12:25	6	20-80			
12:28	7	10-40	6.810	9.0	1.2
12:31	8	0-60			
12:35	9	30-40			
12:38	10	20-100	6.770	9.0	1.1
12:41	11	50-90			
12:43	12	50-110			
12:46	13	50-114			
12:48	14	50-120			
12:50	15	40-160	6.785	9.1	1.2
12:54	13	50-110			
12:57	11	51-89	6.800	9.5	1.3
1:00	9	30-50			
1:02	7	10-46	6.760	9.2	1.1
1:05	5	70-170			
1:08	3	150-260			
1:11	1	200-290	6.780	9.2	0.8

Table 28 Tabulation of unprocessed data for saline at Re=850, 8/14/84

Date: 8/14/84
Barometric pressure: 707 mm Hg
Mean flow rate: 0.14 l/min
Downstream tubing diameter: 1.27 cm
Reynolds number: 850
Transfer gases: 100% O_2 and 100% N_2

Time	x(cm)	Microsensor reading (mm Hg)	pH	pO_2 (mm Hg)	pCO_2 (mm Hg)
3:30	1	110-310	---	9.2	1.2
3:33	2	106-238			
3:35	3	70-130			
3:39	4	52-118	---	9.0	1.1
3:42	5	25-79			
3:45	6	31-93			
3:49	7	60-128	---	10.0	1.5
3:53	8	51-91			
3:56	9	61-113			
3:59	10	55-125			
4:02	11	70-126	---	9.1	1.4
4:05	12	72-148			
4:08	13	113-181			
4:11	14	106-218			
4:14	15	110-258	---	8.9	1.0
4:17	13	98-200			
4:20	11	72-128			
4:24	9	55-119	---	8.8	1.1
4:27	7	63-127			
4:30	5	20-86	---	9.1	1.3
4:33	3	60-140			
4:37	1	90-330	---	9.0	1.2

Table 29 Tabulation of unprocessed data for saline at Re=850, 8/16/84

Date: 8/16/84
Barometric pressure: 707 mm Hg
Mean flow rate: 0.14 l/min
Downstream tubing diameter: 1.27 cm
Reynolds number: 850
Transfer gases: 100% O_2 and 100% N_2

Time	x(cm)	Microsensor reading (mm Hg)	pH	pO_2 (mm Hg)	pCO_2 (mm Hg)
3:55	1	160-280	---	9.8	2.0
3:59	2	110-130			
4.04	3	90-110	---	10.0	1.8
4:09	4	15-85			
4:12	5	10-40	---	9.5	1.3
4:15	6	50-70			
4:19	7	70-90	---	9.8	1.9
4:21	8	100-104			
4:25	9	100-124	---	9.6	2.5
4:29	10	124-170			
4:33	11	130-200	---	9.7	2.4
4:34	12	188-196			
4:35	13	200-216	---	9.8	2.0
4:36	14	200-238			
4:37	15	180-284	---	9.9	2.1
4:40	13	190-210			
4:43	11	140-200			
4:45	9	100-160	---	9.6	2.3
4:47	7	80-100			
4:49	5	12-44	---	9.5	2.2
4:50	3	90-110			
4:53	1	150-292	---	9.8	2.0

Table 30. Tabulation of Unprocessed Data for Whole Blood at Re = 160, 8/3/84

Date: 8/3/84
Barometric pressure: 707 mm Hg.
Mean flow rate: 0.14 ℓ/min.
Downstream tubing diameter: 1.27 cm
Reynolds number: 160
Transfer gases: 100% O_2 and 37% O_2

Time	x(cm)	Microsensor reading (mm Hg)	pH (mm Hg)	PO_2 (mm Hg)	pCO_2 (g/dℓ)	THb	$\%O_2Hb$	%COHb	%MetHb	Vol % O_2
12:50 pm	1	30-56	7.341	20.8	36.4	11.6	26.2	1.1	2.9	4.2
1:02 pm	2	32-38								
1:08 pm	3	20-24								
1:10 pm	4	-20- 4	---	21.5	36.6	11.5	25.5	0.7	3.4	4.1
1:10 pm	5	-20- 2								
1:22 pm	6	-19-(-1)								
1:28 pm	7	-18- 0	---	21.3	35.8	11.6	25.8	0.9	3.2	4.2
1:32 pm	8	-16- 4								
1:36 pm	9	- 8- 4								
1:40 pm	10	- 1- 5								
1:46 pm	11	- 2-12	7.322	20.9	35.8	11.6	25.2	0.9	3.2	4.1
1:50 pm	12	10-14								
1:54 pm	13	18-24								
1:58 pm	14	21-29								
2:04 pm	15	25-31	---	20.5	34.3	11.5	24.4	0.9	3.5	3.9
2:08 pm	16	17-27								
2:12 pm	17	5-15								
2:16 pm	9	- 6- 4	---	18.9	36.2	11.5	24.2	1.1	3.5	3.9
2:21 pm	7	-16- 0								
2:25 pm	5	-18 - 4								
2:29 pm	3	20-30								
2:37 pm	1	30-58	---	20.8	35.4	11.6	32.0	0.9	3.6	3.7

Table 31. Tabulation of Unprocessed Data for Whole Blood at Re = 450

Date: 9/20/84
Barometric pressure: 707 mm Hg.
Mean flow rate: 0.40 ℓ/min. ℓ/min.
Downstream tubing diameter: 1.27 cm
Reynolds number: 450
Transfer gases: 100% O_2 and 3% O_2

Time	x (cm)	Microsensor reading (mm Hg)	pH (mm Hg)	PO_2 (mm Hg)	pCO_2 (g/dℓ)	THb	$\%O_2Hb$	%COHb	%MetHb	Vol % O_2
1:40 pm	1	41-83	7.381	19.4	37.3	11.6	28.0	1.3	2.3	4.5
1:45 pm	2	50-70								
1:48 pm	3	10-50								
1:50 pm	4	5-30	3.385	18.8	35.9	11.5	26.7	1.4	2.8	4.2
1:52 pm	5	1-25								
1:54 pm	6	0-18								
1:56 pm	7	0-28	7.384	18.5	35.8	11.4	25.9	1.3	3.3	4.1
1:59 pm	8	10-26								
2:04 pm	9	10-30								
2:07 pm	10	30-46	7.382	18.4	35.7	11.5	25.9	1.1	3.9	4.1
2:10 pm	11	28-52								
2:12 pm	12	38-58								
2:14 pm	13	30-70								
2:17 pm	14	37-69								
2:21 pm	15	40-76	7.382	18.4	35.1	11.6	26.1	1.2	4.1	4.2
2:23 pm	13	41-65								
2:25 pm	11	29-55								
2:27 pm	9	13-41	7.379	18.8	34.9	11.6	26.0	1.1	4.5	4.1
2:29 pm	7	12-22								
2:32 pm	5	10-15	7.376	18.5	34.7	11.4	26.3	1.3	4.5	4.1
2:35 pm	3	25-36								
2:38 pm	1	34-87	7.372	18.9	35.0	11.4	26.1	1.2	4.6	4.1

The vita has been removed from the scanned document